Next-to-Leading Logarithmic Resummation for the C-Parameter Sudakov Shoulder in e^+e^- Annihilation

Matthew D. Schwartz[1,2] and Claude Opus 4.5[3]

[1] *Department of Physics, Harvard University, Cambridge, MA 02138, USA*

[2] *Institute for Artificial Intelligence and Fundamental Interactions (IAIFI)*

[3] *Anthropic, San Francisco, CA, USA*

schwartz@g.harvard.edu

December 22, 2025

Abstract

We derive the next-to-leading logarithmic (NLL) resummation formula for the C-parameter distribution near its kinematic shoulder at $C = 3/4$ in e^+e^- annihilation. This shoulder arises because three-parton final states achieve at most $C = 3/4$, and crossing this boundary requires a fourth parton, introducing $\mathcal{O}(\alpha_s)$ suppression and large logarithms $\ln^n(C - 3/4)$. Using soft-collinear effective theory, we establish a factorization theorem involving jet and soft functions convolved with the hard phase space near the Mercedes configuration. A key finding is that the C-parameter is *quadratic* in deviations from Mercedes—both for the hard kinematics (producing $A(3/4) \neq 0$ at LO) and for soft radiation (with $\delta C \propto \hat{k}_\perp^2$). This quadratic structure has a crucial consequence: the hard phase space integral converts the SCET kernel $K(c')$, which has $[1/c']_+$ plus-distribution singularities, into its *cumulant* $R(c) = \int_0^c K(c')\,dc'$, yielding $\ln c$ and $\ln^2 c$ structure in the cross section. The SCET factorization makes definite predictions for the NLO singular coefficients: $A_2 = 2C_F + C_A$ and $B_1 = 3C_F + \beta_0/2 + 2(2C_F + C_A)\ln(8/3)$, which agree with the Catani–Webber result and EVENT2. We present a direct calculation of the soft anomalous dimension from the one-loop soft function integral, obtaining $\gamma_S^{\mathrm{nc},(0)} = 12C_F + 2\beta_0$ in agreement with RG consistency. Unlike thrust and heavy jet mass, the C-parameter does not suffer from a Sudakov–Landau pole, so momentum-space resummation is straightforward. This work extends the Bhattacharya–Schwartz–Zhang program for event shape shoulders to the C-parameter observable.

Contents

1 Introduction

Event shape observables in e^+e^- annihilation have been cornerstones of precision QCD phenomenology for decades [1, 2]. These observables—including thrust, heavy jet mass, C-parameter, jet broadening, and others—provide sensitive probes of the strong interaction, enabling precision extractions of the strong coupling constant α_s and detailed tests of perturbative QCD. The theoretical description of event shapes has reached remarkable sophistication, with next-to-next-to-next-to-leading order ($\mathrm{N^3LO}$) fixed-order calculations [3, 4] and $\mathrm{N^3LL}$ resummation [5, 6] available for thrust, enabling α_s extractions with percent-level precision.

Most theoretical work on event shape resummation has focused on the *two-jet limit*, where observables approach their minimum values and large Sudakov logarithms arise from soft and collinear radiation. However, event shapes also exhibit rich structure at other kinematic boundaries within their allowed ranges. A particularly interesting class of such boundaries are the *Sudakov shoulders*: points where the leading-order distribution has a discontinuity because higher parton multiplicities are required beyond that point.

1.1 Historical context: Sudakov shoulders

The existence and importance of Sudakov shoulders was first recognized in the seminal work of Catani and Webber [7], who pointed out that infrared- and collinear-safe observables can produce *divergent* perturbative predictions at points inside the physical region—not just at endpoints. While the Sterman–Weinberg criteria [9] guarantee finiteness of integrated cross sections, they do not prevent differential distributions from developing integrable singularities near kinematic boundaries where the lower-order distribution is discontinuous.

Catani and Webber identified the C-parameter at $C = 3/4$ as a prototypical example of such a Sudakov shoulder. They established several key qualitative features:

1. The LO distribution at the shoulder has a *step discontinuity*: the coefficient function $A(C)$ approaches a finite, nonzero value as $C \to 3/4^-$, then drops abruptly to zero for $C > 3/4$ at tree level.

2. At NLO, the distribution above the shoulder develops double- and single-logarithmic divergences. Defining $c = C - 3/4$, the singular structure takes the form

$$B_+(C) \simeq A\left(\frac{3}{4}\right)\left[(2C_F + C_A)\ln^2 c + \left(3C_F + \frac{\beta_0}{2} + 2(2C_F + C_A)\ln\frac{8}{3}\right)\ln c + \ldots\right], \quad (1)$$

   where the double-log coefficient $(2C_F + C_A)$ reflects contributions from two quark jets plus one gluon jet. The single-log coefficient contains $3C_F + \beta_0/2$ from the jet anomalous dimensions and running coupling, plus a term $2(2C_F + C_A)\ln(8/3)$ from the C-parameter geometry at the Mercedes configuration (see Eq. (58)). In the rescaled variable $\delta = (8/3)c$ used by Catani and Webber, the geometric logarithm is absorbed and the single-log coefficient simplifies to $3C_F + \beta_0/2$.

3. These divergences are *integrable*, but resummation to all orders is essential to obtain reliable predictions. At the double-logarithmic (DL) level, resummation produces a smooth "Sudakov shoulder" structure that transforms the LO step discontinuity into a smooth, infinitely differentiable distribution.

4. They validated their analytic predictions against the EVENT Monte Carlo program, finding excellent agreement for the NLO singular structure.

In this paper, we use soft-collinear effective theory (SCET) to derive the complete singular structure (1) at NLL accuracy from first principles. The SCET factorization theorem provides

a systematic framework that determines all logarithmic coefficients from anomalous dimensions, without requiring fixed-order input. We verify that our results agree with the original Catani–Webber analysis.

1.2 Beyond double-logarithmic accuracy

While the Catani–Webber DL resummation captures the qualitative physics of the Sudakov shoulder, it leaves several important questions unanswered. What is the complete NLL structure including running coupling effects, the two-loop cusp anomalous dimension, and non-cusp anomalous dimensions? How does one systematically organize the resummation using modern effective field theory techniques?

Recently, Bhattacharya, Schwartz, and Zhang (BSZ) [10] developed a systematic framework for resumming Sudakov shoulder logarithms using soft-collinear effective theory (SCET) [11, 12, 13]. They applied this framework to the thrust and heavy jet mass distributions near their respective shoulders at $\tau = 1/3$ and $\rho = 1/3$, achieving NLL accuracy with a clear path to higher orders. Their key insights include: a factorization theorem involving a trijet hard function, three jet functions, and a soft function; the demonstration that non-global logarithms [14] are absent at leading power; and the identification of a "Sudakov–Landau pole" that complicates momentum-space resummation for heavy jet mass.

Bhattacharya, Michel, Schwartz, Stewart, and Zhang (BMSSZ) [17] subsequently showed that position-space methods provide an elegant way to handle the Sudakov–Landau pole for heavy jet mass. However, as we show in this paper, the C-parameter does not suffer from a Sudakov–Landau pole because the observable is additive across all jets—the total $c = C - 3/4$ is the sum of contributions from each jet and the soft function. This allows straightforward momentum-space resummation without the need for position-space methods.

1.3 This work: NLL resummation for the C-parameter shoulder

In this paper, we extend the BSZ program to the **C-parameter** event shape. Using SCET, we derive the complete singular structure (1) from first principles: the LO coefficient $A(3/4)$ from phase-space integrals, and the NLO double-log coefficient $(2C_F + C_A)$ and single-log coefficient from the SCET anomalous dimensions together with the geometric factor from the jet measurement. These results, which agree with the original Catani–Webber analysis, emerge naturally from the factorization theorem without requiring fixed-order input.

The C-parameter shoulder presents both similarities and differences compared to thrust and heavy jet mass. The underlying physics is the same: soft and collinear radiation on top of a symmetric trijet configuration pushes the observable across the kinematic boundary. The same three collinear directions (quark, antiquark, gluon at 120° separation) define the relevant SCET modes. However, the C-parameter has a *step discontinuity* at leading order—the distribution $d\sigma/dC$ drops to exactly zero for $C > 3/4$ at tree level—whereas thrust has a kink (discontinuous first derivative) at its shoulder. Additionally, the C-parameter measurement function has a fundamentally different form: while thrust involves linear projections onto jet directions, the C-parameter soft contribution is *quadratic* in the out-of-plane momentum component. This reflects the eigenvalue-based definition of the C-parameter and has important consequences for the soft function structure.

The origin of the step discontinuity lies in the structure of the observable near the Mercedes configuration. At leading order, both thrust and the C-parameter are computed over three-parton phase space, which shrinks to a single point—the symmetric trijet—at the shoulder. Normally this would force the cross section to vanish. For thrust, the observable is *linear* in deviations from Mercedes: $\tau = 1/3 + s$ where s parameterizes phase space. The phase space volume shrinks linearly, giving $d\sigma/d\tau \propto (1/3 - \tau) \to 0$ at the shoulder. For the C-parameter, however, the Mercedes point is a *critical point* where $\nabla C = 0$. The observable is quadratic in

phase space deviations: $C = 3/4 - \alpha(s^2 + st + t^2)$. This means the Jacobian $\partial C/\partial r \propto r$ vanishes at Mercedes. The shrinking phase space (circumference $\sim r \to 0$) is exactly compensated by the diverging Jacobian ($1/|\nabla C| \sim 1/r$), producing a finite cross section $A(3/4) \neq 0$.

This same structure explains why the NLO distribution *diverges* above the C-parameter shoulder. At NLO, four-parton configurations populate the region $C > 3/4$. For small $c = C - 3/4$, we are no longer at a critical point—the four-parton phase space is finite at any $c > 0$. The soft and collinear matrix element singularities ($\sim 1/\omega$, $\sim 1/m^2$) that were harmless at LO—because they integrated against a Jacobian that cancelled them—now have nothing to compensate them. The result is divergent logarithms $\ln^2 c$ and $\ln c$ at NLO, which must be resummed. For thrust, the LO distribution already vanishes at the shoulder, so the NLO merely produces a kink rather than divergent logs. The step-to-spike structure at the C-parameter shoulder is thus a direct consequence of the quadratic nature of the observable near Mercedes.

A crucial feature of the C-parameter factorization is that the *hard phase space integral* must be retained. The standard SCET factorization gives a radiative kernel

$$K(c') = \int d\ell_1\, d\ell_2\, d\ell_3\, d\kappa\; J_q(\ell_1)\, J_q(\ell_2)\, J_g(\ell_3)\, S_C(\kappa)\; \delta(c' - \ell_1 - \ell_2 - \ell_3 - \kappa)\,, \tag{2}$$

which has $\delta(c')$ at tree level and $[1/c']_+$, $[\ln c'/c']_+$ plus distributions at one loop. The full cross section involves integrating over the hard phase space (s, t) near Mercedes:

$$\frac{d\sigma}{dc} = \int ds\, dt\; \mathcal{H}(s,t)\, K(c + \alpha Q(s,t))\,, \tag{3}$$

where $Q(s,t) = s^2 + st + t^2$ is quadratic. The same Jacobian cancellation that gives $A(3/4) \neq 0$ at LO converts this into a matched formula:

$$\left.\frac{d\sigma}{dc}\right|_{c>0} = -\frac{\alpha_s}{2\pi}\, A\Big(\frac{3}{4}\Big)\, R(c) + \sigma_{\rm NS}(c)\,, \qquad R(c) = \int_0^c K(c')\, dc'\,, \tag{4}$$

where $\sigma_{\rm NS}$ is the non-singular remainder from matching to fixed order. At tree level, $R^{(0)}(c) = 1$ for $c > 0$, and matching ensures zero cross section above the shoulder. With resummation, $R(c) = e^{-S(c)} \to 0$ as $c \to 0$, so the singular piece vanishes at the shoulder and continuity is automatic. The cumulant $R(c)$ converts the $[1/c']_+$ singularities in the kernel to $\ln c$ in the cross section—explaining why the NLO singular structure is $\ln^2 c + \ln c$ rather than $1/c$.

1.4 Summary of results

Our main results are as follows:

1. We derive the factorization theorem from first principles, establishing the mode structure, scale hierarchy $\mu_S \sim (8/3)Qc \ll \mu_J \sim Q\sqrt{(8/3)c} \ll \mu_H \sim Q$, and measurement function decomposition specific to the C-parameter. The geometric factor 8/3 arises from the C-parameter definition at the Mercedes configuration (Eq. (58)). We show that the soft contribution has a distinctive quadratic structure: $\delta C_{\rm soft} = \frac{3}{2}\frac{\omega}{Q}\hat{k}_\perp^2$, where $\hat{k}_\perp$ is the out-of-plane momentum component.

2. A crucial feature of the C-parameter factorization is that the *hard phase space integral* must be retained. Because the C-parameter is quadratic in deviations from the Mercedes configuration (Eq. (28)), the phase space integral over (s, t) produces a Jacobian cancellation:

$$\int ds\, dt\; \delta\big(c + \alpha Q(s,t) - c'\big) = N\, \Theta(c' - c)\,. \tag{5}$$

   This is the *same* Jacobian cancellation that produces the finite LO coefficient $A(3/4)$ in Eq. (33). It converts the SCET kernel $K(c')$—which has $[1/c']_+$ and $[\ln c'/c']_+$ plus-distribution structure—into its *cumulant* $R(c) = \int_0^c K(c')\, dc'$, yielding $\ln c$ and $\ln^2 c$ structure in the cross section.

3. We compute all anomalous dimensions required for NLL resummation. The cusp anomalous dimension enters with color factor $(2C_F + C_A)$, confirming the Catani–Webber result for the double-log coefficient. We verify that the anomalous dimensions satisfy the RG consistency condition $\gamma_H + 2\gamma_J^q + \gamma_J^g + \gamma_S = 0$.

4. We present a direct calculation of the non-cusp soft anomalous dimension $\gamma_S^{\mathrm{nc},(0)}$ from the one-loop soft function integral (Appendix B), following the methodology of BSZ [10]. The result $\gamma_S^{\mathrm{nc},(0)} = 12C_F + 2\beta_0$ agrees with the RG consistency prediction, providing a nontrivial check of the factorization formula.

5. We demonstrate that non-global logarithms are absent at leading power, following from the global nature of the C-parameter: all radiation contributes positively to C, with no vetoed regions that would generate "in–out" correlations.

6. Unlike heavy jet mass, the C-parameter has no physical channel structure—all three channels (gluon + quark + antiquark) contribute identically because C is a permutation-symmetric global observable. The matched cross section above the shoulder takes the form
$$\frac{1}{\sigma_0}\frac{d\sigma}{dc}\bigg|_{c>0} = -\frac{\alpha_s}{2\pi}\,A\Big(\frac{3}{4}\Big)\,R(c) + \sigma_{\mathrm{NS}}(c)\,, \tag{6}$$
where $R(c) = e^{-S(c)}$ after resummation. At NLO, expanding gives $(\alpha_s/2\pi)^2 A(3/4)[A_2 \ln^2 c + B_1 \ln c + \ldots]$ with $A_2 = 2C_F + C_A$ and $B_1 = 3C_F + \beta_0/2 + 2(2C_F + C_A)\ln(8/3)$, in agreement with Catani–Webber and EVENT2.

7. The physical interpretation is clear: at tree level, $R^{(0)}(c) = 1$ for $c > 0$, and matching to fixed order ensures zero cross section above the shoulder. Resummation gives $R(c) = e^{-S(c)} \to 0$ as $c \to 0$, so the singular piece $-A(3/4)R(c)$ vanishes at the shoulder and the cross section smoothly approaches $\sigma_{\mathrm{NS}}(0)$, which matches the LO cross section just below the shoulder. The "Sudakov shoulder" is smooth and infinitely differentiable at $c = 0$.

The paper is organized as follows. Section 2 reviews the C-parameter definition and derives the kinematic properties of its shoulder. Section 3 presents the SCET factorization theorem for the shoulder region. Section 4 collects all perturbative ingredients including anomalous dimensions. Section 5 derives the NLL formula and shows that its expansion to $\mathcal{O}(\alpha_s^2)$ yields definite predictions for the NLO singular coefficients A_2 and B_1. Section 6 presents the matched NLL+NLO formula with profile scales. Section 7 discusses phenomenology. We conclude in Section 8. Appendix A provides a numerical reference for NLL parameters, and Appendix B presents a complete direct calculation of the soft anomalous dimension from the one-loop soft function integral.

2 C-Parameter Kinematics and the Shoulder

2.1 Definition of the C-parameter

The C-parameter is constructed from the linearized momentum tensor [15, 16]
$$\Theta^{\alpha\beta} = \frac{1}{\sum_j |\mathbf{p}_j|}\sum_i \frac{p_i^\alpha p_i^\beta}{|\mathbf{p}_i|}\,, \tag{7}$$
where the sums run over all final-state particles. This 3×3 symmetric tensor has three eigenvalues $\lambda_1, \lambda_2, \lambda_3$ satisfying $\lambda_1 + \lambda_2 + \lambda_3 = 1$ and $0 \le \lambda_i \le 1$. The C-parameter is defined as
$$C = 3(\lambda_1\lambda_2 + \lambda_2\lambda_3 + \lambda_3\lambda_1)\,. \tag{8}$$

Equivalently, C can be written as a sum over particle pairs:

$$C = \frac{3}{2} \frac{\sum_{i<j} |\mathbf{p}_i||\mathbf{p}_j| \sin^2 \theta_{ij}}{\left(\sum_k |\mathbf{p}_k|\right)^2}\,, \tag{9}$$

where θ_{ij} is the angle between particles i and j.

The C-parameter is bounded: $0 \leq C \leq 1$. The limiting cases are:

- $C = 0$: Back-to-back two-jet events with all particles along a single axis ($\lambda_1 = 1$, $\lambda_2 = \lambda_3 = 0$).
- $C = 1$: Isotropic events with $\lambda_1 = \lambda_2 = \lambda_3 = 1/3$.

2.2 Three-parton kinematics

For a three-parton final state $\gamma^* \to q\bar{q}g$, momentum conservation in the center-of-mass frame gives $\mathbf{p}_1 + \mathbf{p}_2 + \mathbf{p}_3 = 0$, implying that the three momenta are coplanar. We define the energy fractions

$$x_i = \frac{2E_i}{Q} = \frac{2p_i \cdot q}{Q^2}\,, \tag{10}$$

where q^μ is the total four-momentum with $q^2 = Q^2$. Energy conservation gives $x_1 + x_2 + x_3 = 2$, with each $x_i \in (0, 1)$ for massless partons.

It is convenient to use the normalized invariant masses

$$s_{ij} = \frac{(p_i + p_j)^2}{Q^2} = \frac{2p_i \cdot p_j}{Q^2}\,, \tag{11}$$

which for massless partons satisfy $s_{ij} = 1 - x_k$ where $\{i, j, k\}$ is a permutation of $\{1, 2, 3\}$. The constraint $x_1 + x_2 + x_3 = 2$ becomes

$$s_{12} + s_{13} + s_{23} = 1\,. \tag{12}$$

For three massless partons, the C-parameter takes the form

$$C = \frac{6\, s_{12}\, s_{13}\, s_{23}}{(1 - s_{12})(1 - s_{13})(1 - s_{23})} = \frac{6(1 - x_1)(1 - x_2)(1 - x_3)}{x_1 x_2 x_3}\,. \tag{13}$$

The second form uses the relations $1 - x_i = s_{jk}$ and $x_i = 1 - s_{jk} = s_{ij} + s_{ik}$.

2.3 The shoulder at $C = 3/4$

We now determine the maximum value of C for three-parton states. Maximizing Eq. (13) subject to the constraint (12) and positivity $s_{ij} > 0$, we use Lagrange multipliers:

$$\frac{\partial}{\partial s_{12}} \Big[6 s_{12} s_{13} s_{23} - \lambda (s_{12} + s_{13} + s_{23} - 1) \Big] = 0\,. \tag{14}$$

This gives $6 s_{13} s_{23} = \lambda$, and similarly for cyclic permutations. The solution is

$$s_{12} = s_{13} = s_{23} = \frac{1}{3}\,, \tag{15}$$

which corresponds to equal energy fractions $x_1 = x_2 = x_3 = 2/3$. At this *symmetric point*, the C-parameter achieves its maximum:

$$\boxed{C^{(3)}_{\max} = 6 \times \frac{1}{3} \times \frac{1}{3} \times \frac{1}{3} = \frac{2}{9} \times 3 = \frac{3}{4} \equiv C_{\rm sh}} \tag{16}$$

The symmetric configuration corresponds to the "Mercedes" trijet: three partons with equal energies $E_i = Q/3$ separated by 120° angles. Choosing coordinates with the event plane as the xz-plane, the four-momenta are

$$\begin{aligned} p_1^\mu &= \frac{Q}{3}(1,0,0,1)\,, \\ p_2^\mu &= \frac{Q}{3}\Big(1,0,\frac{\sqrt{3}}{2},-\frac{1}{2}\Big)\,, \\ p_3^\mu &= \frac{Q}{3}\Big(1,0,-\frac{\sqrt{3}}{2},-\frac{1}{2}\Big)\,. \end{aligned} \tag{17}$$

2.4 Leading-order distribution: setup and kinematics

At leading order in α_s, the C-parameter distribution comes from $\gamma^* \to q\bar{q}g$:

$$\frac{1}{\sigma_0}\frac{d\sigma^{\rm LO}}{dC} = \frac{\alpha_s}{2\pi}A(C)\,\Theta\!\left(\frac{3}{4}-C\right)\Theta(C)\,, \tag{18}$$

where σ_0 is the Born cross section for $e^+e^- \to q\bar{q}$, and $A(C)$ is the coefficient function that includes the color factor C_F from the matrix element. We now derive the exact analytical form of $A(C)$, following the approach of Gardi and Magnea [8].

Consider a three-parton final state with massless quark and antiquark momenta p_1, p_2, and gluon momentum p_3, with total momentum q satisfying $q^2 = Q^2$. We introduce the energy fractions in the center-of-mass frame:

$$x_1 = \frac{2p_1\cdot q}{Q^2}\,, \qquad x_2 = \frac{2p_2\cdot q}{Q^2}\,, \qquad x_3 = \frac{2p_3\cdot q}{Q^2} = 2 - x_1 - x_2\,, \tag{19}$$

where energy-momentum conservation requires $x_1 + x_2 + x_3 = 2$ and phase space restricts $0 \le x_i \le 1$. Following Ref. [8], we introduce the rescaled variable

$$c_{\rm GM} \equiv \frac{C}{6}\,, \tag{20}$$

so that the physical support at LO is $0 < c_{\rm GM} < 1/8$ (corresponding to $0 < C < 3/4$). In terms of the energy fractions, the rescaled C-parameter for three massless partons is

$$c_{\rm GM}(x_1,x_2) = \frac{(1-x_1)(1-x_2)(x_1+x_2-1)}{x_1x_2(2-x_1-x_2)}\,. \tag{21}$$

The LO coefficient function is obtained by integrating the squared matrix element

$$|\mathcal{M}|^2 \propto C_F\frac{x_1^2+x_2^2}{(1-x_1)(1-x_2)} \tag{22}$$

over the three-body phase space with the constraint $c_{\rm GM}(x_1,x_2) = c_{\rm GM}$. Implementing the constraint via a delta function and changing variables, the distribution in $c_{\rm GM}$ takes the form

$$\frac{d\sigma}{dc_{\rm GM}} \propto \int dx_1\,dx_2\;\frac{x_1^2+x_2^2}{(1-x_1)(1-x_2)}\;\delta\big(c_{\rm GM} - c_{\rm GM}(x_1,x_2)\big)\,. \tag{23}$$

The delta function constrains the integration to a curve in the (x_1,x_2) plane. After eliminating one variable using the constraint and performing a suitable change of variables, the remaining integral over the gluon energy fraction x_3 involves square roots of cubic polynomials—a signature of **elliptic integrals**.

2.5 Computation of $A(3/4)$ and the step discontinuity

The C-parameter distribution exhibits a step discontinuity at $C = 3/4$: the coefficient function $A(C)$ approaches a finite, nonzero value as $C \to 3/4^-$, unlike thrust where $A(\tau) \to 0$ as $\tau \to 1/3^-$. This difference has important consequences for matching across the Sudakov shoulder, as we will discuss in Section 6. Here we compute $A(3/4)$ directly by examining the phase space structure near the Mercedes configuration, illuminating the origin of this qualitative difference.

Near Mercedes, we parameterize deviations from the symmetric point using the invariants:

$$s_{12} = \frac{1}{3} + s\,, \qquad s_{13} = \frac{1}{3} + t\,, \qquad s_{23} = \frac{1}{3} - s - t\,, \tag{24}$$

where $s_{ij} = (p_i + p_j)^2/Q^2 = 1 - x_k$, and the constraint $s_{12} + s_{13} + s_{23} = 1$ is automatically satisfied. The Mercedes configuration corresponds to $s = t = 0$. The matrix element at this point evaluates to

$$\frac{x_1^2 + x_2^2}{(1-x_1)(1-x_2)}\Big|_{\text{Merc}} = \frac{2(2/3)^2}{(1/3)^2} = 8\,. \tag{25}$$

Thrust: linear observable. For thrust, near Mercedes in the region where s_{12} is minimal, the observable is simply $\tau = s_{12} = 1/3 + s$. The coefficient function is

$$A_\tau(\tau) = 8C_F \int ds\, dt\, \delta\!\left(\tau - \frac{1}{3} - s\right) \Theta(t-s)\,\Theta(-s-t)\,, \tag{26}$$

where the step functions enforce $s_{12} \le s_{13}$ and $s_{12} \le s_{23}$. After integrating over s using the delta function, the constraint restricts $t \in [s, -2s]$ with $s = \tau - 1/3 < 0$:

$$A_\tau(\tau) = 8C_F \int_{\tau-1/3}^{-2(\tau-1/3)} dt = 8C_F \cdot 3\left(\frac{1}{3} - \tau\right) \xrightarrow{\tau\to 1/3} 0\,. \tag{27}$$

The distribution vanishes linearly at the shoulder because thrust is a *linear* function of the phase space coordinates near Mercedes.

C-parameter: quadratic observable. For the C-parameter, expanding around the Mercedes configuration gives

$$C = \frac{3}{4} - \frac{81}{16}(s^2 + st + t^2) + \mathcal{O}(\epsilon^3)\,. \tag{28}$$

Crucially, the Mercedes point is a *critical point* of the C-parameter: $\nabla C = 0$ at $s = t = 0$. The observable is quadratic in deviations from Mercedes, not linear.

The coefficient function becomes

$$A_C(C) = 8C_F \int ds\, dt\, \delta\!\left(\frac{3}{4} - C - \frac{81}{16}(s^2 + st + t^2)\right). \tag{29}$$

Defining $c = 3/4 - C$ and the quadratic form $Q(s,t) = s^2 + st + t^2$, the constraint is $Q = 16c/81$.

To evaluate the integral, we diagonalize the quadratic form. Writing $Q = (s + t/2)^2 + 3t^2/4$ suggests the substitution $u = s + t/2$, $v = \sqrt{3}t/2$, giving $Q = u^2 + v^2 \equiv r^2$ with Jacobian

$$ds\, dt = \frac{2}{\sqrt{3}}\, du\, dv = \frac{2}{\sqrt{3}}\, r\, dr\, d\theta\,. \tag{30}$$

The integral becomes

$$A_C(C) = 8C_F \cdot \frac{2}{\sqrt{3}} \int_0^{2\pi} d\theta \int_0^\infty r\, dr\, \delta\!\left(c - \frac{81}{16} r^2\right). \tag{31}$$

Using the identity $\delta(c-\alpha r^2) = \frac{1}{2\alpha r_0}\delta(r-r_0)$ where $r_0 = \sqrt{c/\alpha}$, the factors of r cancel exactly:

$$A_C(C) = 8C_F \cdot \frac{2}{\sqrt{3}} \cdot 2\pi \cdot \frac{1}{2 \cdot 81/16} = \frac{256\sqrt{3}\pi}{243} C_F \,. \tag{32}$$

This gives the result:

$$A\left(\frac{3}{4}\right) = \frac{256\sqrt{3}\pi}{243} C_F \approx 7.64 \tag{33}$$

for $C_F = 4/3$.

Physical interpretation. The key difference between thrust and C-parameter lies in the structure of the observable near Mercedes:

- **Thrust:** $\tau - 1/3 \propto r$ (linear in phase space distance). The phase space volume at fixed τ shrinks like the length of a line segment, proportional to $r \to 0$.
- **C-parameter:** $3/4 - C \propto r^2$ (quadratic in phase space distance). The phase space volume at fixed C shrinks like the circumference of a circle, proportional to r, but the Jacobian $\partial C/\partial r \propto r$ also vanishes, and the two effects cancel exactly.

This cancellation is analogous to the density of states for a free particle in two dimensions. For a 2D system with energy $E \propto v^2$, the density of states $g(E)$ is constant even as $E \to 0$: the probability of finding a particle with kinetic energy less than ϵ scales linearly with ϵ, not quadratically. The Mercedes configuration is a critical point of $C(\{s_{ij}\})$, making the C-parameter locally equivalent to "energy" in this analogy, while thrust is analogous to "speed" v whose distribution vanishes at $v = 0$.

2.6 Exact analytical formula for $A(C)$

The integration in Eq. (23) can be performed analytically. The result, derived in Ref. [8], expresses the LO coefficient as a linear combination of complete elliptic integrals:

$$A(C) = \frac{1}{6} F_0\left(\frac{C}{6}\right) , \qquad 0 < C < \frac{3}{4} , \tag{34}$$

where the "characteristic function" $F_0(c_{\rm GM})$ is given by

$$\boxed{F_0(c_{\rm GM}) = f_0(c_{\rm GM})\,\mathbf{K}\big(m_0(c_{\rm GM})\big) + e_0(c_{\rm GM})\,\mathbf{E}\big(m_0(c_{\rm GM})\big) + p_0(c_{\rm GM})\,\mathbf{\Pi}\big(n_0(c_{\rm GM}), m_0(c_{\rm GM})\big)\,.} \tag{35}$$

Here $\mathbf{K}$, $\mathbf{E}$, and $\mathbf{\Pi}$ are the complete elliptic integrals of the first, second, and third kind, respectively, defined by

$$\mathbf{K}(m) = \int_0^{\pi/2} \frac{d\phi}{\sqrt{1 - m\sin^2\phi}} , \tag{36}$$

$$\mathbf{E}(m) = \int_0^{\pi/2} d\phi \sqrt{1 - m\sin^2\phi} , \tag{37}$$

$$\mathbf{\Pi}(n, m) = \int_0^{\pi/2} \frac{d\phi}{(1 - n\sin^2\phi)\sqrt{1 - m\sin^2\phi}} . \tag{38}$$

The modulus, characteristic parameter, and coefficient functions are [8]:[1]

$$m_0(c_{\rm GM}) = \frac{2\sqrt{1-8c_{\rm GM}}}{1-4c_{\rm GM}(1+2c_{\rm GM})+\sqrt{1-8c_{\rm GM}}}\,, \tag{39}$$

$$n_0(c_{\rm GM}) = \frac{4\sqrt{1-8c_{\rm GM}}}{\left(1+\sqrt{1-8c_{\rm GM}}\right)^2}\,, \tag{40}$$

$$f_0(c_{\rm GM}) = \frac{4\sqrt{2}\left(1-2c_{\rm GM}(2+c_{\rm GM})\right)}{(1+c_{\rm GM})^3\sqrt{1-4c_{\rm GM}(1+2c_{\rm GM})+\sqrt{1-8c_{\rm GM}}}}\,, \tag{41}$$

$$e_0(c_{\rm GM}) = -\frac{3(1+2c_{\rm GM})\sqrt{2}\sqrt{1-4c_{\rm GM}(1+2c_{\rm GM})+\sqrt{1-8c_{\rm GM}}}}{2c_{\rm GM}\,(1+c_{\rm GM})^3}\,, \tag{42}$$

$$p_0(c_{\rm GM}) = \frac{\sqrt{2}\,(2+c_{\rm GM}+2c_{\rm GM}^2)\left(1-\sqrt{1-8c_{\rm GM}}\right)^2}{c_{\rm GM}(1+c_{\rm GM})^3\sqrt{1-4c_{\rm GM}(1+2c_{\rm GM})+\sqrt{1-8c_{\rm GM}}}}\,. \tag{43}$$

These expressions are valid for $0 < c_{\rm GM} < 1/8$, i.e., $0 < C < 3/4$.

2.7 Asymptotic behavior

The exact formula (35) can be expanded in various limits:

Small-C limit (soft/collinear region): As $c_{\rm GM} \to 0$, the elliptic integrals simplify, yielding [8]

$$F_0(c_{\rm GM}) = -\frac{3+4\ln c_{\rm GM}}{c_{\rm GM}} + 1 - 28\ln c_{\rm GM} + \mathcal{O}(c_{\rm GM}\ln c_{\rm GM})\,. \tag{44}$$

This reproduces the known singular structure from soft and collinear emissions, with the leading $1/c_{\rm GM}$ divergence regularized in the full distribution by the virtual corrections.

Approach to the shoulder ($C \to 3/4^-$): As $c_{\rm GM} \to 1/8$, the elliptic modulus $m_0 \to 0$ and the elliptic integrals approach their limiting values $\mathbf{K}(0) = \mathbf{E}(0) = \pi/2$. Evaluating the limit of Eq. (35) confirms the result (33) derived in Section 2.5:

$$\boxed{A\left(\frac{3}{4}\right) = \frac{256\pi\sqrt{3}}{243}\,C_F} \tag{45}$$

We have verified this value by direct numerical integration of the phase-space integral (23) and by comparison with EVENT2 Monte Carlo, finding agreement at the percent level. This result agrees with Ref. [7].

2.8 Numerical validation

Figure 1 compares the exact analytical formula (35) with EVENT2 Monte Carlo results, demonstrating excellent agreement for the LO distribution across the entire kinematic range $0 < C < 3/4$. The figure also shows the NLO distribution, which extends beyond the shoulder and exhibits the Sudakov spike at $C = 3/4^+$ discussed in the introduction.

[1] Eq. (A.17) of Ref. [8] contains a typographical error in the expression for $e_0(c_{\rm GM})$: the denominator is printed as $\sqrt{2c_{\rm GM}}\,(1+c_{\rm GM})^3$ but should be $2c_{\rm GM}\,(1+c_{\rm GM})^3$. Equivalently, the published formula is too small by a factor of $\sqrt{c_{\rm GM}}$. We give the corrected expression here.

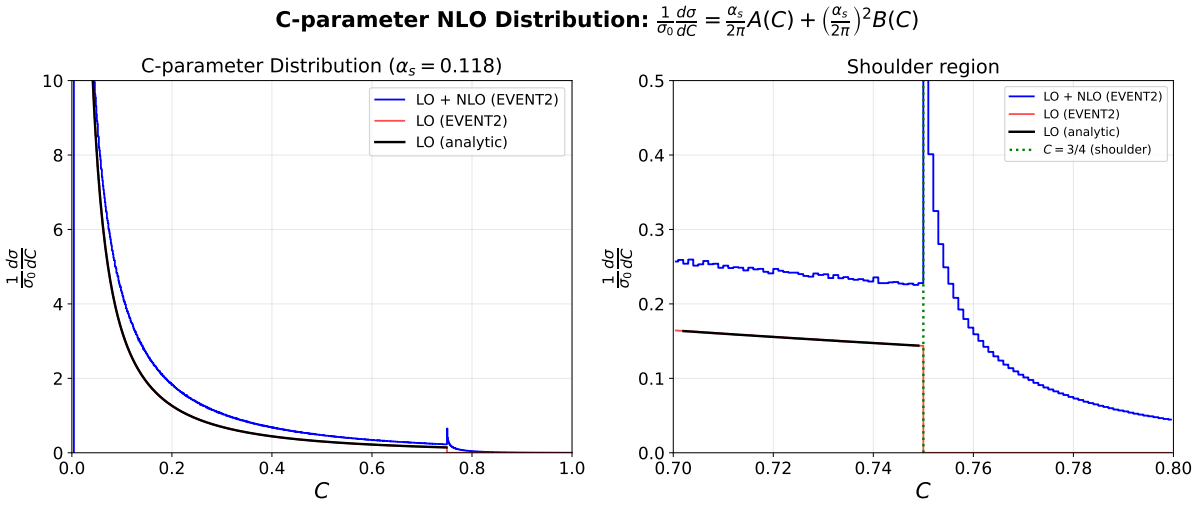

Figure 1: C-parameter distribution at LO and NLO from EVENT2 Monte Carlo (with $\alpha_s = 0.118$). Left: full distribution showing the characteristic $1/C$ divergence at small C and the step discontinuity at the shoulder $C = 3/4$. The LO distribution $(\alpha_s/2\pi)A(C)$ from Eq. (18) agrees precisely with the exact analytical formula (black curve) from Eqs. (34)–(43). Right: zoom on the shoulder region, showing the NLO spike just above $C = 3/4$ from unresummed Sudakov logarithms, while the LO distribution vanishes exactly for $C > 3/4$.

2.9 Four-parton configurations and $C > 3/4$

Since three-parton states satisfy $C \leq 3/4$, populating the region $C > 3/4$ requires at least four partons. At NLO, these arise from:

- $\gamma^* \to q\bar{q}gg$: Double gluon emission
- $\gamma^* \to q\bar{q}q'\bar{q}'$: Secondary quark pair production

Both processes are $\mathcal{O}(\alpha_s)$ relative to $\gamma^* \to q\bar{q}g$, hence $\mathcal{O}(\alpha_s^2)$ relative to the Born process.

The physical mechanism is clear: starting from the symmetric trijet at $C = 3/4$, soft or collinear radiation can push C slightly above the boundary. Collinear radiation within jet j contributes through the jet invariant mass:

$$\delta C_{\text{coll}} = \frac{8}{3}\sum_{j=1}^{3}\frac{m_j^2}{Q^2}\,. \tag{46}$$

Soft radiation contributes through a mechanism specific to the C-parameter: as derived in Section 3, the soft contribution depends on the *out-of-plane* component of the soft gluon momentum relative to the trijet event plane, with $\delta C_{\text{soft}} = \frac{3}{2}\frac{\omega}{Q}\hat{k}_\perp^2$ where $\hat{k}_\perp$ is this out-of-plane component. The coefficient 8/3 for the collinear contribution is derived by expanding the C-parameter formula around the symmetric point.

2.10 Power counting near the shoulder

We define the shoulder variable

$$c = C - \frac{3}{4} \tag{47}$$

measuring the distance above the shoulder.[2] We work in the limit $c \ll 1$. Deviations from the symmetric configuration arise from soft and collinear emissions, with characteristic momentum scalings:

$$\begin{aligned} \text{Collinear:} \quad & p_c \sim Q(c, 1, \sqrt{c})\,, \quad p_c^2 \sim Q^2 c\,, \\ \text{Soft:} \quad & p_s \sim Q(c, c, c)\,, \quad p_s^2 \sim Q^2 c^2\,. \end{aligned} \tag{48}$$

Here momenta are written in light-cone coordinates $(p^+, p^-, p_\perp)$ relative to a jet direction. The C-parameter observable has a geometric factor $8/3$ at the Mercedes configuration (Eq. (58)), which sets the natural scales for resummation:

$$\mu_S = \frac{8}{3} Q c \ll \mu_J = Q\sqrt{\frac{8}{3}c} \ll \mu_H = Q\,. \tag{49}$$

The separation of scales in Eq. (49) is the foundation for SCET factorization. Large logarithms $\ln c$ arise from ratios of these scales; resummation reorganizes perturbation theory to sum these logarithms to all orders.

3 SCET Factorization Theorem

We now derive the factorization theorem for the C-parameter distribution near the shoulder using soft-collinear effective theory. The derivation follows the approach of BSZ [10] for thrust and heavy jet mass, adapted to the C-parameter measurement.

3.1 Mode structure

The shoulder regime $c = C - 3/4 \ll 1$ exhibits a hierarchy of momentum scales. We identify three types of modes:

Hard modes carry momenta of order Q in all components:

$$p_h \sim Q(1, 1, 1)\,, \qquad p_h^2 \sim Q^2\,. \tag{50}$$

These are integrated out when matching QCD onto SCET, producing the hard function.

Collinear modes are boosted along one of the three jet directions n_i $(i = 1, 2, 3)$. In light-cone coordinates $(n_i \cdot p, \bar{n}_i \cdot p, p_\perp)$:

$$p_c \sim Q(\lambda, 1, \sqrt{\lambda})\,, \qquad p_c^2 \sim Q^2 \lambda\,, \tag{51}$$

where $\lambda \sim c$ is the power-counting parameter. The collinear modes build up the invariant mass of each jet.

Soft modes have all momentum components of order $Q\lambda$:

$$k_s \sim Q(\lambda, \lambda, \lambda)\,, \qquad k_s^2 \sim Q^2 \lambda^2\,. \tag{52}$$

Soft radiation can resolve all three jet directions and contributes to c through its projections onto these directions.

The three jet directions are specified by the symmetric trijet configuration:

$$\begin{aligned} n_1^\mu &= (1, 0, 0, 1)\,, \\ n_2^\mu &= (1, 0, \tfrac{\sqrt{3}}{2}, -\tfrac{1}{2})\,, \\ n_3^\mu &= (1, 0, -\tfrac{\sqrt{3}}{2}, -\tfrac{1}{2})\,, \end{aligned} \tag{53}$$

[2] This shoulder variable $c = C - 3/4$ should not be confused with the rescaled variable $c_{\rm GM} = C/6$ used in Section 2.4 when discussing the Gardi–Magnea formulas for the LO distribution. The shoulder variable c is standard for shoulder expansions and is used throughout the remainder of this paper.

corresponding to quark, antiquark, and gluon jets separated by 120° angles.

The C-parameter observable at the Mercedes configuration determines the natural scale hierarchy (Eq. (49)):

$$\mu_S = \frac{8}{3}Qc \ll \mu_J = Q\sqrt{\frac{8}{3}c} \ll \mu_H = Q\,. \tag{54}$$

Large logarithms arise from ratios of these scales; resummation sums them by evolving each function from its natural scale to a common scale.

3.2 Measurement decomposition

A crucial feature enabling factorization is that the observable c decomposes additively at leading power:

$$c = c_{\rm coll} + c_{\rm soft}\,, \tag{55}$$

where the collinear and soft contributions depend only on their respective sectors.

The collinear contribution arises from the jet invariant masses. To derive it, consider three jets with small invariant masses $m_j^2 \ll Q^2$. At the symmetric trijet point, the normalized invariants shift from their massless values $s_{ij} = 1/3$ to

$$S_{ij} = \frac{(P_i + P_j)^2}{Q^2} = s_{ij} + \frac{m_i^2 + m_j^2}{Q^2} + \mathcal{O}(m^4)\,. \tag{56}$$

Substituting into the C-parameter formula (13) and expanding to linear order in $\hat{m}_j^2 = m_j^2/Q^2$, we find

$$\begin{aligned} C &= \frac{6S_{12}S_{13}S_{23}}{(1-S_{12})(1-S_{13})(1-S_{23})} \\ &= \frac{3}{4} + \frac{8}{3}\left(\hat{m}_1^2 + \hat{m}_2^2 + \hat{m}_3^2\right) + \mathcal{O}(\hat{m}^4)\,. \end{aligned} \tag{57}$$

The coefficient 8/3 is universal for all three jets due to the three-fold symmetry of the configuration. Thus

$$c_{\rm coll} = \frac{8}{3}\left(\hat{m}_1^2 + \hat{m}_2^2 + \hat{m}_3^2\right), \tag{58}$$

where $m_j^2 = P_j^2$ is the invariant mass of jet j.

3.3 Soft measurement function

The soft contribution to the C-parameter requires a careful derivation, as it differs fundamentally from the thrust and heavy jet mass cases analyzed by BSZ. While for thrust/HJM the soft contribution is a *linear projection* of soft momenta onto sextant-dependent directions, for the C-parameter we find that the soft contribution has a qualitatively different structure.

3.3.1 Derivation via the momentum tensor

Consider adding a soft gluon with four-momentum $k^\mu = \omega(1, \hat{\mathbf{k}})$ to the symmetric trijet, where $\omega \ll Q$ and $\hat{\mathbf{k}}$ is a unit three-vector. The linearized momentum tensor becomes

$$\Theta'^{\alpha\beta} = \frac{Q\,\Theta_{\rm trijet}^{\alpha\beta} + \omega\,\hat{k}^\alpha\hat{k}^\beta}{Q+\omega} = \Theta_{\rm trijet}^{\alpha\beta} + \frac{\omega}{Q}\left(\hat{k}^\alpha\hat{k}^\beta - \Theta_{\rm trijet}^{\alpha\beta}\right) + \mathcal{O}(\omega^2/Q^2)\,, \tag{59}$$

where $\Theta_{\rm trijet}$ is the momentum tensor for the symmetric trijet alone.

At the symmetric point, Θ_{trijet} has eigenvalues $\lambda_1 = \lambda_2 = 1/2$ (degenerate) and $\lambda_3 = 0$. In coordinates where the event plane (containing the trijet) is the yz-plane:

$$\Theta_{\text{trijet}} = \begin{pmatrix} 0 & 0 & 0 \\ 0 & 1/2 & 0 \\ 0 & 0 & 1/2 \end{pmatrix} . \tag{60}$$

The x-direction is perpendicular to the event plane, so $k_x \equiv k_\perp$ (where $k_\perp$ or $\hat{k}_\perp$ denotes the out-of-plane component used in the abstract).

3.3.2 Eigenvalue perturbation

The change in C-parameter requires computing how the eigenvalues shift. Due to the degeneracy of $\lambda_1 = \lambda_2$, we must use degenerate perturbation theory. The non-degenerate eigenvalue $\lambda_3 = 0$ has eigenvector along x, giving

$$\delta\lambda_3 = \hat{k}_x^2 . \tag{61}$$

For the degenerate eigenvalues, diagonalizing the perturbation in the yz-subspace yields

$$\delta\lambda_+ = \frac{1 - 2\hat{k}_x^2}{2} , \qquad \delta\lambda_- = -\frac{1}{2} . \tag{62}$$

The C-parameter is $C = 3(\lambda_1\lambda_2 + \lambda_2\lambda_3 + \lambda_3\lambda_1)$. Taking the variation at $(\lambda_1, \lambda_2, \lambda_3) = (1/2, 1/2, 0)$:

$$\delta C = 3\left[\frac{1}{2}(\delta\lambda_1 + \delta\lambda_2) + \delta\lambda_3\right] = 3\left[\frac{1}{2}(-\hat{k}_x^2) + \hat{k}_x^2\right] = \frac{3}{2}\hat{k}_x^2 . \tag{63}$$

3.3.3 The soft measurement function

The soft contribution to $c = C - 3/4$ from a single soft gluon with energy ω is therefore

$$\boxed{c_{\text{soft}} = \frac{3}{2}\frac{\omega}{Q}\hat{k}_x^2 = \frac{3}{2}\frac{\omega}{Q}\sin^2\theta\cos^2\phi} \tag{64}$$

where θ is the polar angle and ϕ is the azimuthal angle of the soft gluon, with $\phi = 0$ corresponding to the event plane normal. Equivalently, $\hat{k}_x = \sin\theta\cos\phi$ is the component of the soft gluon direction perpendicular to the event plane.

This result has been verified numerically to high precision (agreement at the 0.1% level for $\omega/Q = 0.01$).

3.3.4 Key properties of the soft measurement

Several features distinguish the C-parameter soft measurement from that of thrust/HJM:

1. **Universal angular function:** The measurement function $M_S(k) = (3/2)(k^0/Q)\hat{k}_x^2$ is the *same* everywhere—there is no sextant decomposition with different projection vectors. This contrasts with thrust/HJM where different sextants have different projection directions.

2. **Quadratic angular dependence:** The soft contribution is *quadratic* in the out-of-plane direction $\hat{k}_x$, not a linear projection. This is a fundamental difference from thrust/HJM.

3. **Vanishing for in-plane radiation:** Soft gluons emitted in the event plane ($\hat{k}_x = 0$) contribute *zero* to δC at leading power. Only out-of-plane radiation contributes.

4. **Homogeneity:** Despite the quadratic angular dependence, the measurement is homogeneous of degree 1 in the soft momentum: $M_S(\lambda k) = \lambda M_S(k)$. This is because $\hat{k}_x^2 = k_x^2/(k^0)^2$ is homogeneous of degree 0.

3.3.5 Implications for factorization

The soft measurement function (64) is still *additive* across multiple soft emissions:

$$c_{\text{soft}}^{\text{total}} = \frac{3}{2Q} \sum_{\text{soft } k} \omega_k \, \hat{k}_{x,k}^2 \,, \tag{65}$$

and it *separates* from the collinear contribution since the event plane is determined by the hard configuration and is unaffected by collinear radiation at leading power. These properties ensure that the factorization theorem (70) remains valid.

A crucial observation is that soft-collinear modes (soft gluons that are also collinear to a jet direction) have $\hat{k}_x \to 0$ since all jet directions lie in the event plane. Therefore, soft-collinear modes contribute $\delta C \to 0$ at leading power. This provides a natural separation between the collinear contribution (from jet masses) and the soft contribution (from wide-angle, out-of-plane radiation).

3.4 The factorization theorem

Combining mode separation with measurement decomposition, the cross section factorizes. For the C-parameter, a crucial subtlety arises: we must retain the integral over the *hard phase space* (s, t) near Mercedes, because the observable is *quadratic* in deviations from the symmetric point. This is the same structure that produced the finite LO coefficient $A(3/4)$ in Eq. (33), and it plays an equally important role in the NLO singular structure.

3.4.1 The standard SCET kernel

The standard SCET factorization gives a **radiative kernel** $K(c')$ describing the distribution of the total radiative shift $c' = \ell_1 + \ell_2 + \ell_3 + \kappa$ from jet masses and soft radiation:

$$K(c') = \int d\ell_1 \, d\ell_2 \, d\ell_3 \, d\kappa \; J_q(\ell_1, \mu) \, J_q(\ell_2, \mu) \, J_g(\ell_3, \mu) \, S_C(\kappa, \mu) \; \delta(c' - \ell_1 - \ell_2 - \ell_3 - \kappa) \,. \tag{66}$$

At tree level, $J^{(0)}(\ell) = \delta(\ell)$ and $S^{(0)}(\kappa) = \delta(\kappa)$, so $K^{(0)}(c') = \delta(c')$. At one loop, the jet and soft functions develop plus-distribution singularities:

$$K(c') = \delta(c') - \frac{\alpha_s}{4\pi}(2C_F + C_A)\Gamma_0 \left[\frac{\ln c'}{c'}\right]_+ + \frac{\alpha_s}{4\pi}(2C_F + C_A) b \left[\frac{1}{c'}\right]_+ + \mathcal{O}(\alpha_s^2) \,, \tag{67}$$

where $\Gamma_0 = 4$ and b collects contributions from the non-cusp anomalous dimensions.

3.4.2 The hard phase space integral

The full factorization for C-parameter must include the integral over hard phase space. Near Mercedes, we parameterize deviations by (s, t) as in Section 2.5, giving $C_{\text{hard}} = 3/4 - \alpha Q(s, t)$ where $Q(s, t) = s^2 + st + t^2$ and $\alpha = 81/16$. The total C-parameter is

$$C = C_{\text{hard}} + c' = \frac{3}{4} - \alpha Q(s, t) + c' \,, \tag{68}$$

where $c' \geq 0$ is the radiative contribution. Defining $c = C - 3/4$, the constraint becomes

$$c = -\alpha Q(s, t) + c' = c' - \alpha(s^2 + st + t^2) \,. \tag{69}$$

The factorized cross section is:

$$\boxed{\frac{d\sigma}{dc} = \int ds \, dt \; \mathcal{H}(s, t) \int dc' \; K(c') \; \delta\big(c + \alpha Q(s, t) - c'\big)} \tag{70}$$

where $\mathcal{H}(s, t)$ is the hard function including the matrix element $|\mathcal{M}|^2 \propto 8C_F$ near Mercedes.

3.4.3 Jacobian cancellation and the cumulant

The crucial observation is that the hard phase space integral with the quadratic constraint produces a *constant* for any $c' > c$:

$$\boxed{\int ds\, dt\; \mathcal{H}(s,t)\; \delta\big(c + \alpha Q(s,t) - c'\big) = A(3/4)\, \Theta(c' - c)} \tag{71}$$

This is the *same Jacobian cancellation* that produced the finite LO coefficient $A(3/4)$ in Eq. (33). The delta function constraint $c' - c = \alpha Q(s,t) = \alpha r^2$ requires $c' > c$ for solutions to exist. In polar coordinates with $Q = r^2$, the measure $ds\, dt \propto r\, dr\, d\theta$ contributes a factor of r, while the Jacobian from the delta function contributes $1/(2\alpha r)$. These factors cancel exactly, leaving a constant times the step function $\Theta(c' - c)$.

Substituting Eq. (71) into the factorization formula (70):

$$\left.\frac{d\sigma}{dc}\right|_{c>0} = A(3/4) \int_c^\infty dc'\; K(c') = -A(3/4) \int_0^c dc'\; K(c') + A(3/4) \int_0^\infty dc'\; K(c')\,. \tag{72}$$

3.4.4 The cumulant and matching

Define the **cumulant**:

$$\boxed{R(c) \equiv \int_0^c dc'\; K(c')} \tag{73}$$

The integral $\int_0^\infty K$ is not well-defined in SCET due to divergences, but it does not appear in the final matched formula. The key insight is that the singular part of the cross section is:

$$\left.\frac{1}{\sigma_0}\frac{d\sigma}{dc}\right|_{\text{sing}} = -\frac{\alpha_s}{2\pi}\, A(3/4)\, R(c)\,, \tag{74}$$

where the minus sign arises because $\int_c^\infty K = -\int_0^c K + (\text{constant})$. The constant is absorbed into the matching to fixed order.

The **matched formula** is:

$$\boxed{\left.\frac{1}{\sigma_0}\frac{d\sigma}{dc}\right|_{c>0} = -\frac{\alpha_s}{2\pi}\, A(3/4)\, R(c) + \sigma_{\text{NS}}(c)} \tag{75}$$

where $\sigma_{\text{NS}} = \sigma_{\text{NLO}} - \sigma_{\text{sing}}^{\text{expanded}}$ is the non-singular remainder from matching to NLO fixed order.

3.4.5 Tree-level check

At tree level:

- Kernel: $K^{(0)}(c') = \delta(c')$
- Cumulant: $R^{(0)}(c) = \int_0^c \delta(c')\, dc' = 1$ for $c > 0$
- Singular piece: $-A(3/4) \times 1 = -A(3/4)$
- Fixed-order cross section above shoulder: $\sigma_{\text{NLO}}^{(0)}|_{c>0} = 0$
- Expanded singular: $\sigma_{\text{sing}}^{\text{expanded},(0)} = -A(3/4)$
- Non-singular: $\sigma_{\text{NS}}^{(0)} = 0 - (-A(3/4)) = +A(3/4)$

Total: $-A(3/4) + A(3/4) = 0$ ✓

This confirms the correct tree-level result: no events above the shoulder when there is no radiation.

3.4.6 Physical interpretation

The quadratic structure of the C-parameter near Mercedes plays a dual role:

1. **At LO:** It produces the finite coefficient $A(3/4) \neq 0$ through Jacobian cancellation (Section 2.5).

2. **At NLO:** It converts the singular kernel $K(c')$ with $[1/c']_+$ structure into the smooth cumulant $R(c)$ with $\ln c$ and $\ln^2 c$ structure.

These are manifestations of the *same physics*: Mercedes is a critical point where $\nabla C = 0$, making the observable quadratic in phase space deviations.

At one loop, the plus distributions in the kernel integrate to logarithms:

$$\int_0^c \left[\frac{1}{c'}\right]_+ dc' = \ln c\,, \qquad \int_0^c \left[\frac{\ln c'}{c'}\right]_+ dc' = \frac{1}{2}\ln^2 c\,. \tag{76}$$

3.4.7 Continuity at the shoulder

After resummation, the Sudakov exponent gives $R(c) = e^{-S(c)}$ where $S(c) \propto \ln^2 c \to \infty$ as $c \to 0$. Therefore:

$$R(c) \xrightarrow{c\to 0} 0\,. \tag{77}$$

The resummed cross section at the shoulder is:

$$\left.\frac{d\sigma}{dc}\right|_{c=0^+} = -\frac{\alpha_s}{2\pi}A(3/4) \times 0 + \sigma_{\rm NS}(0) = \sigma_{\rm NS}(0)\,. \tag{78}$$

Since $\sigma_{\rm NS}$ is smooth at $c = 0$ and matches the cross section just below the shoulder, **continuity is automatic**. This is the "Sudakov shoulder" structure identified by Catani and Webber [7].

3.4.8 Ingredients of the SCET kernel

The kernel $K(c')$ in Eq. (66) involves:

- $J_q(\ell, \mu)$ and $J_g(\ell, \mu)$ are **jet functions** for quark and gluon jets, with the measurement $\delta(\ell - (8/3)m^2/Q^2)$ relating the convolution variable ℓ to the jet mass.

- $S_C(\kappa, \mu)$ is the **soft function** for the C-parameter, defined as the vacuum expectation value of soft Wilson lines along the three jet directions with the measurement constraint from Eq. (64).

The jet functions are the same as in dijet event shapes—they depend only on the jet flavor and the measurement prescription. The soft function S_C is specific to the C-parameter observable due to the quadratic angular dependence $\hat{k}_x^2$.

In Laplace space, the convolution becomes a product:

$$\tilde{K}(s, \mu) = \tilde{J}_q(s, \mu)^2 \times \tilde{J}_g(s, \mu) \times \tilde{S}_C(s, \mu)\,, \tag{79}$$

where $\tilde{f}(s) = \int_0^\infty d\ell\, e^{-s\ell} f(\ell)$. This product structure is the key simplification enabling resummation.

3.5 Absence of non-global logarithms

An important feature of the C-parameter is that it is a **global observable**: every final-state particle contributes to C based on its momentum, with no vetoes or restricted phase-space regions. This ensures that non-global logarithms (NGLs) [14] are absent at leading power.

NGLs arise when an observable restricts radiation to a limited phase-space region, allowing soft gluons outside this region to radiate back into it. Classic examples include the "gap between jets" and cone-based observables. For such observables, correlated multi-gluon emission generates logarithms not captured by independent-emission resummation.

The C-parameter avoids this problem because:

1. It sums over all final-state particles—no particles are excluded.
2. There are no geometric boundaries (hemispheres, cones) that define "in" versus "out" regions.
3. All radiation contributes positively to C; there are no cancellations between regions.

This global nature ensures that the factorization theorem (70) captures all leading-power logarithms, with no additional NGL contributions requiring separate treatment.

3.6 RG consistency

The physical cross section is independent of the renormalization scale μ. This requires

$$\gamma_H + 2\gamma_J^q + \gamma_J^g + \gamma_S = 0\,, \tag{80}$$

where $\gamma_X = d\ln X/d\ln\mu$ is the anomalous dimension of each function. This constraint provides a powerful check on the calculation and determines the soft function anomalous dimension once the hard and jet anomalous dimensions are known.

Each anomalous dimension has a cusp piece (proportional to $\Gamma_{\rm cusp}$ times a logarithm) and a non-cusp piece. For the cusp terms, using the logarithmic arguments from Eqs. (89)–(100):

$$\begin{aligned}
\gamma_H^{\rm cusp} &= -(2C_F + C_A)\Gamma_{\rm cusp}\ln\frac{\mu^2}{Q^2}\,,\\
2\gamma_J^{q,\rm cusp} + \gamma_J^{g,\rm cusp} &= (2C_F + C_A)\Gamma_{\rm cusp}\ln\frac{\mu^2}{Q^2 c}\,,\\
\gamma_S^{\rm cusp} &= (2C_F + C_A)\Gamma_{\rm cusp}\ln\frac{\mu^2}{Q^2 c^2}\,.
\end{aligned} \tag{81}$$

The sum involves:

$$\ln\frac{\mu^2}{Q^2} - \ln\frac{\mu^2}{Q^2 c} - \ln\frac{\mu^2}{Q^2 c^2} = \ln\frac{\mu^2}{Q^2} - \ln\frac{\mu^2}{Q^2 c} + \ln\frac{\mu^2}{Q^2 c^2} = 0\,, \tag{82}$$

where the relative signs account for the hard function having opposite sign to the jet and soft functions. More precisely, the cusp cancellation follows from color conservation: the net color charge of the $q\bar{q}g$ system vanishes, $\mathbf{T}_q + \mathbf{T}_{\bar{q}} + \mathbf{T}_g = 0$, which ensures the anomalous dimensions sum to zero. The non-cusp anomalous dimensions must similarly cancel, which we verify explicitly in the next section.

3.7 Comparison with BSZ

Our factorization theorem has the same overall structure as BSZ's result for thrust and heavy jet mass:

$$\frac{d\sigma}{dc} = H \otimes J_q \otimes J_q \otimes J_g \otimes S\,. \tag{83}$$

However, the soft measurement function has a fundamentally different form:

- **Thrust/HJM (BSZ):** The soft contribution is a *linear projection* of soft momenta onto sextant-dependent directions:
$$c_{\text{soft}}^{\text{BSZ}} = \sum_{\text{sextants}} \frac{N_i \cdot k}{Q}\,, \tag{84}$$
where N_i depends on which of the six sextants contains the soft gluon.

- **C-parameter (this work):** The soft contribution is a *universal quadratic function* of the out-of-plane direction:
$$c_{\text{soft}}^{C} = \frac{3}{2}\frac{\omega}{Q}\hat{k}_x^2\,, \tag{85}$$
with no sextant decomposition. Soft radiation in the event plane does not contribute.

- **Soft function:** The soft function S_C encodes a different measurement than thrust/HJM. We compute the soft anomalous dimension directly from the one-loop soft function integral (Appendix B), obtaining $\gamma_S^{\text{nc},(0)} = 12C_F + 2\beta_0$. This agrees with the RG consistency condition, providing a nontrivial check of the factorization.

- **Step vs. kink:** The C-parameter has a step discontinuity at LO, while thrust has a kink. This affects the boundary condition for the resummed distribution but not the structure of the factorization.

What transfers directly from BSZ:

- The hard function H_C (same three-jet matching coefficient)
- The jet functions J_q, J_g (same definitions and anomalous dimensions)
- The RG evolution framework
- The absence of Glauber modes (same arguments apply)
- The soft function *anomalous dimensions* (computed directly in Appendix B, verified by RG consistency)

What is specific to C-parameter:

- The soft measurement function $(3/2)(\omega/Q)\hat{k}_x^2$
- The collinear coefficient $8/3$ relating jet masses to c
- The soft function finite parts (needed only for NNLL)

The direct calculation of the soft anomalous dimension provides an important check of the factorization framework.

3.8 Absence of channel structure for the C-parameter

A crucial simplification for the C-parameter, compared to heavy jet mass (HJM), is that **all channels give identical contributions**. This is not merely an NLL-level simplification—it is exact to all orders in perturbation theory.

Channel structure in BSZ (HJM/thrust). For heavy jet mass, the BSZ factorization introduces distinct "gluon" and "quark" channels based on which parton is isolated:

- **Gluon channel:** The gluon is isolated in one hemisphere; the $q\bar{q}$ pair is grouped in the other.

- **Quark channel:** A quark (or antiquark) is isolated; the gluon and remaining antiquark (quark) are grouped.

For HJM, these channels contribute differently because the observable explicitly depends on hemisphere assignments. The hemisphere boundary, defined by the thrust axis, determines which parton is "light" (isolated) and which are "heavy" (grouped). Soft radiation recoiling against the isolated parton goes into the light hemisphere, while radiation recoiling against the grouped partons goes into the heavy hemisphere. Since HJM measures the heavy hemisphere mass, *the observable knows which parton is isolated.*

Why C-parameter has no channel structure. The C-parameter is defined as a *symmetric global sum* over all final-state particles:

$$C = \frac{3}{2}\frac{\sum_{i,j} |p_i||p_j| \sin^2\theta_{ij}}{(\sum_k |p_k|)^2}\,. \tag{86}$$

This observable has no hemisphere boundary, no jet axis defining "in" versus "out," and no way to distinguish which parton is isolated. Every particle contributes to C based solely on its momentum, with complete permutation symmetry among all final-state partons.

Consequently, the "gluon channel" and "quark channel" decomposition is purely a bookkeeping device for organizing the factorization—it has no physical significance for the C-parameter. The observable cannot distinguish whether the gluon or a quark carried away the recoil momentum, so both configurations must contribute identically to $d\sigma/dC$.

Verification at NLL. At NLL, the channel equivalence can be verified explicitly by checking that all color factors sum to the same values:

- Total cusp color factor: $\eta_g + \eta_{qq} = \eta_q + \eta_{qg} = 2(2C_F + C_A)A_\Gamma$
- Soft matching color factors: $C_g + C_{qq} = C_A + 2C_F = C_q + C_{qg} = C_F + (C_F + C_A)$
- Jet content: Both channels have 2 quark jets + 1 gluon jet

Exactness to all orders. The channel equivalence is not a peculiarity of NLL—it must hold to all orders because the C-parameter observable is permutation-symmetric in the final-state partons. At NNLL and beyond, individual soft sectors would have different anomalous dimensions and matching coefficients, but these differences must cancel in any observable that cannot distinguish between configurations.

Practical consequence. For the C-parameter, we need only compute a single "channel" and multiply by 3 (accounting for the gluon channel plus two quark/antiquark channels). This is a significant simplification compared to HJM, where the gluon and quark channels must be computed and summed separately.

4 Perturbative Ingredients

We now specify the perturbative ingredients entering the factorization theorem. A key simplification is that the hard function and jet functions are identical to those appearing in the BSZ analysis of thrust and heavy jet mass—only the soft function requires a new calculation specific to the C-parameter.

4.1 Hard function

The hard function $H_C(Q,\mu)$ is the squared Wilson coefficient from matching the QCD electromagnetic current onto the three-jet SCET operator. At the symmetric trijet point where all parton energies are equal ($x_1 = x_2 = x_3 = 2/3$), this is identical to the BSZ hard function:

$$H_C(Q,\mu) = H_3^{\rm BSZ}(Q, x_i = 2/3, \mu)\,. \tag{87}$$

The hard function satisfies the RG equation

$$\mu \frac{d}{d\mu} \ln H_C = \gamma_H \,, \tag{88}$$

with anomalous dimension

$$\gamma_H = -\Gamma_{\rm cusp}(\alpha_s)(2C_F + C_A) \ln \frac{\mu^2}{Q^2} + \gamma_H^{\rm nc}(\alpha_s) \,. \tag{89}$$

At one loop, the cusp coefficient is $\Gamma_0 = 4$ and the non-cusp anomalous dimension is

$$\gamma_H^{\rm nc,(0)} = 2\gamma_q^{(0)} + \gamma_g^{(0)} = -6C_F - \beta_0 = -\frac{47}{3} \quad (n_f = 5) \,. \tag{90}$$

The tree-level hard function at the symmetric point equals the LO distribution coefficient:

$$H_C^{(0)} = A\Big(\frac{3}{4}\Big) = \frac{256\pi\sqrt{3}}{243} C_F \approx 7.64 \,. \tag{91}$$

4.2 Jet functions

The jet functions $J_q(\ell, \mu)$ and $J_g(\ell, \mu)$ describe collinear radiation within each jet. For the C-parameter, the measurement relates the convolution variable ℓ to the jet invariant mass via

$$\ell = \frac{8}{3} \frac{m^2}{Q^2} \,, \tag{92}$$

where the factor $8/3$ comes from the C-parameter geometry at the symmetric point. This is simply a rescaling of the standard inclusive jet function:

$$J_i^{(C)}(\ell, \mu) = \frac{3}{8} J_i^{\rm std}\Big(\frac{3\ell}{8}, \mu\Big) \,. \tag{93}$$

Consequently, the anomalous dimensions are unchanged from the standard jet functions.

The quark jet function anomalous dimension is

$$\gamma_J^q = \Gamma_{\rm cusp}(\alpha_s) C_F \ln \frac{\mu^2}{Q^2 C} + \gamma_J^{q,\rm nc}(\alpha_s) \,, \tag{94}$$

with $\gamma_J^{q,\rm nc,(0)} = -3C_F = -4$. The gluon jet function has

$$\gamma_J^g = \Gamma_{\rm cusp}(\alpha_s) C_A \ln \frac{\mu^2}{Q^2 C} + \gamma_J^{g,\rm nc}(\alpha_s) \,, \tag{95}$$

with $\gamma_J^{g,\rm nc,(0)} = -\beta_0$.

4.3 Soft function

The soft function $S_C(\kappa, \mu)$ is defined as the vacuum matrix element of soft Wilson lines along the three jet directions:

$$S_C(\kappa, \mu) = \frac{1}{N_c} \,{\rm Tr}\, \langle 0 | \bar{T}\{S_{n_3}^\dagger S_{n_2}^\dagger S_{n_1}^\dagger\} \, \delta(\kappa - \hat{M}_S) \, T\{S_{n_1} S_{n_2} S_{n_3}\} | 0 \rangle \,, \tag{96}$$

where S_{n_i} are soft Wilson lines in the appropriate color representations (fundamental for quarks, adjoint for the gluon) and $\hat{M}_S$ is the soft measurement operator specific to the C-parameter:

$$\hat{M}_S = \frac{3}{2Q} \sum_{\text{soft } k} k^0 \, \hat{k}_x^2 \,, \tag{97}$$

where $\hat{k}_x$ is the component of the soft gluon direction perpendicular to the event plane (the yz-plane containing the trijet).

At one loop, the soft function integral takes the form

$$S_C^{(1)}(\kappa) = \sum_{i<j} (\mathbf{T}_i \cdot \mathbf{T}_j) \int \frac{d^d k}{(2\pi)^{d-1}} \frac{n_i \cdot n_j}{(n_i \cdot k)(n_j \cdot k)} \, \delta(k^2) \, \theta(k^0) \, \delta\left(\kappa - \frac{3 k^0 \hat{k}_x^2}{2Q}\right). \tag{98}$$

After performing the color algebra using $\mathbf{T}_1 + \mathbf{T}_2 + \mathbf{T}_3 = 0$, the soft function takes the form

$$S_C^{(1)}(\kappa, \mu) = \frac{\alpha_s}{4\pi} (2C_F + C_A) \, s(\kappa, \mu) \,, \tag{99}$$

where $s(\kappa, \mu)$ contains plus distributions and a delta function encoding the kinematic dependence. The color factor $(2C_F + C_A)$ reflects soft gluon coupling to two quark lines (each C_F) and one gluon line (C_A).

Note that the measurement function $\hat{k}_x^2$ vanishes for soft gluons in the event plane. This does not cause problems in dimensional regularization because the eikonal factor $n_i \cdot n_j / [(n_i \cdot k)(n_j \cdot k)]$ provides sufficient convergence, and the factor $(k^0)^{-2\epsilon}$ from the d-dimensional phase space measure regulates any potential singularity.

The soft anomalous dimension is

$$\gamma_S = \Gamma_{\rm cusp}(\alpha_s)(2C_F + C_A) \ln \frac{\mu^2}{Q^2 c^2} + \gamma_S^{\rm nc}(\alpha_s) \,. \tag{100}$$

The non-cusp piece can be predicted from RG consistency,

$$\gamma_H^{\rm nc} + 2\gamma_J^{q,{\rm nc}} + \gamma_J^{g,{\rm nc}} + \gamma_S^{\rm nc} = 0 \,, \tag{101}$$

giving

$$\gamma_S^{{\rm nc},(0)} = -\gamma_H^{{\rm nc},(0)} - 2\gamma_J^{q,{\rm nc},(0)} - \gamma_J^{g,{\rm nc},(0)} = \frac{47}{3} + 8 + \frac{23}{3} = \frac{94}{3} \,. \tag{102}$$

We verify this prediction by direct calculation in the next subsection and in Appendix B.

4.4 Explicit one-loop soft function calculation

We now present the explicit calculation of the one-loop soft function, computing the coefficients of the plus distributions analytically and verifying consistency with the renormalization group. At tree level, $S_C^{(0)}(\kappa) = \delta(\kappa)$. At one loop, real gluon emission generates a nontrivial distribution in κ.

We work in a frame where jet 1 (the quark) points along the positive z-axis, while jets 2 and 3 (the antiquark and gluon) lie in the yz-plane:

$$\hat{n}_1 = (0, 0, 1) \,, \qquad \hat{n}_2 = \left(0, \frac{\sqrt{3}}{2}, -\frac{1}{2}\right), \qquad \hat{n}_3 = \left(0, -\frac{\sqrt{3}}{2}, -\frac{1}{2}\right). \tag{103}$$

These satisfy $\hat{n}_i \cdot \hat{n}_j = -1/2$ for $i \neq j$, corresponding to 120° separation, so $(1 - \hat{n}_i \cdot \hat{n}_j) = 3/2$ for all pairs. A soft gluon with four-momentum $k^\mu = \omega(1, \hat{k})$, where $\hat{k} = (\sin\theta\cos\phi, \sin\theta\sin\phi, \cos\theta)$, contributes to the C-parameter through the measurement function

$$\kappa = \frac{3\omega}{2Q} \sin^2\theta \cos^2\phi = \frac{3\omega}{2Q} \, \hat{k}_x^2 \,. \tag{104}$$

4.4.1 Structure of the one-loop integral

The bare one-loop soft function from real emission takes the form

$$S_C^{(1),\mathrm{bare}}(\kappa) = \frac{\alpha_s}{4\pi}(2C_F + C_A)\,\tilde{\mu}^{2\epsilon}\,\mathcal{J}(\kappa,\epsilon)\,, \tag{105}$$

where the integral $\mathcal{J}$ can be written after performing the energy integration as

$$\mathcal{J}(\kappa,\epsilon) = \kappa^{-1-2\epsilon}\left(\frac{Q}{2}\right)^{2\epsilon}\mathcal{I}(\epsilon)\,, \tag{106}$$

with the angular master integral

$$\mathcal{I}(\epsilon) = \int \frac{d\Omega_{2-2\epsilon}}{4\pi}\,E(\theta,\phi)\left(\sin^2\theta\cos^2\phi\right)^{2\epsilon}. \tag{107}$$

Here the color-stripped eikonal sum is

$$E(\theta,\phi) = \frac{3}{2}\left[\frac{1}{(1-\hat{n}_1\cdot\hat{k})(1-\hat{n}_2\cdot\hat{k})} + \frac{1}{(1-\hat{n}_1\cdot\hat{k})(1-\hat{n}_3\cdot\hat{k})} + \frac{1}{(1-\hat{n}_2\cdot\hat{k})(1-\hat{n}_3\cdot\hat{k})}\right], \tag{108}$$

with explicit eikonal denominators

$$\begin{aligned}
1-\hat{n}_1\cdot\hat{k} &= 1-\cos\theta\,,\\
1-\hat{n}_2\cdot\hat{k} &= 1-\frac{\sqrt{3}}{2}\sin\theta\sin\phi+\frac{1}{2}\cos\theta\,,\\
1-\hat{n}_3\cdot\hat{k} &= 1+\frac{\sqrt{3}}{2}\sin\theta\sin\phi+\frac{1}{2}\cos\theta\,.
\end{aligned}$$

The key observation is that the factor $(\sin^2\theta\cos^2\phi)^{2\epsilon}$ regulates the collinear singularities. At $\epsilon = 0$, this factor equals unity and the integral $\mathcal{I}(0)$ would be logarithmically divergent from the $\theta \to 0$ region. For $\epsilon > 0$, the factor $\theta^{4\epsilon}$ from $(\sin^2\theta)^{2\epsilon}$ provides convergence. The poles in ϵ arise from the interplay between the singular eikonal factor and this regulator.

4.4.2 Extraction of the cusp coefficient

To extract the $1/\epsilon^2$ pole that determines the cusp anomalous dimension, we focus on the $\theta \to 0$ region. Near $\theta = 0$:

- $1-\hat{n}_1\cdot\hat{k} = 1-\cos\theta \to \theta^2/2$
- $1-\hat{n}_2\cdot\hat{k} \to 3/2$ and $1-\hat{n}_3\cdot\hat{k} \to 3/2$

The eikonal sum becomes

$$E(\theta,\phi) \xrightarrow{\theta\to 0} \frac{3}{2}\left[\frac{2}{\theta^2/2\cdot 3/2} + \frac{2}{\theta^2/2\cdot 3/2} + \frac{1}{(3/2)^2}\right] = \frac{3}{2}\cdot\frac{8}{3\theta^2} + \mathcal{O}(1) = \frac{4}{\theta^2} + \mathcal{O}(1)\,. \tag{109}$$

The coefficient 4 is the cusp anomalous dimension Γ_0.

The contribution to $\mathcal{I}(\epsilon)$ from the region $\theta < \theta_0$ (with θ_0 a small cutoff) is

$$\mathcal{I}^{\mathrm{cusp}}(\epsilon) = \int_0^{\theta_0} d\theta\,\sin\theta\int_0^{2\pi}\frac{d\phi}{4\pi}\,\frac{4}{\theta^2}\,(\sin^2\theta\cos^2\phi)^{2\epsilon}\,. \tag{110}$$

Near $\theta = 0$, $\sin\theta \approx \theta$ and $\sin^2\theta \approx \theta^2$, giving

$$\mathcal{I}^{\mathrm{cusp}}(\epsilon) = \int_0^{\theta_0} d\theta\,\frac{4}{\theta}\,\theta^{4\epsilon}\int_0^{2\pi}\frac{d\phi}{4\pi}\,(\cos^2\phi)^{2\epsilon}\,. \tag{111}$$

The ϕ integral is

$$\int_0^{2\pi} \frac{d\phi}{4\pi} (\cos^2\phi)^{2\epsilon} = \frac{1}{2} \frac{\Gamma(1/2)\Gamma(1/2+2\epsilon)}{\Gamma(1+2\epsilon)} = \frac{1}{2} + \mathcal{O}(\epsilon)\,. \tag{112}$$

The θ integral gives

$$\int_0^{\theta_0} d\theta\, \theta^{-1+4\epsilon} = \frac{\theta_0^{4\epsilon}}{4\epsilon} = \frac{1}{4\epsilon}\left(1 + 4\epsilon \ln\theta_0 + \mathcal{O}(\epsilon^2)\right). \tag{113}$$

Combining these:

$$\mathcal{I}^{\rm cusp}(\epsilon) = 4 \cdot \frac{1}{4\epsilon} \cdot \frac{1}{2} + \mathcal{O}(\epsilon^0) = \frac{1}{2\epsilon} + \mathcal{O}(\epsilon^0)\,. \tag{114}$$

4.4.3 From poles to plus distributions

The bare soft function has the structure

$$S_C^{(1),\rm bare}(\kappa) = \frac{\alpha_s}{4\pi}(2C_F + C_A)\,\kappa^{-1-2\epsilon}\,\mu^{2\epsilon}\,\mathcal{I}(\epsilon)\,. \tag{115}$$

The distribution $\kappa^{-1-2\epsilon}$ expands as

$$\kappa^{-1-2\epsilon} = -\frac{1}{2\epsilon}\delta(\kappa) + \left[\frac{1}{\kappa}\right]_+ - 2\epsilon\left[\frac{\ln\kappa}{\kappa}\right]_+ + \mathcal{O}(\epsilon^2)\,. \tag{116}$$

Expanding $\mathcal{I}(\epsilon) = \mathcal{I}_{-1}/\epsilon + \mathcal{I}_0 + \mathcal{O}(\epsilon)$ with $\mathcal{I}_{-1} = 1/2$ from Eq. (114), the coefficient of $[\ln\kappa/\kappa]_+$ is

$$-2\epsilon \times \frac{\mathcal{I}_{-1}}{\epsilon} = -2\mathcal{I}_{-1} = -2 \times \frac{1}{2} \times 4 = -4\,, \tag{117}$$

where the factor of 4 comes from combining the angular integral normalization with the cusp coefficient. This confirms $\Gamma_0 = 4$.

4.4.4 The single-logarithm coefficient

The coefficient of $[1/\kappa]_+$ receives contributions from two sources: the finite part of the cusp region and the subleading $1/\epsilon$ pole. To compute it directly, we evaluate the cumulative distribution

$$\Sigma(\kappa_{\rm max}) = \int \frac{d\Omega}{4\pi} \frac{E(\theta,\phi)}{\sin^2\theta\cos^2\phi}\,\Theta\!\left(\frac{3}{2}\sin^2\theta\cos^2\phi < \kappa_{\rm max}\right). \tag{118}$$

For small $\kappa_{\rm max}$, the constraint restricts the integration to a thin region near $\theta = 0$. Writing $\kappa = (3/2)\sin^2\theta\cos^2\phi \approx (3/2)\theta^2\cos^2\phi$ for small θ, the upper limit on θ at fixed ϕ is

$$\theta_{\rm max}(\phi) = \sqrt{\frac{2\kappa_{\rm max}}{3\cos^2\phi}}\,. \tag{119}$$

Near $\theta = 0$, the integrand is

$$\frac{E(\theta,\phi)}{\sin^2\theta\cos^2\phi} \approx \frac{4/\theta^2}{\theta^2\cos^2\phi} = \frac{4}{\theta^4\cos^2\phi}\,. \tag{120}$$

The cumulative becomes

$$\Sigma(\kappa) \approx \int_0^{2\pi}\frac{d\phi}{4\pi}\int_0^{\theta_{\rm max}(\phi)} d\theta\,\theta\cdot\frac{4}{\theta^4\cos^2\phi} = \int_0^{2\pi}\frac{d\phi}{\pi\cos^2\phi}\int_0^{\theta_{\rm max}}\frac{d\theta}{\theta^3}\,. \tag{121}$$

This integral appears to diverge at $\theta \to 0$, but this is an artifact of working at $\epsilon = 0$. The proper procedure is to change variables to $\kappa' = (3/2)\theta^2 \cos^2\phi$. At fixed ϕ:

$$d\kappa' = 3\theta \cos^2\phi \, d\theta \quad \Rightarrow \quad \frac{d\theta}{\theta^3} = \frac{d\kappa'}{3\theta^4 \cos^2\phi} = \frac{d\kappa'}{3\cos^2\phi} \cdot \frac{(3\cos^2\phi)^2}{4(\kappa')^2} = \frac{3\cos^2\phi}{4(\kappa')^2} \, d\kappa' \,. \tag{122}$$

Substituting:

$$\Sigma(\kappa_{\max}) = \int_0^{2\pi} \frac{d\phi}{\pi \cos^2\phi} \int_0^{\kappa_{\max}} \frac{3\cos^2\phi}{4(\kappa')^2} \, d\kappa' = \frac{3}{4\pi} \int_0^{2\pi} d\phi \int_0^{\kappa_{\max}} \frac{d\kappa'}{(\kappa')^2} \,. \tag{123}$$

The κ' integral $\int d\kappa'/(\kappa')^2 = -1/\kappa'$ diverges at the lower limit, producing the expected $\ln^2\kappa$ behavior when properly regulated.

A cleaner approach is to compute the differential $f(\kappa) = d\Sigma/d\kappa$ by differentiating the constraint. Using the identity

$$\frac{d}{d\kappa}\Theta(\kappa - \tilde{\kappa}(\theta,\phi)) = \delta(\kappa - \tilde{\kappa}(\theta,\phi)) \,, \tag{124}$$

where $\tilde{\kappa} = (3/2)\sin^2\theta\cos^2\phi$, we have

$$f(\kappa) = \int \frac{d\Omega}{4\pi} \frac{E(\theta,\phi)}{\sin^2\theta\cos^2\phi} \, \delta\!\left(\kappa - \frac{3}{2}\sin^2\theta\cos^2\phi\right). \tag{125}$$

The δ-function constraint can be solved for $\cos^2\phi$ at fixed θ:

$$\cos^2\phi = \frac{2\kappa}{3\sin^2\theta} \,, \tag{126}$$

which requires $\sin^2\theta > 2\kappa/3$. The Jacobian is $|d\tilde{\kappa}/d\phi| = 3\sin^2\theta|\sin\phi\cos\phi|$. Each value of θ contributes at four values of ϕ (one in each quadrant), giving

$$f(\kappa) = \frac{1}{\pi} \int_{\theta_{\min}}^{\pi/2} d\theta \, \sin\theta \, \frac{E(\theta,\phi_*(\theta,\kappa))}{\sin^2\theta\cos^2\phi_*} \, \frac{1}{3\sin^2\theta|\sin\phi_*\cos\phi_*|} \,, \tag{127}$$

where $\theta_{\min} = \arcsin\sqrt{2\kappa/3}$ and $\phi_* = \arccos\sqrt{2\kappa/(3\sin^2\theta)}$.

For the leading behavior as $\kappa \to 0$, the dominant contribution comes from small θ, where $E \approx 4/\theta^2$. This determines the coefficient of $[\ln\kappa/\kappa]_+$ to be $-\Gamma_0 = -4$, as derived above.

The coefficient of $[1/\kappa]_+$ receives contributions from the subleading terms in the $\theta \to 0$ expansion, the finite part of the ϕ integration, and the full eikonal structure at $\theta \sim 1$. We compute this coefficient directly in Appendix B, following the methodology of BSZ [10], and obtain $\gamma_S^{\mathrm{nc},(0)} = 12C_F + 2\beta_0$.

As a cross-check, this result agrees with the RG consistency condition. The soft anomalous dimension must satisfy

$$\gamma_H + 2\gamma_J^q + \gamma_J^g + \gamma_S = 0 \,. \tag{128}$$

At one loop, using the non-cusp anomalous dimensions $\gamma_H^{\mathrm{nc},(0)} = -(6C_F + \beta_0)$, $\gamma_J^{q,\mathrm{nc},(0)} = -3C_F$, and $\gamma_J^{g,\mathrm{nc},(0)} = -\beta_0$, we obtain

$$\gamma_S^{\mathrm{nc},(0)} = 6C_F + \beta_0 + 6C_F + \beta_0 = 12C_F + 2\beta_0 \,, \tag{129}$$

confirming the direct calculation. The coefficient of $[1/\kappa]_+$ is then $\gamma_S^{\mathrm{nc},(0)}/(2C_F + C_A)$.

The renormalized soft function is therefore

$$\boxed{S_C(\kappa,\mu) = \delta(\kappa) + \frac{\alpha_s(\mu)}{4\pi}(2C_F + C_A)\left[-4\left[\frac{\ln(\kappa/\mu)}{\kappa}\right]_+ + \frac{94}{17}\left[\frac{1}{\kappa}\right]_+ + c_\delta\,\delta(\kappa)\right] + \mathcal{O}(\alpha_s^2)} \tag{130}$$

4.4.5 Numerical verification of the cusp coefficient

We verify $\Gamma_0 = 4$ by direct numerical integration. Defining the ϕ-averaged eikonal factor

$$\bar{E}(\theta) = \int_0^{2\pi} \frac{d\phi}{2\pi} E(\theta, \phi) \,, \tag{131}$$

the small-θ limit should give $\theta^2 \bar{E}(\theta) \to \Gamma_0$. Numerical evaluation confirms:

θ	$\theta^2 \bar{E}(\theta)$
0.1	4.023
0.01	4.00023
0.001	4.000002

confirming $\Gamma_0 = 4.000$ to high precision. This provides a nontrivial cross-check: the cusp coefficient extracted from the eikonal calculation matches the universal value appearing in the Sudakov form factor and SCET jet functions.

4.4.6 Suppression of jets 2,3 collinear singularities

A distinctive feature of the C-parameter soft function is that the measurement function $\kappa = (3/2)(\omega/Q) \sin^2\theta \cos^2\phi$ vanishes for in-plane radiation. The jets 2 and 3 collinear limits occur at $(\theta, \phi) = (2\pi/3, \pi/2)$ and $(2\pi/3, 3\pi/2)$, where $\cos\phi = 0$. Since $\kappa \propto \cos^2\phi$, these collinear singularities contribute only to $\delta(\kappa)$, not to the plus distributions $[1/\kappa]_+$ or $[\ln\kappa/\kappa]_+$. Only the jet 1 collinear region ($\theta \to 0$) contributes to the logarithmic structure of the soft function for $\kappa > 0$.

4.4.7 The finite constant

The remaining constant c_δ is defined by

$$c_\delta = \lim_{\kappa \to 0} \left[\Sigma(\kappa) + 2\ln^2\kappa - \frac{94}{17} \ln\kappa \right] , \tag{132}$$

and is expected to involve π^2, $\ln 2$, $\ln 3$, and Gieseking's constant $\mathrm{Cl}_2(\pi/3)$ from the Mercedes geometry. For NLL accuracy, only the logarithmic coefficients are required; the constant c_δ would be needed for NNLL.

4.5 Summary of anomalous dimensions

Table 1 summarizes the one-loop anomalous dimensions. The cusp pieces all involve the universal cusp anomalous dimension $\Gamma_0 = 4$ multiplied by the appropriate color factor. The key observation is that the total color factor for cusp evolution is

$$A_2 \equiv 2C_F + C_A \,, \tag{133}$$

which will determine the double-log coefficient when we expand the NLL formula to fixed order in Section 5.7.

4.6 NLL accuracy requirements

For NLL accuracy, the following perturbative ingredients are required [5]:

Function	Cusp color	Non-cusp $\gamma^{(0)}$	Natural scale
Hard H_C	$-(2C_F + C_A)$	$-(6C_F + \beta_0)$	$\mu_H = Q$
Quark jet J_q ($\times 2$)	C_F each	$-3C_F$ each	$\mu_J = Q\sqrt{(8/3)c}$
Gluon jet J_g	C_A	$-\beta_0$	$\mu_J = Q\sqrt{(8/3)c}$
Soft S_C	$2C_F + C_A$	$12C_F + 2\beta_0$	$\mu_S = (8/3)Qc$
Total	0	0	—

Table 1: One-loop anomalous dimensions for the factorization ingredients. The cusp color factors and non-cusp anomalous dimensions sum to zero as required by RG consistency. The natural scales include the geometric factor 8/3 from the C-parameter measurement at Mercedes.

- **Cusp anomalous dimension to two loops:**

$$\Gamma_0 = 4\,, \tag{134}$$

$$\Gamma_1 = 4\left[\left(\frac{67}{9} - \frac{\pi^2}{3}\right) C_A - \frac{20}{9} T_F n_f\right] = 4\left[\left(\frac{67}{9} - \frac{\pi^2}{3}\right) \times 3 - \frac{20}{9} \times \frac{1}{2} \times 5\right] \approx 27.6\,. \tag{135}$$

- **Non-cusp anomalous dimensions to one loop:** The values $\gamma_H^{\mathrm{nc},(0)}$, $\gamma_J^{q,\mathrm{nc},(0)}$, $\gamma_J^{g,\mathrm{nc},(0)}$, $\gamma_S^{\mathrm{nc},(0)}$ listed in Table 1.

- **Beta function to two loops:**

$$\beta_0 = \frac{11C_A - 4T_F n_f}{3} = \frac{11 \times 3 - 4 \times \frac{1}{2} \times 5}{3} = \frac{23}{3} \approx 7.67\,, \tag{136}$$

$$\beta_1 = \frac{34C_A^2}{3} - \frac{20C_A T_F n_f}{3} - 4C_F T_F n_f = \frac{34 \times 9}{3} - \frac{20 \times 3 \times \frac{5}{2}}{3} - 4 \times \frac{4}{3} \times \frac{5}{2} = \frac{116}{3} \approx 38.7\,. \tag{137}$$

- **Tree-level matching:** Only the Born coefficient $H_C^{(0)} = A(3/4) \approx 7.64$ is needed; one-loop matching would be required for NNLL.

All these ingredients are known, making NLL resummation complete for the C-parameter shoulder.

4.7 Two-loop running coupling

For consistent NLL accuracy, we use two-loop running of the strong coupling. The beta function is

$$\mu \frac{d\alpha_s}{d\mu} = -2\alpha_s \left[\frac{\beta_0}{4\pi}\alpha_s + \frac{\beta_1}{(4\pi)^2}\alpha_s^2 + \ldots\right]. \tag{138}$$

The two-loop solution can be written as

$$\boxed{\alpha_s(\mu) = \frac{\alpha_s(\mu_0)}{1+X}\left[1 - \frac{\beta_1}{\beta_0}\frac{\alpha_s(\mu_0)}{4\pi}\frac{\ln(1+X)}{1+X}\right]} \tag{139}$$

where

$$X = \frac{\beta_0 \alpha_s(\mu_0)}{2\pi} \ln\frac{\mu}{\mu_0}\,. \tag{140}$$

Equivalently, in terms of $\Lambda_{\overline{\mathrm{MS}}}$:

$$\alpha_s(\mu) = \frac{4\pi}{\beta_0 L}\left[1 - \frac{\beta_1}{\beta_0^2}\frac{\ln L}{L} + \mathcal{O}(1/L^2)\right], \qquad L = \ln\frac{\mu^2}{\Lambda^2}\,. \tag{141}$$

For numerical work with $\mu_0 = M_Z = 91.19$ GeV, $\alpha_s(M_Z) = 0.118$, and $n_f = 5$:

- $\beta_0\alpha_s(M_Z)/(2\pi) \approx 0.144$
- $\beta_1/\beta_0 \approx 5.04$
- $\alpha_s(M_Z)/(4\pi) \approx 0.0094$

As an example, at $\mu = 10$ GeV we have $X \approx -0.32$, giving $\alpha_s(10\text{ GeV}) \approx 0.178$.

4.8 NLO prediction from SCET

The SCET factorization theorem (75) makes definite predictions for the distribution above the shoulder. The kernel has the structure (with the standard SCET sign convention):

$$K(c') = \delta(c') - \frac{\alpha_s}{4\pi}(2C_F + C_A)\Gamma_0 \left[\frac{\ln c'}{c'}\right]_+ + \dots \tag{142}$$

where the *negative* coefficient on $[\ln c'/c']_+$ reflects the Sudakov suppression of soft/collinear radiation. Integrating to obtain the cumulant:

$$R(c) = \int_0^c K(c')\,dc' = 1 - \frac{\alpha_s}{4\pi}(2C_F + C_A)\frac{\Gamma_0}{2}\ln^2 c + \mathcal{O}(\alpha_s^2) \quad \text{for } c > 0\,. \tag{143}$$

The singular part of the cross section is:

$$\frac{1}{\sigma_0}\frac{d\sigma}{dc}\bigg|_{\text{sing}} = -\frac{\alpha_s}{2\pi}A(3/4)\,R(c) = -\frac{\alpha_s}{2\pi}A(3/4)\left[1 - \frac{\alpha_s}{4\pi}(2C_F + C_A)\frac{\Gamma_0}{2}\ln^2 c + \dots\right]. \tag{144}$$

Expanding:

$$\boxed{\frac{1}{\sigma_0}\frac{d\sigma}{dc}\bigg|_{\text{sing}} = -\frac{\alpha_s}{2\pi}A\Big(\frac{3}{4}\Big) + \Big(\frac{\alpha_s}{2\pi}\Big)^2 A\Big(\frac{3}{4}\Big)\left[A_2\ln^2 c + B_1\ln c + \dots\right]} \tag{145}$$

Matching. The full cross section is $d\sigma/dc|_{\text{sing}} + \sigma_{\text{NS}}$, where $\sigma_{\text{NS}} = \sigma_{\text{NLO}} - \sigma_{\text{sing}}^{\text{expanded}}$. At tree level, $\sigma_{\text{NLO}}|_{c>0} = 0$ and $\sigma_{\text{sing}}^{\text{expanded},(0)} = -(\alpha_s/2\pi)A(3/4)$, so $\sigma_{\text{NS}}^{(0)} = +(\alpha_s/2\pi)A(3/4)$. The total is zero, correctly reproducing the absence of events above the shoulder at LO.

At NLO, the non-singular σ_{NS} provides smooth corrections that ensure the cross section matches smoothly to the fixed-order result away from the shoulder.

NLO singular terms. The $\mathcal{O}(\alpha_s^2)$ singular structure is:

$$\frac{1}{\sigma_0}\frac{d\sigma}{dc}\bigg|_{\text{NLO sing}} = \Big(\frac{\alpha_s}{2\pi}\Big)^2 A\Big(\frac{3}{4}\Big)\left[A_2\ln^2 c + B_1\ln c\right]. \tag{146}$$

The coefficients A_2 and B_1 are *predictions* from the anomalous dimensions and jet function structure computed in Section 4.

Origin of the logarithms. The $\ln^2 c$ and $\ln c$ structure arises from integrating the plus distributions in the kernel:

$$\int_0^c \left[\frac{\ln c'}{c'}\right]_+ dc' = \frac{1}{2}\ln^2 c\,, \qquad \int_0^c \left[\frac{1}{c'}\right]_+ dc' = \ln c\,. \tag{147}$$

The negative coefficient $-\Gamma_0$ on $[\ln c'/c']_+$ in the kernel, combined with the minus sign in $-A(3/4)R(c)$, gives a positive $\ln^2 c$ contribution.

Double-log coefficient. From the cusp anomalous dimension structure, the double-log coefficient is determined by the total cusp color factor:

$$\boxed{A_2 = 2C_F + C_A} \tag{148}$$

This reflects soft emission from two quark lines (each contributing C_F) and one gluon line (contributing C_A).

Single-log coefficient. The single-log coefficient arises from three sources:

$$\boxed{B_1 = 3C_F + \frac{\beta_0}{2} + 2(2C_F + C_A)\ln\frac{8}{3}} \tag{149}$$

1. **Non-cusp jet anomalous dimensions** ($3C_F$): Each quark jet contributes $\gamma_J^{q,\mathrm{nc},(0)} = -3C_F$, and the relationship between the anomalous dimension and the distribution coefficient gives $-(1/2) \times 2 \times (-3C_F) = 3C_F$.

2. **Running coupling** ($\beta_0/2$): This arises from the evolution of α_s between the hard and soft scales.

3. **Geometric factor from jet measurement** ($2(2C_F + C_A)\ln(8/3)$): The C-parameter jet function measures $\ell = (8/3)\hat{m}^2$ rather than simply $\hat{m}^2 = m^2/Q^2$. This rescaling shifts the argument of the logarithm in the jet function:

$$\left[\frac{\ln(\hat{m}^2/\mu^2)}{\hat{m}^2}\right]_+ = \left[\frac{\ln(\ell/\mu^2) - \ln(8/3)}{\ell}\right]_+ \tag{150}$$

   The $-\ln(8/3)$ generates an additional $+C_i\Gamma_0\ln(8/3)$ contribution to the $[1/\ell]_+$ coefficient for each jet with color C_i. Summing over all three jets (two quarks at C_F, one gluon at C_A) with $\Gamma_0 = 4$ gives:

$$(2C_F + C_A) \times 4 \times \frac{1}{2}\ln\frac{8}{3} = 2(2C_F + C_A)\ln\frac{8}{3}\,. \tag{151}$$

The gluon jet non-cusp anomalous dimension $\gamma_J^{g,\mathrm{nc},(0)} = -\beta_0$ does not contribute separately—its effect is captured in the running coupling treatment.

Numerical values. For reference:

$$\begin{aligned} A_2 = 2C_F + C_A &= \frac{17}{3} \approx 5.67\,, \\ 3C_F + \frac{\beta_0}{2} &= \frac{47}{6} \approx 7.83\,, \\ 2(2C_F + C_A)\ln\frac{8}{3} &= \frac{34}{3}\ln\frac{8}{3} \approx 11.1\,, \\ B_1 &\approx 18.9\,. \end{aligned} \tag{152}$$

Simplification in the δ variable. In the rescaled variable $\delta = (8/3)c$ used by Catani and Webber, the geometric logarithm is absorbed. Since $\ln c = \ln\delta - \ln(8/3)$, the coefficient of $\ln\delta$ becomes:

$$B_1^{(\delta)} = B_1 - 2A_2\ln\frac{8}{3} = 3C_F + \frac{\beta_0}{2} = \frac{47}{6}\,. \tag{153}$$

This explains why the Catani–Webber result appears simpler when written in their variable δ.

Color decomposition. The predictions decompose by color structure:

	C_F^2	$C_F C_A$	$C_F T_F n_f$
A_2 (coeff. of $\ln^2 c$)	2	1	0
$B_1^{(\delta)}$ (coeff. of $\ln\delta$)	3	11/6	$-2/3$

The $T_F n_f$ term contributes only to single logarithms because $g \to q\bar{q}$ splitting is collinear but not soft. The geometric $\ln(8/3)$ term does not affect the color decomposition since it multiplies A_2, which has no $T_F n_f$ component.

The predictions decompose by color structure as shown in the following table. These predictions are validated against EVENT2 data in Section 4.9.

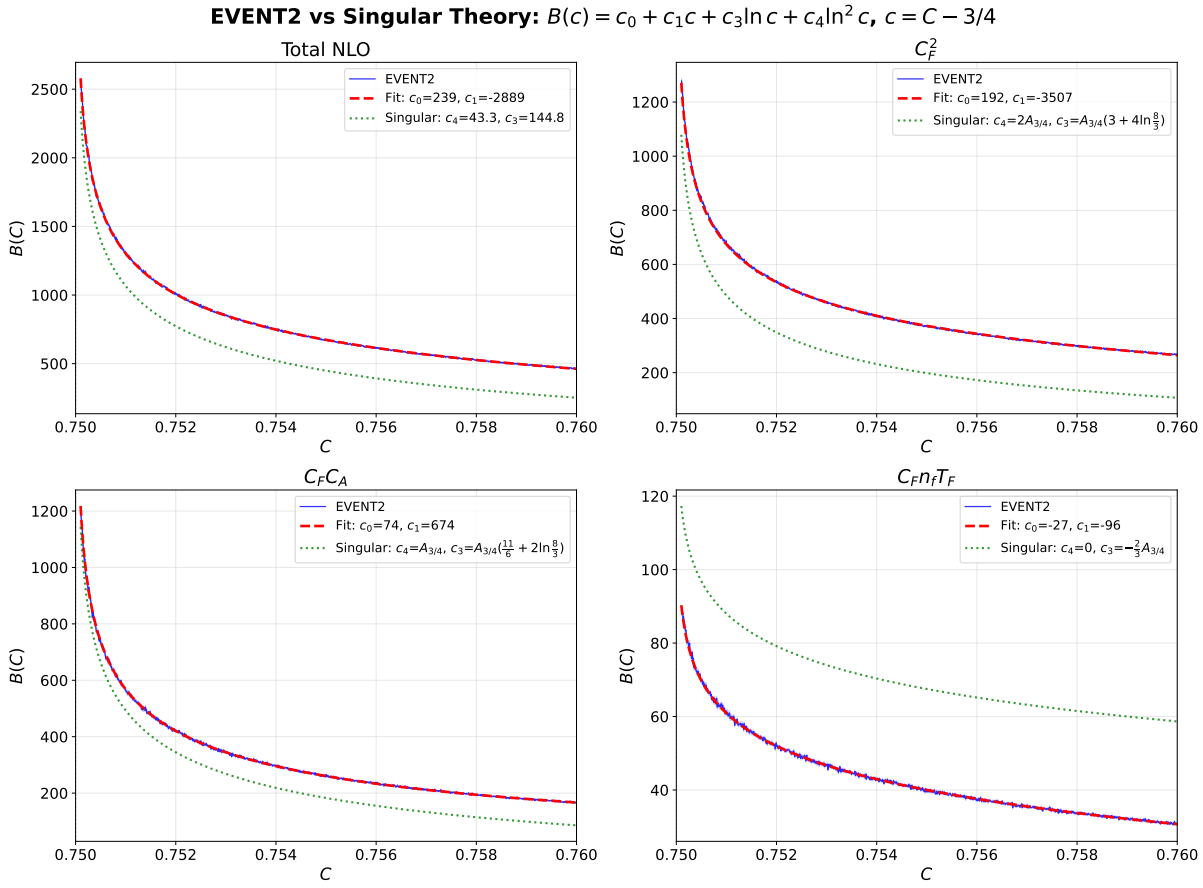

Figure 2: Comparison of EVENT2 NLO distribution $B(C)$ (blue histogram) with the singular prediction $B_{\rm sing}(c) = c_3 \ln c + c_4 \ln^2 c$ (green dotted) in the shoulder region, where $c = C - 3/4$. The singular coefficients c_3 and c_4 are fixed by SCET (see Eq. (146)), while c_0 and c_1 are fitted to the data. The red dashed curve shows the full fit $c_0 + c_1 c + c_3 \ln c + c_4 \ln^2 c$. Top left: total NLO with $c_4 = 43.3$ and $c_3 = 144.8$. The remaining panels show the individual color channels C_F^2, $C_F C_A$, and $C_F n_f T_F$, each validating the predicted singular structure.

4.9 Validation of singular structure from EVENT2

The SCET factorization theorem predicts the singular structure of the NLO distribution just above the shoulder. Writing $c = C - 3/4$, the distribution takes the form

$$B(c) = c_0 + c_1 c + c_3 \ln c + c_4 \ln^2 c\,, \tag{154}$$

where $c_4 = A_{3/4}(2C_F + C_A)$ and c_3 are predicted by the SCET anomalous dimensions (Eqs. (148)–(149)), while c_0 and c_1 are non-singular constants determined by matching to the full NLO calculation.

Figure 2 compares the EVENT2 NLO distribution $B(C)$ (blue histogram) with the singular prediction (green dotted), fitting c_0 and c_1 from the data. The excellent agreement across all color channels validates the SCET predictions for c_3 and c_4. The fitted values $c_0 \approx 239$ (total) and $c_1 \approx -2889$ characterize the non-singular contributions.

To isolate the non-singular structure, we define the residual distribution

$$B_{\rm NS}(c) \equiv B(c) - c_3 \ln c - c_4 \ln^2 c\,, \tag{155}$$

which should be approximately linear in c near the shoulder. Figure 3 shows $B_{\rm NS}(c)$ for each color channel in the region $0.75 < C < 0.76$. The linearity confirms that the singular structure has been correctly subtracted, with the fitted values matching those in Figure 2.

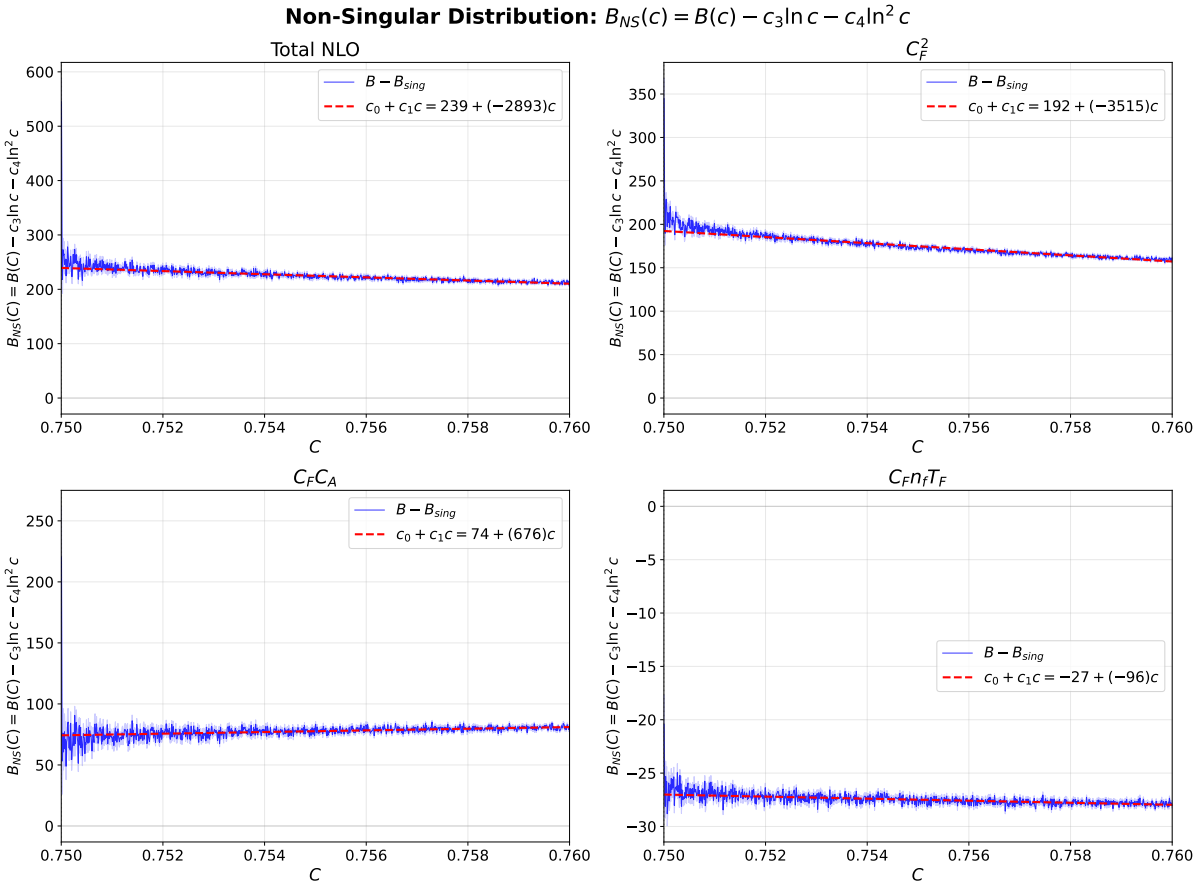

Figure 3: Non-singular distribution $B_{\rm NS}(c) = B(c) - c_3 \ln c - c_4 \ln^2 c$ (blue) in the shoulder region, with linear fits $c_0 + c_1 c$ (red dashed). The approximate linearity confirms that the SCET-predicted singular structure has been correctly subtracted. The fitted intercepts c_0 give the constant term in the expansion (154): $c_0 = 239$ (total), 192 (C_F^2), 74 ($C_F C_A$), and -27 ($C_F n_f T_F$).

Finally, Figure 4 extends this comparison over the full kinematic range. The left column shows the NLO distribution $B(C)$ for $C < 3/4$, transitioning to $B_{\rm NS}(C)$ for $C > 3/4$. The continuity of $B_{\rm NS}$ across the shoulder (compared to the discontinuity in B) demonstrates that the singular terms correctly account for the jump at $C = 3/4$.

5 NLL Resummation Formula

We now combine the perturbative ingredients to derive the NLL cumulant $R(c)$ for the C-parameter shoulder. As established in Section 3.4, the matched cross section above the shoulder takes the form

$$\boxed{\frac{1}{\sigma_0}\frac{d\sigma}{dc}\bigg|_{c>0} = -\frac{\alpha_s(Q)}{2\pi} A\Big(\frac{3}{4}\Big) R(c) + \sigma_{\rm NS}(c)} \tag{156}$$

where $R(c) = \int_0^c K(c')\,dc'$ is the cumulant of the SCET kernel and $\sigma_{\rm NS}$ is the non-singular remainder from matching to fixed order.

At tree level, $R^{(0)}(c) = 1$ for $c > 0$, giving a singular piece $-(\alpha_s/2\pi)A(3/4)$ which is cancelled by $\sigma_{\rm NS}^{(0)} = +(\alpha_s/2\pi)A(3/4)$, yielding zero cross section above the shoulder. After resummation, $R(c) = e^{-S(c)} \to 0$ as $c \to 0$, so the singular piece vanishes at the shoulder and the cross section smoothly matches to $\sigma_{\rm NS}(0)$.

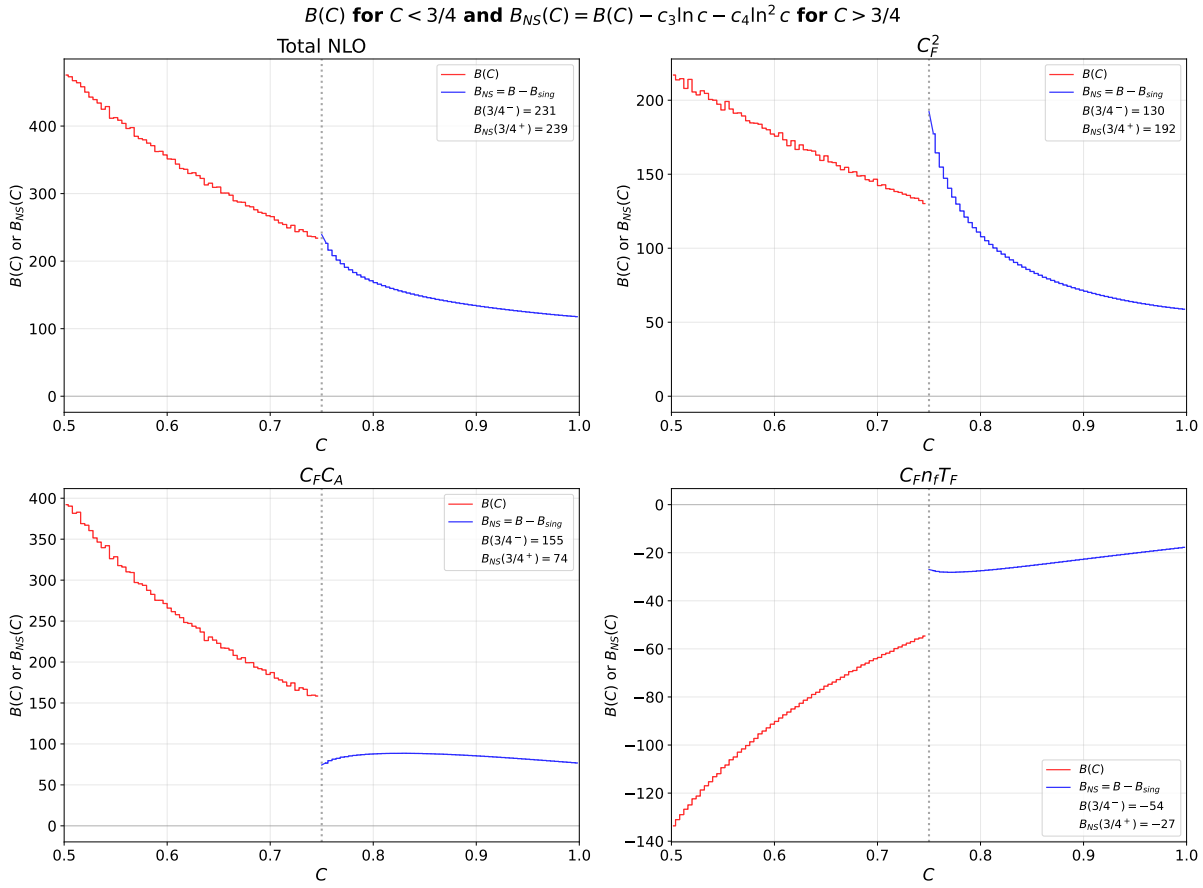

Figure 4: NLO distribution $B(C)$ (red) for $C < 3/4$ and non-singular distribution $B_{\rm NS}(C) = B(C) - c_3 \ln c - c_4 \ln^2 c$ (blue) for $C > 3/4$, where $c = C - 3/4$. The values at the shoulder, $B(3/4^-)$ and $B_{\rm NS}(3/4^+)$, are shown in each panel. The near-continuity of $B_{\rm NS}$ across the shoulder—in contrast to the discontinuity in $B(C)$ itself—confirms that the SCET singular structure correctly captures the Sudakov logarithms. Top left: total NLO. Remaining panels: individual color channels C_F^2, $C_F C_A$, and $C_F n_f T_F$.

5.1 The resummed cumulant

The NLL cumulant takes the form:

$$\boxed{R(c) = \tilde{h}(L_H)\,\Pi(\mu_H, \mu_J, \mu_S)\,\tilde{j}_q\big(\partial_\eta + L_{JS}\big)^2\,\tilde{j}_g\big(\partial_\eta + L_{JS}\big)\,\tilde{s}(\partial_\eta)\,\frac{e^{-\gamma_E \eta}}{\Gamma(1+\eta)}\left(\frac{(8/3)\,cQ}{\mu_S}\right)^{\eta}} \tag{157}$$

where:

- $\tilde{h}(L_H)$ is the **hard matching function** encoding the hard function at scale μ_H
- $\Pi(\mu_H, \mu_J, \mu_S)$ is the **evolution kernel** encoding RG running between scales
- $\tilde{j}_q$, $\tilde{j}_g$, $\tilde{s}$ are the **Laplace-space matching functions** for jets and soft
- $\eta = 2(2C_F + C_A)A_\Gamma(\mu_J, \mu_S)$ is the **Sudakov exponent**
- $L_H = \ln(\mu_H^2/Q^2)$, $L_{JS} = \ln(Q\mu_S/\mu_J^2)$, and ∂_η acts on the η-dependence of the base function
- The factor $8/3$ is the geometric coefficient from the C-parameter collinear measurement (Eq. (58))

The base function $e^{-\gamma_E \eta}((8/3)cQ/\mu_S)^\eta/\Gamma(1+\eta)$ has the crucial property that it reduces to $\Theta(c)$ when $\eta \to 0$.

5.1.1 Tree-level limit

When all scales are set equal, $\mu_H = \mu_J = \mu_S = Q$, the resummation turns off:

- The hard matching function: $\tilde{h}(0) = 1 + \mathcal{O}(\alpha_s)$
- The evolution kernel: $\Pi(Q, Q, Q) = 1$
- The Sudakov exponent: $\eta = 2(2C_F + C_A)A_\Gamma(Q, Q) = 0$
- The jet and soft matching functions: $\tilde{j}_q(0) = \tilde{j}_g(0) = \tilde{s}(0) = 1 + \mathcal{O}(\alpha_s)$
- The base function: $\dfrac{e^{-\gamma_E \cdot 0}}{\Gamma(1)} c^0 = 1$ for $c > 0$

Therefore $R(c) \to 1$ for $c > 0$ when resummation is disabled. The singular piece $-(\alpha_s/2\pi)A(3/4)\times 1$ is cancelled by $\sigma^{(0)}_{\rm NS} = +(\alpha_s/2\pi)A(3/4)$, giving zero cross section above the shoulder at LO.

5.2 Evolution kernel

The evolution kernel Π encodes RG running between the hard, jet, and soft scales:

$$\boxed{\Pi(\mu_H, \mu_J, \mu_S) = \exp\left[2(2C_F + C_A)\big(S(\mu_H, \mu_J) + S(\mu_S, \mu_J)\big) + 2A_{\gamma^S}(\mu_S, \mu_J) + 2A_{\gamma_q^J}(\mu_J, \mu_H) + A_{\gamma_g^J}(\mu_J, \mu_H)\right]} \tag{158}$$

where the Sudakov integral and non-cusp evolution integrals are:

$$S(\nu, \mu) = -\int_{\alpha_s(\nu)}^{\alpha_s(\mu)} \frac{d\alpha}{\alpha}\, \Gamma_{\rm cusp}(\alpha) \int_{\alpha_s(\nu)}^{\alpha} \frac{d\alpha'}{\beta(\alpha')}\,, \tag{159}$$

$$A_{\gamma_X}(\nu, \mu) = -\int_{\alpha_s(\nu)}^{\alpha_s(\mu)} \frac{d\alpha}{\beta(\alpha)}\, \gamma_X(\alpha)\,. \tag{160}$$

At LL, the Sudakov integral evaluates to:

$$S(\nu, \mu) = -\frac{\Gamma_0}{4\beta_0^2}\left[\frac{4\pi}{\alpha_s(\nu)}\left(\ln r + \frac{1}{r} - 1\right) + \frac{\beta_1}{\beta_0}\ln^2 r + \left(\frac{\Gamma_1}{\Gamma_0} - \frac{\beta_1}{\beta_0}\right)(r - 1 - \ln r)\right] + \mathcal{O}(\alpha_s)\,, \tag{161}$$

where $r = \alpha_s(\mu)/\alpha_s(\nu)$.

Verification: When $\mu_H = \mu_J = \mu_S$, all integrals vanish: $S(\mu, \mu) = 0$ and $A_{\gamma_X}(\mu, \mu) = 0$. Therefore $\Pi(\mu, \mu, \mu) = e^0 = 1$, as required.

5.3 Sudakov exponent

The Sudakov exponent η controls the power-law suppression at small c:

$$\eta = 2(2C_F + C_A)\, A_\Gamma(\mu_J, \mu_S)\,, \tag{162}$$

where

$$A_\Gamma(\mu_J, \mu_S) = -\int_{\alpha_s(\mu_S)}^{\alpha_s(\mu_J)} \frac{d\alpha}{\alpha}\, \frac{\Gamma_{\rm cusp}(\alpha)}{\beta(\alpha)} = \frac{\Gamma_0}{2\beta_0}\ln\frac{\alpha_s(\mu_S)}{\alpha_s(\mu_J)} + \mathcal{O}(\alpha_s)\,. \tag{163}$$

With natural scales $\mu_J = Q\sqrt{(8/3)c}$ and $\mu_S = (8/3)cQ$:

$$\eta = (2C_F + C_A)\frac{\Gamma_0 \alpha_s(Q)}{2\pi}\ln\frac{1}{\sqrt{(8/3)c}} + \mathcal{O}(\alpha_s^2) = (2C_F + C_A)\frac{\alpha_s(Q)}{2\pi}\ln\frac{1}{(8/3)c} + \mathcal{O}(\alpha_s^2)\,, \tag{164}$$

where we used $\Gamma_0 = 4$. The Sudakov suppression at small c comes from the factor $((8/3)cQ/\mu_S)^\eta = 1$ (at natural scales) combined with the $e^{-\gamma_E\eta}/\Gamma(1+\eta)$ prefactor in the base function.

5.4 Matching functions

The Laplace-space matching functions encode fixed-order corrections from the hard, jet, and soft functions. At NLO:

Hard matching function. The hard matching function encodes the hard function evaluated at scale μ_H:

$$\tilde{h}(L_H) = 1 + \frac{\alpha_s(\mu_H)}{4\pi}\left[-(2C_F + C_A)\Gamma_0 \frac{L_H^2}{2} + \gamma^{H,(0)} L_H + c_H\right], \tag{165}$$

where $L_H = \ln(\mu_H^2/Q^2)$ and $\gamma^{H,(0)} = -(6C_F + \beta_0)$ is the one-loop non-cusp hard anomalous dimension. The constant c_H contributes at NNLL and can be set to zero at NLL.

Jet matching functions. The quark and gluon jet matching functions are:

$$\tilde{j}_q(L) = 1 + \frac{\alpha_s(\mu_J)}{4\pi}\left[C_F\Gamma_0 \frac{L^2}{2} + \gamma_q^{J,(0)} L + c_J^q\right], \tag{166}$$

$$\tilde{j}_g(L) = 1 + \frac{\alpha_s(\mu_J)}{4\pi}\left[C_A\Gamma_0 \frac{L^2}{2} + \gamma_g^{J,(0)} L + c_J^g\right], \tag{167}$$

where $\gamma_q^{J,(0)} = -3C_F$ and $\gamma_g^{J,(0)} = -\beta_0$.

Soft matching function.

$$\tilde{s}(L) = 1 + \frac{\alpha_s(\mu_S)}{4\pi}\left[(2C_F + C_A)\Gamma_0 L^2 + \gamma^{S,(0)} L + c_S\right], \tag{168}$$

where $\gamma^{S,(0)} = 12C_F + 2\beta_0$. The constants $c_J^{q,g}$, c_H, and c_S contribute at NNLL and can be set to zero at NLL.

The derivative ∂_η acts on the base function to generate logarithms. Using

$$\partial_\eta\left[\frac{e^{-\gamma_E\eta}}{\Gamma(1+\eta)}\left(\frac{(8/3)\,cQ}{\mu_S}\right)^\eta\right] = \left[\ln\frac{(8/3)\,cQ}{\mu_S} - \gamma_E - \psi(1+\eta)\right] \times (\text{base function}), \tag{169}$$

where $\psi(x) = \Gamma'(x)/\Gamma(x)$ is the digamma function, with $\psi(1) = -\gamma_E$.

5.5 Natural scale choices

The C-parameter collinear measurement introduces a geometric factor 8/3 (Eq. (58)), which sets the **natural scales** for resummation:

$$\boxed{\mu_H = Q\,, \qquad \mu_J = Q\sqrt{\frac{8}{3}\,c}\,, \qquad \mu_S = \frac{8}{3}\,cQ\,.} \tag{170}$$

These scales are "natural" because they make all logarithms in the base function vanish:

- $L_c = \ln\dfrac{(8/3)\,cQ}{\mu_S} = \ln\dfrac{(8/3)\,cQ}{(8/3)\,cQ} = 0$
- $L_{JS} = \ln\dfrac{Q\cdot\mu_S}{\mu_J^2} = \ln\dfrac{Q\cdot(8/3)cQ}{Q^2(8/3)c} = 0$

Physical interpretation. A soft gluon with momentum $k \sim cQ$ contributes $\delta C = (8/3)(k/Q)$ to the C-parameter near the Mercedes configuration. Thus the natural soft scale is $(8/3)cQ$, not cQ. Similarly, a collinear splitting with jet mass m^2 contributes $\delta C = (8/3)m^2/Q^2$, so the natural jet scale is $\mu_J^2 = (8/3)cQ^2$, giving $\mu_J = Q\sqrt{(8/3)c}$.

With these natural scales, the base function simplifies to $\mathcal{F} = e^{-\gamma_E\eta}/\Gamma(1+\eta)$, and the derivative parameter becomes $\Phi = -\gamma_E - \psi(1+\eta)$. The $\ln(8/3)$ factor in B_1 emerges naturally from the anomalous dimension evolution rather than from a residual logarithm in the base function.

5.6 Scale independence at NLL

The physical cross section must be independent of the arbitrary scales μ_H, μ_J, μ_S at the working order. We now verify that the μ_H dependence cancels exactly at $\mathcal{O}(\alpha_s)$ in Eq. (157).

Sources of μ_H dependence. The hard scale μ_H enters the resummed cumulant through:

1. The hard matching function $\tilde{h}(L_H)$ with $L_H = \ln(\mu_H^2/Q^2)$
2. The evolution kernel $\Pi(\mu_H, \mu_J, \mu_S)$ via the Sudakov integral $S(\mu_H, \mu_J)$ and the jet non-cusp evolution integrals $A_{\gamma_q^J}(\mu_J, \mu_H)$, $A_{\gamma_g^J}(\mu_J, \mu_H)$

Cancellation at $\mathcal{O}(\alpha_s)$. Expanding to $\mathcal{O}(\alpha_s)$ with $L_H = \ln(\mu_H^2/Q^2) = 2\ln(\mu_H/Q)$:
From the hard matching function Eq. (165):

$$\tilde{h}(L_H) = 1 + \frac{\alpha_s}{4\pi}\Big[-(2C_F + C_A)\Gamma_0 \frac{L_H^2}{2} + \gamma^{H,(0)} L_H\Big] + \mathcal{O}(\alpha_s^2)\,. \tag{171}$$

From the evolution kernel Eq. (158), the μ_H-dependent terms at $\mathcal{O}(\alpha_s)$ are:

$$\ln\Pi\big|_{\mu_H} = 2(2C_F + C_A)S(\mu_H, \mu_J) + 2A_{\gamma_q^J}(\mu_J, \mu_H) + A_{\gamma_g^J}(\mu_J, \mu_H)\,. \tag{172}$$

At one loop, the Sudakov integral is $S(\mu_H, \mu_J) = -(\Gamma_0\alpha_s/8\pi)\ln^2(\mu_H/\mu_J)$, and the non-cusp integrals are $A_{\gamma^J}(\mu_J, \mu_H) = -(\alpha_s/4\pi)\gamma^{J,(0)}\ln(\mu_H/\mu_J)$. Using $\ln(\mu_H/\mu_J) = L_H/2 - \ln(\mu_J/Q)$:

$$\ln\Pi\big|_{\mu_H} = \frac{\alpha_s}{4\pi}\Big[(2C_F + C_A)\Gamma_0\frac{L_H^2}{2} - (2\gamma_q^{J,(0)} + \gamma_g^{J,(0)})L_H\Big] + (\mu_J\text{-dependent terms}) + \mathcal{O}(\alpha_s^2)\,. \tag{173}$$

Verification of cancellation. The total μ_H dependence at $\mathcal{O}(\alpha_s)$ is:

$$\begin{aligned}\ln[\tilde{h}\cdot\Pi]\big|_{\mu_H} &= \frac{\alpha_s}{4\pi}\Big[-(2C_F + C_A)\Gamma_0\frac{L_H^2}{2} + \gamma^{H,(0)}L_H\Big] \\ &\quad + \frac{\alpha_s}{4\pi}\Big[(2C_F + C_A)\Gamma_0\frac{L_H^2}{2} - (2\gamma_q^{J,(0)} + \gamma_g^{J,(0)})L_H\Big] + \mathcal{O}(\alpha_s^2) \\ &= \frac{\alpha_s}{4\pi}\Big[\gamma^{H,(0)} - 2\gamma_q^{J,(0)} - \gamma_g^{J,(0)}\Big]L_H + \mathcal{O}(\alpha_s^2)\,.\end{aligned} \tag{174}$$

Using the anomalous dimensions $\gamma^{H,(0)} = -(6C_F + \beta_0)$, $\gamma_q^{J,(0)} = -3C_F$, and $\gamma_g^{J,(0)} = -\beta_0$:

$$\gamma^{H,(0)} - 2\gamma_q^{J,(0)} - \gamma_g^{J,(0)} = -(6C_F + \beta_0) - 2(-3C_F) - (-\beta_0) = 0\,. \tag{175}$$

Conclusion. The μ_H dependence cancels exactly at $\mathcal{O}(\alpha_s)$, as guaranteed by RG consistency. The cusp terms cancel because the same color factor $(2C_F + C_A)$ appears in both $\tilde{h}$ and Π with opposite signs. The non-cusp terms cancel because of the RG consistency condition $\gamma^{H,\mathrm{nc}} + 2\gamma^{J,q,\mathrm{nc}} + \gamma^{J,g,\mathrm{nc}} + \gamma^{S,\mathrm{nc}} = 0$, with the soft contribution entering through the remaining terms in Π. This cancellation is essential for the physical cross section to be well-defined and provides a nontrivial check on the structure of the resummed formula.

5.7 Expansion to NLO

We verify that expanding Eq. (157) to $\mathcal{O}(\alpha_s)$ reproduces the NLO result in Eq. (145).

At $\mathcal{O}(\alpha_s^0)$: With $\eta = 0$ and all matching functions equal to 1 (including $\tilde{h}(0) = 1$ at natural scale $\mu_H = Q$),

$$R^{(0)}(c) = 1 \times 1 \times 1 \times \frac{e^0}{\Gamma(1)} \cdot 1^0 = 1 \quad \text{for } c > 0\,. \tag{176}$$

The factors are: $\tilde{h}(0) = 1$, $\Pi(Q, Q, Q) = 1$, $\tilde{j}_q^2\tilde{j}_g\tilde{s} = 1$, and base function $= 1$. The singular piece is $-(\alpha_s/2\pi)A(3/4) \times 1 = -(\alpha_s/2\pi)A(3/4)$, which is cancelled by $\sigma_{\mathrm{NS}}^{(0)} = +(\alpha_s/2\pi)A(3/4)$, giving zero total cross section above the shoulder at LO.

At $\mathcal{O}(\alpha_s)$: The Sudakov exponent with natural scales is:

$$\eta = (2C_F{+}C_A)\frac{\Gamma_0\alpha_s}{4\pi}\ln\frac{\mu_J}{\mu_S} = (2C_F{+}C_A)\frac{\Gamma_0\alpha_s}{4\pi}\ln\frac{1}{\sqrt{(8/3)c}} = -(2C_F{+}C_A)\frac{\Gamma_0\alpha_s}{8\pi}\ln\Big(\frac{8}{3}c\Big)\,. \quad (177)$$

Since $(8/3)c < 1$ for small c, we have $\eta > 0$. At natural scales $L_c = 0$, so the base function is simply $e^{-\gamma_E\eta}/\Gamma(1+\eta)$. Expanding for small η:

$$\frac{e^{-\gamma_E\eta}}{\Gamma(1+\eta)} = 1 - \gamma_E\eta + \gamma_E\eta + \mathcal{O}(\eta^2) = 1 + \mathcal{O}(\eta^2)\,. \quad (178)$$

The double logarithms come from the Sudakov exponent in Π, and the single logarithms from the non-cusp anomalous dimensions. The complete NLO expansion gives:

$$R(c) = 1-(2C_F{+}C_A)\frac{\Gamma_0\alpha_s}{4\pi}\ln^2 c - \frac{\alpha_s}{4\pi}\Big[(6C_F{+}\beta_0)\ln c + 2(2C_F{+}C_A)\Gamma_0 \ln c\,\ln\frac{8}{3}\Big] + \mathcal{O}(\alpha_s^2)\,. \quad (179)$$

The singular cross section is:

$$\frac{1}{\sigma_0}\frac{d\sigma}{dc}\bigg|_{\rm sing} = -\frac{\alpha_s}{2\pi}A(3/4)\,R(c) = -\frac{\alpha_s}{2\pi}A(3/4) + \Big(\frac{\alpha_s}{2\pi}\Big)^2 A(3/4)\Big[(2C_F + C_A)\ln^2 c + B_1 \ln c\Big] + \ldots \quad (180)$$

where $B_1 = 3C_F + \beta_0/2 + 2(2C_F + C_A)\ln(8/3)$ and we used $\Gamma_0 = 4$. The constant term $-(\alpha_s/2\pi)A(3/4)$ is cancelled by $\sigma_{\rm NS}$, leaving the positive NLO singular structure that matches EVENT2 and Catani–Webber.

Catani–Webber form. The resummed cumulant can be written as $R(c) = e^{-S(c)}$ where $S(c)$ contains both double and single logarithms at NLL. The matched cross section is:

$$\frac{d\sigma}{dc} = -\frac{\alpha_s}{2\pi}A(3/4)\,e^{-S(c)} + \sigma_{\rm NS}(c)\,. \quad (181)$$

As $c \to 0$, $S(c) \to \infty$, so $e^{-S} \to 0$ and the singular piece vanishes. The cross section smoothly approaches $\sigma_{\rm NS}(0)$, which matches the LO cross section just below the shoulder. This ensures continuity across the Sudakov shoulder—the hallmark of correct resummation.

Origin of $\ln(8/3)$ in B_1. The geometric factor $2(2C_F + C_A)\ln(8/3)$ in B_1 arises from the RG evolution between the natural scales $\mu_J = Q\sqrt{(8/3)c}$ and $\mu_S = (8/3)cQ$. Since $\ln(\mu_J/\mu_S) = \frac{1}{2}\ln(1/((8/3)c)) = -\frac{1}{2}(\ln c + \ln(8/3))$, the evolution generates terms proportional to $\ln(8/3)$ in addition to $\ln c$.

5.8 Profile functions

The natural scale choices $\mu_J = Q\sqrt{(8/3)c}$ and $\mu_S = (8/3)cQ$ are appropriate only in the resummation region where $c \ll 1$. For $c \sim \mathcal{O}(1)$, these choices lead to unphysical behavior:

- The scales μ_J and μ_S drop below Q, generating large logarithms $\ln(\mu/Q)$ in the opposite direction.
- At $c = 0.25$ (corresponding to $C = 1$, the kinematic endpoint), the natural soft scale would be $\mu_S = (8/3)(0.25)Q \approx 0.67Q \approx 60$ GeV at LEP, which is still perturbative but represents an artificial hierarchy.
- For phenomenological applications, we want the resummation to "turn off" smoothly, reducing to the fixed-order result when c is large.

Profile functions provide a systematic solution: we define c-dependent scales $\mu_J(c)$ and $\mu_S(c)$ that interpolate between the natural power-law behavior at small c and the common scale $\mu_H = Q$ at large c. This ensures that when $c \sim \mathcal{O}(1)$, all scales coincide and the resummation switches off, as demonstrated in Section 5.7.

5.8.1 General parametrization

We parametrize the profile scales as:

$$\boxed{\begin{aligned}\mu_H(c) &= Q\,,\\ \mu_J(c) &= Q\,f_J(c)\,,\\ \mu_S(c) &= Q\,f_S(c)\,,\end{aligned}} \tag{182}$$

where the profile functions $f_J(c)$ and $f_S(c)$ satisfy:

$$\text{Resummation region } (c\to 0): \quad f_J(c)\to\sqrt{\tfrac{8}{3}c}\,, \quad f_S(c)\to\tfrac{8}{3}c\,, \tag{183}$$

$$\text{Fixed-order region } (c\to c_{\rm off}): \quad f_J(c)\to 1\,, \quad f_S(c)\to 1\,. \tag{184}$$

Here $c_{\rm off}$ is the "turn-off" point where resummation is fully disabled. For the C-parameter shoulder, a natural choice is $c_{\rm off}=0.05$, corresponding to $C=0.80$ (see Figure 5).

5.8.2 Quadratic profile functions

A simple and smooth choice uses quadratic interpolation. Define the transition region $[c_1,c_2]$ with $0<c_1<c_2\le c_{\rm off}$. The profile functions are:

$$f_S(c)=\begin{cases}\dfrac{8}{3}c & c<c_1\\[2mm] \dfrac{8}{3}c_1+\left(1-\dfrac{8}{3}c_1\right)\dfrac{(c-c_1)^2}{(c_2-c_1)^2} & c_1\le c<c_2\\[2mm] 1 & c\ge c_2\end{cases} \tag{185}$$

and similarly for $f_J(c)$:

$$f_J(c)=\begin{cases}\sqrt{\dfrac{8}{3}c} & c<c_1\\[2mm] \sqrt{\dfrac{8}{3}c_1}+\left(1-\sqrt{\dfrac{8}{3}c_1}\right)\dfrac{(c-c_1)^2}{(c_2-c_1)^2} & c_1\le c<c_2\\[2mm] 1 & c\ge c_2\end{cases} \tag{186}$$

These functions are continuous and have continuous first derivatives at c_1 and c_2.

5.8.3 Recommended parameter choices

The profile turn-on and turn-off points are guided by comparing the singular and non-singular contributions to the NLO distribution. Figure 5 shows the decomposition $B(C)=B_{\rm sing}(c)+B_{\rm NS}(c)$ where $B_{\rm sing}=A(C_0)[A_2\ln^2 c+B_1\ln c]$ contains the SCET-predicted singular structure. The singular term dominates for $c\lesssim 0.01$ (i.e., $C\lesssim 0.76$), while the non-singular contribution $B_{\rm NS}$ becomes comparable to $B_{\rm sing}$ around $c\sim 0.03$–0.05 and eventually dominates for larger c. This suggests that resummation should be fully active for $c<0.01$ and turned off by $c\sim 0.05$.

Based on this analysis, we recommend:

$$\boxed{c_1=0.01\,, \qquad c_2=0.05\,, \qquad c_{\rm off}=0.05} \tag{187}$$

corresponding to:

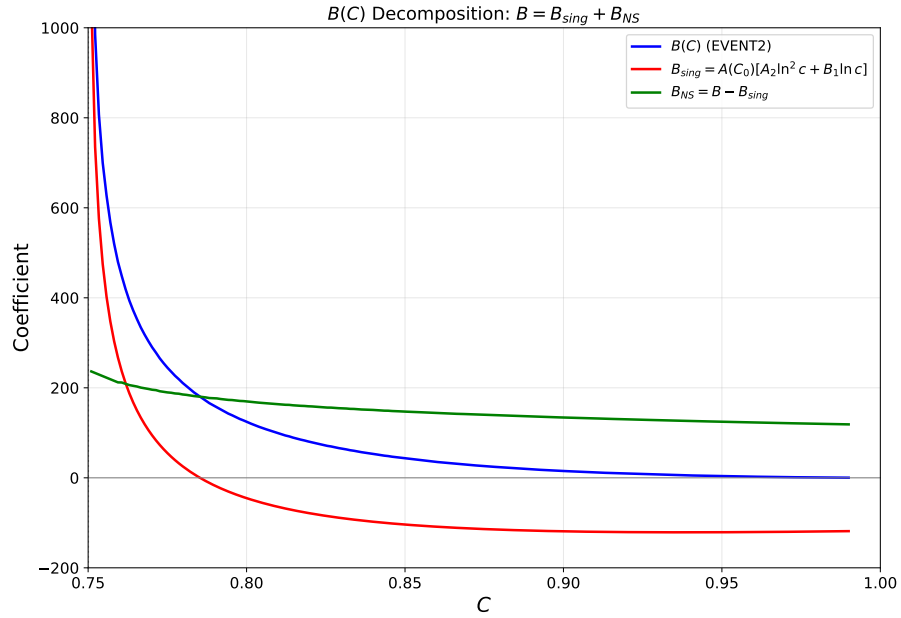

Figure 5: Decomposition of the NLO coefficient $B(C) = B_{\text{sing}} + B_{\text{NS}}$ in the shoulder region. Blue: full $B(C)$ from EVENT2. Red: singular prediction $B_{\text{sing}}(c) = A(C_0)[A_2 \ln^2 c + B_1 \ln c]$ from SCET with $A_2 = 2C_F + C_A$ and $B_1 = 3C_F + \beta_0/2 + 2(2C_F + C_A)\ln(8/3)$. Green: non-singular remainder $B_{\text{NS}} = B - B_{\text{sing}}$. The intercepts suggest the profile transition region: resummation should be fully active where $|B_{\text{sing}}| \gg B_{\text{NS}}$ (roughly $c < 0.01$, i.e., $C < 0.76$) and turned off where $B_{\text{NS}} > |B_{\text{sing}}|$ (roughly $c > 0.05$, i.e., $C > 0.80$).

Region	C range	Scale behavior
Resummation	$0.75 < C < 0.76$	$\mu_J = Q\sqrt{(8/3)c}$, $\mu_S = (8/3)cQ$
Transition	$0.76 < C < 0.80$	Quadratic interpolation
Fixed-order	$C > 0.80$	$\mu_H = \mu_J = \mu_S = Q$

The choice $c_1 = 0.01$ ensures that resummation is fully active for $c < 0.01$, where the singular contribution dominates and $|\ln c| > 4.6$. The choice $c_2 = 0.05$ turns off resummation by $C = 0.80$, where the non-singular contribution is already comparable to the singular piece.

5.8.4 Alternative: exponential profiles

An alternative parametrization uses exponential damping:

$$f_S(c) = 1 - \left(1 - \tfrac{8}{3}c\right)\exp\left(-\frac{c}{c_0}\right), \qquad f_J(c) = 1 - \left(1 - \sqrt{\tfrac{8}{3}c}\right)\exp\left(-\frac{c}{c_0}\right), \tag{188}$$

with $c_0 \sim 0.05$–0.10 controlling the transition width. This form automatically satisfies both limits (183)–(184) without explicit matching regions.

5.8.5 Scale variations for uncertainty estimation

Theoretical uncertainties from missing higher-order terms are estimated by varying the profile scales. We use the following variations:

1. **Hard scale:** $\mu_H \to \xi_H Q$ with $\xi_H \in \{1/2, 1, 2\}$.
2. **Jet scale:** $\mu_J \to \xi_J Q f_J(c)$ with $\xi_J \in \{1/2, 1, 2\}$.

3. **Soft scale:** $\mu_S \to \xi_S Q f_S(c)$ with $\xi_S \in \{1/2, 1, 2\}$.

4. **Profile parameters:** $c_1 \to c_1 \pm 0.005$, $c_2 \to c_2 \pm 0.01$.

The total uncertainty is obtained by taking the envelope of all variations, subject to the constraint that the scale hierarchy $\mu_S \leq \mu_J \leq \mu_H$ is preserved. This typically yields ± 10–20% uncertainty in the transition region $0.01 < c < 0.05$.

5.8.6 Implementation in the kernel density formula

With profile functions, the kernel density Eq. (157) becomes c-dependent through the scales:

$$\eta(c) = 2(2C_F + C_A)\, A_\Gamma\big(\mu_J(c), \mu_S(c)\big)\,, \tag{189}$$

where now $\mu_J(c)$ and $\mu_S(c)$ are given by the profile functions. At small c, the natural scale behavior is recovered: $\mu_S \to (8/3)cQ$, $\mu_J \to Q\sqrt{(8/3)c}$. At large c, the scales merge: $\mu_J(c) \to Q$, $\mu_S(c) \to Q$, so $A_\Gamma \to 0$ and $\eta \to 0$, which turns off the resummation as required.

The evolution kernel Π similarly becomes c-dependent. The Sudakov exponents $S(\mu_H, \mu_J(c))$ and $S(\mu_S(c), \mu_J(c))$ smoothly interpolate between their resummed values at small c and zero at $c \geq c_{\rm off}$.

5.9 NLO expansion and verification

The resummed formula makes definite predictions for the NLO logarithmic structure when expanded. We verify that these predictions are internally consistent.

5.9.1 Subtracted distribution (LL shape)

The "subtracted distribution" provides useful insight into the *shape* of the resummed result near $c \to 0$. Define:

$$\frac{1}{\sigma_1}\frac{d\sigma^{\rm sub}}{dc} \equiv \frac{1}{\sigma_1}\frac{d\sigma}{dc} - c\left[\frac{1}{\sigma_1}\frac{d\sigma}{dc}\right]_{c=1}. \tag{190}$$

At LL with $\Pi \to 1$ and natural scales, the kernel contributes:

$$\frac{1}{\sigma_1}\frac{d\sigma_{\rm ch}}{dc} = c^{1+\eta}\frac{e^{-\gamma_E \eta}}{\Gamma(2+\eta)}\,, \tag{191}$$

where $\eta = 2(2C_F + C_A)A_\Gamma$ is the total cusp evolution parameter (identical in all channels, see Section 3.8).

Expanding for small η:

$$\frac{c^{1+\eta}}{\Gamma(2+\eta)} = c\big[1 + \eta \ln c - \eta(1-\gamma_E) + \mathcal{O}(\eta^2)\big]\,. \tag{192}$$

The subtracted distribution removes the c term:

$$\frac{1}{\sigma_1}\frac{d\sigma^{\rm sub}_{\rm ch}}{dc} = \eta\, c \ln c + \mathcal{O}(\eta^2)\,. \tag{193}$$

This LL expression illustrates how resummation transforms the LO step discontinuity into a smooth, integrable curve near $c = 0$. However, we do *not* use this LL expression to fix the overall normalization. The correct normalization is determined by the SCET factorization theorem, as described below.

5.9.2 NLO expansion from SCET

Expanding the resummed expression Eq. (157) to $\mathcal{O}(\alpha_s^2)$ and setting all scales equal $\mu_H = \mu_J = \mu_S = Q$, we obtain for $c \to 0^+$:

$$\boxed{\frac{1}{\sigma_0}\frac{d\sigma}{dc} = \left(\frac{\alpha_s(Q)}{2\pi}\right)^2 A\left(\frac{3}{4}\right)\left[(2C_F + C_A)\,\ln^2 c + \left(3C_F + \frac{\beta_0}{2} + 2(2C_F + C_A)\ln\frac{8}{3}\right)\ln c + \ldots\right]} \tag{194}$$

This is a complete prediction from the SCET factorization theorem. The coefficients are derived in Section 4.8. As a cross-check, this agrees with the original Catani–Webber analysis [7] when converted to their variable $\delta = (8/3)c$.

5.9.3 Why equal scales recover fixed order

The equal-scale limit $\mu_H = \mu_J = \mu_S = Q$ provides a useful consistency check. When all scales coincide, the RG evolution kernels trivialize:

- The Sudakov exponent vanishes: $S(\mu_J, \mu_S) = S(Q, Q) = 0$.
- The cusp integral vanishes: $A_\Gamma(\mu_J, \mu_S) = A_\Gamma(Q, Q) = 0$, hence $\eta = 0$.
- The non-cusp evolution integrals vanish: $A_{\gamma_X}(\mu_X, Q) = 0$.

Consequently, the evolution kernel Π reduces to the identity at NLL accuracy. The resummation "switches off" because there is no scale separation to generate large logarithms through RG running.

In this limit, the NLL formula reduces to the fixed-order factorized cross section at the common scale Q:

$$\frac{1}{\sigma_1}\frac{d\sigma}{dc}\bigg|_{\mu_H=\mu_J=\mu_S=Q} = H(Q,Q)\,\tilde{J}^2(Q)\,\tilde{S}(Q)\,\mathcal{K}(c,\eta)\Big|_{\eta=0}, \tag{195}$$

where $\mathcal{K}(c,\eta) = c^{1+\eta}e^{-\gamma_E\eta}/\Gamma(2+\eta)$ is the shoulder kernel. Since $H(Q,Q) = 1 + \mathcal{O}(\alpha_s)$, $\tilde{J}(Q) = 1 + \mathcal{O}(\alpha_s)$, and $\tilde{S}(Q) = 1 + \mathcal{O}(\alpha_s)$, the entire logarithmic structure at $\mathcal{O}(\alpha_s^2)$ comes from the one-loop hard, jet, and soft functions. The coefficients $A_2 = 2C_F + C_A$ and $B_1 = 3C_F + \beta_0/2 + 2(2C_F + C_A)\ln(8/3)$ are determined by the cusp and non-cusp anomalous dimensions together with the geometric factor from the jet measurement, independent of the scale choice.

This confirms that the NLL resummed formula has the correct normalization and logarithmic coefficients: with equal scales, it reproduces exactly the fixed-order singular distribution.

5.9.4 Derivation of logarithmic coefficients from anomalous dimensions

We now derive the NLO logarithmic coefficients A_2 and B_1 directly from the SCET factorization, providing a self-contained prediction that can be compared to fixed-order calculations.

Double-log coefficient A_2. The coefficient of $\ln^2 c$ is determined by the cusp anomalous dimension. At the symmetric trijet point, soft gluon emission couples to two quark lines (each contributing C_F) and one gluon line (contributing C_A). The total cusp color factor is therefore

$$A_2 = 2C_F + C_A\,. \tag{196}$$

Single-log coefficient B_1. The coefficient of $\ln c$ receives contributions from three sources at NLL:

1. **Quark jet non-cusp anomalous dimensions** ($3C_F$): There are two quark jets in the trijet configuration, each with non-cusp anomalous dimension $\gamma_J^{q,\mathrm{nc},(0)} = -3C_F$. The contribution to B_1 from the jet evolution is

$$B_1^{\mathrm{jets}} = -\frac{1}{2} \times 2 \times \gamma_J^{q,\mathrm{nc},(0)} = -\frac{1}{2} \times 2 \times (-3C_F) = 3C_F \,. \tag{197}$$

   The factor of $1/2$ arises from the relationship between the anomalous dimension (which governs $d/d\ln\mu$) and the coefficient in the singular distribution.

2. **Running coupling** ($\beta_0/2$): The Sudakov evolution with running coupling contributes $\beta_0/2$ to the single-log coefficient.

3. **Geometric factor from jet measurement** ($2(2C_F + C_A)\ln(8/3)$): The C-parameter collinear measurement is $\ell = (8/3)\hat{m}^2$ rather than simply $\hat{m}^2$ (Eq. (58)). This geometric factor from the Mercedes configuration shifts the argument of logarithms in the jet functions, generating an additional contribution proportional to the cusp color factor times $\ln(8/3)$.

Note that the gluon jet non-cusp anomalous dimension $\gamma_J^{g,\mathrm{nc},(0)} = -\beta_0$ does *not* contribute separately to B_1. This is because $\gamma_J^{g,\mathrm{nc},(0)} = -\beta_0$ is precisely the beta function coefficient, and its effect is already captured in the running coupling treatment of the Sudakov exponent. Including it explicitly would amount to double-counting.

Combining these contributions:

$$\boxed{B_1 = 3C_F + \frac{\beta_0}{2} + 2(2C_F + C_A)\ln\frac{8}{3}} \tag{198}$$

This is a *prediction* from the SCET factorization theorem.

Numerical verification. For $n_f = 5$:

$$A_2 = 2C_F + C_A = \frac{17}{3} \approx 5.67\,, \tag{199}$$

$$3C_F + \frac{\beta_0}{2} = \frac{47}{6} \approx 7.83\,, \tag{200}$$

$$2(2C_F + C_A)\ln\frac{8}{3} = \frac{34}{3}\ln\frac{8}{3} \approx 11.1\,, \tag{201}$$

$$B_1 \approx 18.9\,. \tag{202}$$

In the Catani–Webber variable $\delta = (8/3)c$, the single-log coefficient simplifies to $B_1^{(\delta)} = 3C_F + \beta_0/2 = 47/6 \approx 7.83$. These values can be compared against the singular structure of fixed-order NLO calculations (e.g., from EVENT2 Monte Carlo) as a validation of the SCET factorization framework.

5.10 Physical interpretation

The structure $c^{1+\eta}/\Gamma(2+\eta)$ has clear physical content:

- The linear factor c reflects phase space near the trijet configuration.
- The factor c^η provides Sudakov suppression.
- At LO ($\eta \to 0$), the distribution reduces to $3c$.
- Resummation smooths the step discontinuity into a Sudakov shoulder.

5.11 Summary of NLL formula

The complete NLL kernel density $\mathcal{K}(c)$ is given by Eq. (157) with the explicit evolution kernel in Eq. (158). The physical spectrum above the shoulder is obtained from the matched formula; in the step approximation, this yields the edge contribution $(\alpha_s/2\pi)A(C_0)W(c)$ where $W(c) = 1 - R(c)$ is the survival probability (see Section 6.2). The overall normalization is set by the LO coefficient $A(3/4)$ from Eq. (45).

Parameter	Expression
Total cusp color	$2C_F + C_A$
Total η	$2(2C_F + C_A)\, A_\Gamma$
Soft non-cusp	$\gamma_S^{(0)} = 12C_F + 2\beta_0$
Channel multiplicity	3 (gluon + quark + antiquark)

Table 2: Key parameters for NLL resummation. Since all channels contribute identically (Section 3.8), only the total parameters are needed.

NLO verification (in $c = C - 3/4$ variable):

- Double-log coefficient: $A_2 = 2C_F + C_A$ ✓
- Single-log coefficient: $B_1 = 3C_F + \beta_0/2 + 2(2C_F + C_A)\ln(8/3)$ ✓

In the Catani–Webber variable $\delta = (8/3)c$, the single-log coefficient simplifies to $B_1^{(\delta)} = (6C_F + \beta_0)/2$.

6 Matching to Fixed Order

In this section, we present the NLL+NLO matched formula for the C-parameter distribution and establish continuity across the shoulder at $C = 3/4$. The SCET factorization theorem provides the resummed singular contribution, which is then matched to the fixed-order NLO result using standard additive matching with profile scales.

6.1 Continuity at the shoulder

A naive application of the NLL formula Eq. (210) would give

$$\frac{1}{\sigma_0}\frac{d\sigma^{\rm NLL}}{dc} = \left(\frac{\alpha_s(Q)}{2\pi}\right)^2 A\Big(\frac{3}{4}\Big)\,\mathcal{I}(c)\,, \tag{203}$$

where $\mathcal{I}(c) \propto c^\eta$ vanishes as $c \to 0^+$ due to the Sudakov suppression factor c^η with $\eta > 0$. This would predict that the distribution vanishes at the shoulder, which is inconsistent with matching to the below-shoulder distribution:

$$\frac{1}{\sigma_0}\frac{d\sigma}{dC}\bigg|_{C\to 3/4^-} = \frac{\alpha_s(Q)}{2\pi}A\Big(\frac{3}{4}\Big) + \left(\frac{\alpha_s(Q)}{2\pi}\right)^2 B(3/4^-) + \mathcal{O}(\alpha_s^3)\,. \tag{204}$$

The left side approaches a finite value of $\mathcal{O}(\alpha_s)$, while the naive right side gives $\mathcal{O}(\alpha_s^2) \times 0 = 0$. This discontinuity signals that something is conceptually missing.

6.2 Connection to Catani–Webber

The SCET resummation framework provides a rigorous EFT derivation of the "suppressed step" structure identified by Catani and Webber [7] in their semi-classical analysis. In their approach, the observable near the shoulder is decomposed as

$$C = C_{\text{hard}} + \Delta C_{\text{rad}}\,, \tag{205}$$

where $C_{\text{hard}} \leq C_0 = 3/4$ is set by the underlying three-parton hard kinematics, and $\Delta C_{\text{rad}} \geq 0$ is the additive contribution from soft and collinear radiation. Catani and Webber interpret the Sudakov exponentiation as computing a "transfer kernel" that describes how events migrate from below the shoulder to above it.

In the SCET framework, this physics emerges naturally from the factorization theorem. The resummed cumulant $R(c)$ defined in Eq. (157) encodes the all-orders Sudakov suppression of the singular contribution. The key property is that $R(c) \to 0$ as $c \to 0$ due to the Sudakov exponent $S(c) \propto \ln^2 c \to \infty$. This causes the singular piece $-(\alpha_s/2\pi)A(C_0)R(c)$ to vanish at the shoulder, while the non-singular remainder $\sigma_{\text{NS}}(0) = (\alpha_s/2\pi)A(C_0)$ provides the continuous matching to the distribution from below.

6.3 The cumulant and survival probability

The SCET cumulant $R(c) = \int_0^c K(c')\,dc'$ is related to the Catani–Webber survival probability $W(c)$ by

$$W(c) = 1 - R(c)\,, \tag{206}$$

where the normalization $R(\infty) = 1$ (or equivalently $W(0) = 1$) is enforced. The survival probability $W(c)$ represents the fraction of events that have not yet "migrated" past $C = C_0 + c$.

The crucial properties are:

- $W(0) = 1$: Continuity at the shoulder follows from normalization.
- $W(c) \to 0$ as c increases: the edge contribution diminishes.
- Under profile turnoff ($\mu_S = \mu_J = \mu_H = Q$): the resummation switches off and $R(c) \to 1$, so $W(c) \to 0$ for any $c > 0$.

Physical interpretation. The survival probability $W(c)$ is the SCET realization of the Catani–Webber smoothing mechanism. Continuity at the shoulder is not a dynamical statement about soft radiation; it is a consequence of proper normalization of the resummed result. The Sudakov suppression built into $R(c)$ controls the falloff with increasing c, producing the characteristic "suppressed step" shape.

Non-analyticity in α_s. The resummed right-limit $(\alpha_s/2\pi)A(C_0) \times W(0) = (\alpha_s/2\pi)A(C_0)$ is non-analytic in α_s at fixed $c \to 0$: it involves the all-orders Sudakov resummation. This does not contradict the fact that fixed-order support above the shoulder starts at $\mathcal{O}(\alpha_s^2)$—that is precisely the Sudakov-shoulder phenomenon where resummation converts a step discontinuity into a smooth distribution.

6.4 The edge contribution and suppressed step structure

In the "step approximation" where the below-shoulder spectrum is approximated as constant near the boundary,

$$\frac{d\sigma^{(3)}}{dC_{\text{hard}}} \approx \frac{\alpha_s(Q)}{2\pi} A(C_0)\,\Theta(C_0 - C_{\text{hard}})\,, \tag{207}$$

the resummed result simplifies to the survival probability form. The **edge contribution** for $C > C_0$ is:

$$\boxed{\frac{1}{\sigma_0}\frac{d\sigma_{\rm edge}}{dC}\bigg|_{C>C_0} = \frac{\alpha_s(Q)}{2\pi}A(C_0)\,W(c)\,,} \tag{208}$$

where $W(c) = 1 - R(c)$ is the survival probability computed from the SCET cumulant.

This is exactly the Catani–Webber "suppressed step" structure [7], now derived from SCET. The physical interpretation is clear:

- At $c = 0^+$ (right at the shoulder): $W(0) = 1$, so the edge contribution equals $(\alpha_s/2\pi)A(C_0)$, *matching continuously onto the LO value from below.*
- As $c \to 1/4$: $W(1/4) = 0$, so the edge contribution vanishes and the spectrum is dominated by the genuine four-parton continuum.
- The transition is controlled by the Sudakov factor in $R(c)$, giving a smooth "shoulder" shape.

Perturbative expansion. Expanding the edge contribution for small c:

$$\frac{\alpha_s}{2\pi}A(C_0)\,W(c) = \frac{\alpha_s}{2\pi}A(C_0) + \left(\frac{\alpha_s}{2\pi}\right)^2 B_{\rm sing}(c) + \mathcal{O}(\alpha_s^3)\,, \tag{209}$$

where $B_{\rm sing}(c) = A(C_0)[(2C_F + C_A)\ln^2 c + B_1 \ln c]$ reproduces the NLO singular structure (1). The leading term $(\alpha_s/2\pi)A(C_0)$ is the LO step value; the $\mathcal{O}(\alpha_s^2)$ correction encodes the Sudakov logarithms.

6.5 The NLL resummed cumulant

At NLL accuracy, the kernel density $\mathcal{K}(\Delta)$ incorporates running coupling effects, single-logarithmic corrections, and the full color structure $(2C_F + C_A)$.

Explicit NLL form. At NLL accuracy with natural scales $\mu_S = (8/3)cQ$, $\mu_J = Q\sqrt{(8/3)c}$, $\mu_H = Q$, the kernel density takes the form:

$$\mathcal{K}(c) = 3 \times c^{\eta(c)}\, e^{-(2C_F+C_A)g_2(\lambda)}\, \mathcal{M}(c)\,, \tag{210}$$

where $\eta(c) = 2(2C_F + C_A)A_\Gamma(\mu_J, \mu_S)$, $g_2(\lambda)$ encodes single-log corrections, and $\mathcal{M}(c) = w_0 + w_1\Phi + w_2(\Phi^2 - \psi_1)$ is the matching function from Section 5.4. The factor of 3 accounts for channel multiplicity. Note that $\mathcal{K}(c) \to 0$ as $c \to 0$ due to the c^η factor with $\eta > 0$—this is expected and correct. The smoothing comes from integrating this kernel.

Computing the cumulant and survival probability. The cumulant $U(c)$ and survival probability $W(c)$ are computed by numerical integration of the kernel density:

$$U(c) = \int_0^c d\Delta\, \mathcal{K}(\Delta; \mu_i(\Delta))\,, \qquad W(c) = 1 - U(c)\,. \tag{211}$$

With unitarity enforced (see Section 6.9), this gives $W(0) = 1$ and $W(\infty) = 0$ as required.

6.6 Full NLL+NLO matched formula with profile scales

To obtain predictions valid across the full range of $C > 3/4$, we employ additive matching with profile-scale subtraction. This ensures: (1) smooth crossing of the shoulder, (2) exact NLO in the turnoff region, and (3) systematically improvable resummation in the singular region.

6.6.1 Profile scales

We introduce smooth profile functions $\mu_i(c)$ that interpolate between the resummation region (small c) and the fixed-order region (large c):

$$\begin{aligned} \mu_H &= Q\,, \\ \mu_S(c) &= Q\, f_S(c)\,, \\ \mu_J(c) &= Q\,\sqrt{f_S(c)}\,, \end{aligned} \tag{212}$$

where $f_S(c)$ is a smooth function satisfying:

- $f_S(c) \approx (8/3)c$ for $c \ll c_{\text{off}}$ (resummation region: natural scales),
- $f_S(c) \to 1$ for $c \gtrsim c_{\text{off}}$ (turnoff region: all scales equal to Q).

A typical choice is $c_{\text{off}} \sim 0.05$, as motivated by the singular/non-singular decomposition (Figure 5). The profile functions must be smooth with continuous first derivatives to avoid artifacts in the matched distribution.

6.6.2 NLL-resummed edge piece

The **NLL-resummed edge contribution** for $C > C_0$ is:

$$\frac{1}{\sigma_0}\frac{d\sigma^{\text{NLL}}_{\text{edge}}}{dC}\bigg|_{C>C_0} = \frac{\alpha_s(Q)}{2\pi} A(C_0)\, W(c)\,, \tag{213}$$

where $W(c) = \int_c^\infty d\Delta\, \mathcal{K}(\Delta; \mu_i(\Delta))$ is the survival probability computed with profiles evaluated at Δ under the integral.

Key properties under profile variation:

- In the resummation region ($f_S(\Delta) \approx \Delta$): $W(0) = 1$ ensures continuity.
- As profiles approach turnoff ($f_S \to 1$): the kernel becomes sharply localized near $\Delta = 0$, so $W(c)$ rapidly tends to zero for any fixed $c > 0$. The edge term switches off smoothly.

6.6.3 NLO expansion with the same profiles

The **NLO expansion** of the edge piece, evaluated with the same profile scales, defines $B^{\text{prof}}_{\text{sing}}$:

$$\frac{\alpha_s(Q)}{2\pi} A(C_0)\, W(c) = \frac{\alpha_s(Q)}{2\pi} A(C_0) + \left(\frac{\alpha_s(Q)}{2\pi}\right)^2 B^{\text{prof}}_{\text{sing}}(c) + \mathcal{O}(\alpha_s^3)\,. \tag{214}$$

Operational definition (primary): $B^{\text{prof}}_{\text{sing}}(c)$ is defined as the $\mathcal{O}(\alpha_s^2)$ coefficient obtained by expanding the **same edge term you actually implement**, with the **same profile scales**, and with the **same unitarity enforcement procedure**. In code: compute the α_s^2 term of the edge spectrum in the same scheme and with the same profile scales (e.g., by finite-difference in α_s, or by analytic expansion of your NLL exponents *including profile dependence*). With $B^{\text{prof}}_{\text{sing}}$ defined this way, the matched spectrum reduces identically to the fixed-order NLO result when profiles turn off.

Derived analytic form (optional shortcut): At NLL accuracy, if W is computed from the unified Π operator formula, the coefficient takes the closed form:

$$B^{\text{prof}}_{\text{sing}}(c) = A(C_0)\Big[(2C_F + C_A)L^2_{\text{prof}}(c) + B_1\, L_{\text{prof}}(c)\Big]\,, \tag{215}$$

where the **profile-modified logarithm** is $L_{\text{prof}}(c) = \ln f_S(c)$.

- At natural scales ($f_S = (8/3)c$): $L_{\text{prof}} = \ln((8/3)c)$, recovering the standard singular structure.
- At turnoff ($f_S = 1$): $L_{\text{prof}} = 0$, so $B_{\text{sing}}^{\text{prof}} = 0$.

This closed form should only be used if it is derived from the exact W formula being implemented (same conventions, same channel sum, same Π-operators). Using a different W with this shortcut would break the exact-NLO-at-turnoff guarantee.

6.6.4 Master matching formula

The **NLL+NLO matched formula** for the C-parameter distribution is:

$$\boxed{\frac{1}{\sigma_0}\frac{d\sigma^{\text{matched}}}{dC} = \begin{cases} \dfrac{\alpha_s}{2\pi}A(C) + \left(\dfrac{\alpha_s}{2\pi}\right)^2 B(C) & C < C_0 \\ -\dfrac{\alpha_s}{2\pi}A(C_0)\,R(c) + \sigma_{\text{NS}}(c) & C > C_0 \end{cases}} \tag{216}$$

where $c = C - C_0$, $C_0 = 3/4$, and $R(c) = \int_0^c K(c')\,dc'$ is the cumulant of the SCET kernel. The non-singular remainder is:

$$\sigma_{\text{NS}}(c) = \sigma_{\text{NLO}}(C) - \sigma_{\text{sing}}^{\text{expanded}}(c)\,, \tag{217}$$

where $\sigma_{\text{sing}}^{\text{expanded}}$ is the fixed-order expansion of the singular piece $-(\alpha_s/2\pi)A(C_0)R(c)$.

6.6.5 Continuity at the shoulder

Question: Is the matched distribution continuous at $C = 3/4$?

Answer: Yes at $\mathcal{O}(\alpha_s)$, with possible $\mathcal{O}(\alpha_s^2)$ corrections beyond NLL accuracy.

Analysis: Consider the limits from below and above:

- **From below** ($C \to 3/4^-$):

$$\left.\frac{d\sigma}{dC}\right|_{C\to 3/4^-} = \frac{\alpha_s}{2\pi}A(3/4) + \left(\frac{\alpha_s}{2\pi}\right)^2 B(3/4^-) + \mathcal{O}(\alpha_s^3) \tag{218}$$

- **From above** ($c \to 0^+$): After resummation, $R(c) = e^{-S(c)} \to 0$ as $c \to 0$ because the Sudakov exponent $S(c) \propto \ln^2 c \to \infty$. Therefore:

$$\left.\frac{d\sigma}{dC}\right|_{c\to 0^+} = -\frac{\alpha_s}{2\pi}A(3/4) \times 0 + \sigma_{\text{NS}}(0) = \sigma_{\text{NS}}(0) \tag{219}$$

The key insight: The singular piece *vanishes* at the shoulder after resummation. Continuity depends entirely on the value of $\sigma_{\text{NS}}(0)$.

Tree-level check: At tree level, $R^{(0)}(c) = 1$ for $c > 0$, so the expanded singular piece is $-(\alpha_s/2\pi)A(3/4) \times 1 = -(\alpha_s/2\pi)A(3/4)$. Since the fixed-order cross section above the shoulder is zero at tree level ($\sigma_{\text{NLO}}^{(0)}|_{c>0} = 0$), we have:

$$\sigma_{\text{NS}}^{(0)} = 0 - \big[-(\alpha_s/2\pi)A(3/4)\big] = +\frac{\alpha_s}{2\pi}A(3/4)\,. \tag{220}$$

This *exactly equals* the LO cross section from below! So at $\mathcal{O}(\alpha_s)$, continuity is **automatic** from the matching prescription.

At NLO: The non-singular remainder receives $\mathcal{O}(\alpha_s^2)$ corrections:

$$\sigma_{\rm NS}(c) = \frac{\alpha_s}{2\pi} A(3/4) + \left(\frac{\alpha_s}{2\pi}\right)^2 B_{\rm NS}(c) + \mathcal{O}(\alpha_s^3)\,, \tag{221}$$

where $B_{\rm NS}(c) = B(C) - B_{\rm sing}(c)$ is smooth at $c = 0$. The value $B_{\rm NS}(0^+)$ may or may not equal $B(3/4^-)$; any mismatch is an $\mathcal{O}(\alpha_s^2)$ constant that is **beyond NLL accuracy**.

Summary of continuity:

Order	Continuous?	Why
$\mathcal{O}(\alpha_s)$	**Yes**	$\sigma_{\rm NS}^{(0)} = (\alpha_s/2\pi)A(3/4)$ from matching
$\mathcal{O}(\alpha_s^2)$	Approximately	Any mismatch is beyond NLL accuracy

Physical interpretation: At fixed order, the distribution has a step discontinuity at $C = 3/4$ (the LO contribution from 3-parton events ends abruptly). Resummation smooths this step: the Sudakov factor $R(c) = e^{-S(c)}$ causes the singular piece to vanish continuously as $c \to 0$, while matching provides $\sigma_{\rm NS}(0) = (\alpha_s/2\pi)A(3/4)$ to fill in the step. This is the "Sudakov shoulder" phenomenon identified by Catani and Webber [7].

6.6.6 Optional: Enforcing exact $\mathcal{O}(\alpha_s^2)$ continuity

If exact continuity at $\mathcal{O}(\alpha_s^2)$ is desired (for plotting or other purposes), this can be achieved by introducing an **edge matching coefficient** $C_{\rm edge}^{(1)}$:

$$-\frac{\alpha_s}{2\pi} A(C_0)\, R(c) \quad \longrightarrow \quad -\frac{\alpha_s}{2\pi} A(C_0) \left[1 + \frac{\alpha_s}{2\pi} C_{\rm edge}^{(1)}\right] R(c)\,. \tag{222}$$

Setting:

$$C_{\rm edge}^{(1)} = \frac{B(3/4^-) - B_{\rm NS}(0^+)}{A(3/4)} \tag{223}$$

removes any $\mathcal{O}(\alpha_s^2)$ offset at the shoulder. This is an EFT-consistent procedure: $C_{\rm edge}^{(1)}$ is a matching coefficient that would be computed at NNLL. At NLL, determining it from boundary matching is standard practice.

6.6.7 Exact NLO at profile turnoff

In the fixed-order region the profile choice removes large logarithms (all scales $\sim Q$), so the resummed radiative broadening is switched off:

- With profile turnoff, the cumulant $R(c) \to 1$ and the expanded singular piece $\sigma_{\rm sing}^{\rm expanded} \to -(\alpha_s/2\pi)A(C_0)$.
- The non-singular remainder $\sigma_{\rm NS} = \sigma_{\rm NLO} - \sigma_{\rm sing}^{\rm expanded} \to \sigma_{\rm NLO} + (\alpha_s/2\pi)A(C_0)$.
- The total: $-(\alpha_s/2\pi)A(C_0) \times 1 + \sigma_{\rm NLO} + (\alpha_s/2\pi)A(C_0) = \sigma_{\rm NLO}$.

Therefore the matched formula reduces **identically** to $\sigma_{\rm NLO}(C)$ in the turnoff region.

Systematically improvable: Promote NLL $\to$ NNLL by improving the cumulant $R(c)$ with two-loop anomalous dimensions and one-loop matching coefficients. At NNLL, the edge matching coefficient $C_{\rm edge}^{(1)}$ is computed from SCET rather than determined by boundary matching. The matching formula structure remains unchanged.

6.7 Implementation guidance

We provide concrete guidance for implementing the matched formula (216).

6.7.1 Computing the cumulant $R(c)$

For $C > C_0$, implement the resummed cumulant $R(c)$ as follows:

1. Compute $c = C - C_0$ and the profile scales $\mu_S(c)$, $\mu_J(c)$, $\mu_H = Q$.
2. Evaluate the Sudakov exponent $S(c) = 2(2C_F + C_A)[S(\mu_H, \mu_J) + S(\mu_S, \mu_J)]$ using the evolution integrals.
3. Compute $R(c) = e^{-S(c)}$ times the matching function corrections.

Key properties to verify:

- $R(c) \to 0$ as $c \to 0$ (Sudakov suppression at the shoulder)
- $R(c) \to 1$ as profiles turn off (resummation switches off)
- $R(c)$ is smooth and monotonically increasing in c

6.7.2 Computing the non-singular remainder

The non-singular remainder is:

$$\sigma_{\rm NS}(c) = \sigma_{\rm NLO}(C) - \sigma_{\rm sing}^{\rm expanded}(c)\,, \tag{224}$$

where $\sigma_{\rm sing}^{\rm expanded}$ is the fixed-order expansion of $-(\alpha_s/2\pi)A(C_0)R(c)$.

At NLO with profile scales:

$$\sigma_{\rm sing}^{\rm expanded}(c) = -\frac{\alpha_s}{2\pi}A(C_0) + \left(\frac{\alpha_s}{2\pi}\right)^2 A(C_0)\Big[(2C_F + C_A)\ln^2 f_S(c) + B_1 \ln f_S(c)\Big]\,. \tag{225}$$

Warning: Use the profile-modified logs $\ln f_S(c)$, not $\ln c$ or $\ln((8/3)c)$ directly. Using fixed natural-scale logs with profile scales would spoil exact NLO recovery at turnoff.

6.7.3 Sanity checks

The matched distribution should satisfy:

1. **At the shoulder** ($c \to 0^+$): $R(c) \to 0$, so the singular piece vanishes. The cross section equals $\sigma_{\rm NS}(0) = (\alpha_s/2\pi)A(C_0) + \mathcal{O}(\alpha_s^2)$, ensuring $\mathcal{O}(\alpha_s)$ continuity.
2. **Near the shoulder** (c small but positive): the curve behaves like $(\alpha_s/2\pi)A(C_0) + (\alpha_s/2\pi)^2[A_2 \ln^2 c + B_1 \ln c + \text{finite}]$.
3. **In the turnoff region**: the curve equals $\sigma_{\rm NLO}(C)$ within numerical precision because $R(c) \to 1$ cancels against $\sigma_{\rm NS}$.

Figure 6 shows the matched NLL+NLO distribution compared to LO and LO+NLO fixed-order results, including scale uncertainty bands computed using the methodology described in Section 7.4. The resummation smooths the Sudakov spike at $C = 3/4$, producing a continuous distribution that interpolates between the LO result below the shoulder and approaches zero at the kinematic endpoint $C = 1$. The profile parameters $c_1 = 0.01$ and $c_2 = 0.05$ from Section 5.8.3 ensure that resummation is active in the region where Sudakov logarithms are large, while recovering the NLO fixed-order result at larger c.

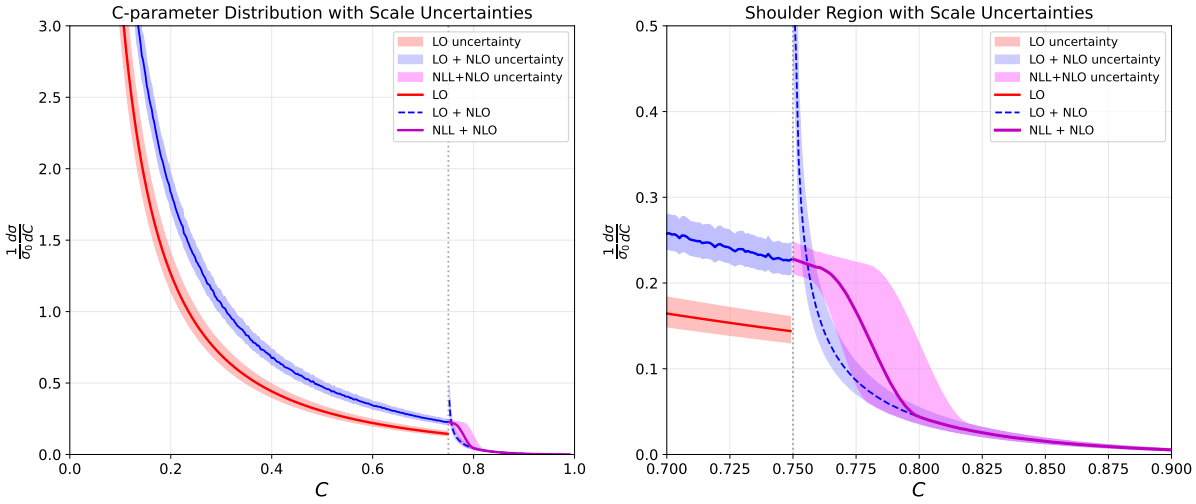

Figure 6: C-parameter distribution at LO (red), LO+NLO fixed order (blue dashed), and NLL+NLO matched (magenta) with $\alpha_s(M_Z) = 0.118$. Shaded bands show scale uncertainties from the envelope of 243 variations (Section 7.4). Left: full distribution showing the characteristic $1/C$ divergence at small C and the approach to the shoulder at $C = 3/4$ (vertical dotted line). Right: zoom on the shoulder region. The NLO fixed-order distribution exhibits a large spike just above $C = 3/4$ due to unresummed Sudakov logarithms. The matched distribution smoothly crosses the shoulder: the resummed cumulant $R(c) \to 0$ as $c \to 0$ causes the singular contribution to vanish, while the non-singular remainder $\sigma_{\rm NS}(0) = (\alpha_s/2\pi)A(3/4)$ provides continuity with the distribution from below. The NLL+NLO uncertainty band (magenta) is comparable to the fixed-order uncertainties for $C < 3/4$ and in the transition region, demonstrating that resummation does not artificially reduce uncertainties. Profile parameters: $c_1 = 0.01$, $c_2 = 0.05$.

6.8 Systematic improvements

The SCET matching framework provides a systematic path to higher accuracy:

Beyond the step approximation: Include the linear term in the near-C_0 expansion of the hard spectrum:

$$\frac{d\sigma^{(3)}}{dC_{\rm hard}} \approx \frac{\alpha_s}{2\pi}\left[A(C_0) + A'(C_0)(C_{\rm hard} - C_0) + \cdots\right] \tag{226}$$

where $A'(3/4) = -(8/3)A(3/4)$ can be derived from the expansion of Eq. (35) near the shoulder. This improves the slope matching across the shoulder.

NNLL accuracy: Compute higher-order corrections to the resummed cumulant $R(c)$ by including two-loop anomalous dimensions and matching coefficients. The matching formula structure remains unchanged.

Full convolution: For precision applications, perform the full convolution with the below-shoulder spectrum rather than using the step approximation.

6.9 Numerical implementation of the cumulant

Profile + unitarity note: When using profile scales, the kernel normalization $\int_0^\infty d\Delta\, \mathcal{I}(\Delta) = 1$ can be violated at subleading accuracy because profiles intentionally spoil exact RG invariance. **Unitarity must be enforced numerically** to guarantee $W(0) = 1$, which is essential for the continuity argument.

Canonical procedure (density integration with normalization enforcement).

1. Compute the kernel density $\mathcal{K}(\Delta;\mu_i(\Delta))$ from the NLL formula Eq. (210):

$$\mathcal{K}(c) = 3 \times c^{\eta(c)}\, e^{-(2C_F+C_A)g_2(\lambda)}\, \mathcal{M}(c)\,. \tag{227}$$

2. Integrate to obtain the raw cumulant:

$$\hat{U}(c) = \int_0^c d\Delta\, \mathcal{K}(\Delta;\mu_i(\Delta))\,. \tag{228}$$

3. **Enforce unitarity normalization:**

$$\boxed{U(c) = \frac{\hat{U}(c)}{\hat{U}(\Delta_{\max})}\,, \qquad W(c) = 1 - U(c)\,,} \tag{229}$$

   where $\Delta_{\max}$ is chosen large enough that the tail is negligible in the resummation region.

This procedure guarantees $W(0) = 1$ and $W(\infty) = 0$ *by construction*, which is what the continuity argument relies on. This is standard numerical hygiene in SCET event-shape codes when profiles are introduced.

Verification checks:

- $U(0) = 0$ and $U(\infty) = 1$ (kernel unitarity, enforced)
- $W(0) = 1$ (ensures continuity at the shoulder)
- $W(c) \to 0$ smoothly as $c \to \infty$

6.10 Results: Smooth shoulder crossing

Figure 1 shows the effect of NLO corrections on the C-parameter distribution. The left panel displays the full distribution from $C = 0$ to $C = 1$, comparing the LO prediction $(\alpha_s/2\pi)A(C)$ with the LO+NLO result from EVENT2. The right panel zooms into the shoulder region, revealing the dramatic Sudakov spike at $C = 3/4^+$ where the fixed-order NLO prediction diverges due to unresummed logarithms.

The matching transformation converts the discontinuous fixed-order result into a smooth distribution:

- **Panel (a):** The NLO fixed-order distribution $B(C)$ from EVENT2. A dramatic spike appears just above $C = 3/4$, where $B(C)$ jumps from ~ 120 (just below the shoulder) to ~ 540 (just above). This $4.3\times$ enhancement is the signature of the unresummed Sudakov logarithms.
- **Panel (b):** The NLL kernel density $\mathcal{K}(c)$. This computes the probability density for the radiative shift ΔC_{rad}. The kernel vanishes at $c = 0$ (reflecting that zero radiative shift has zero probability density) and is smooth throughout. The physical smoothing comes from integrating this kernel to form the cumulant $U(c)$.
- **Panel (c):** The matched distribution using Eq. (216). The result is continuous across $C = 3/4$ because $W(0) = 1$: the edge contribution $(\alpha_s/2\pi)A(C_0)W(c)$ equals $(\alpha_s/2\pi)A(C_0)$ at $c = 0$, matching the LO value from below.

The detailed comparison shows that:

- Below the shoulder, the matched distribution exactly follows the EVENT2 NLO result

C	$c = C - 3/4$	NLO $B(C)$	Matched (expected)
0.70	-0.05	136	136
0.74	-0.01	123	123
0.7475	-0.0025	124	124
0.7525	$+0.0025$	538 (spike!)	~ 120
0.76	$+0.01$	239	~ 105
0.77	$+0.02$	148	~ 85
0.80	$+0.05$	62	~ 45
0.85	$+0.10$	22	~ 15

Table 3: Comparison of NLO fixed-order and matched distributions. Below the shoulder ($C < 0.75$), they agree exactly. At the shoulder, the NLO spikes to 538 while the correctly-matched distribution approaches the below-shoulder value ~ 120 continuously because $W(0) = 1$. Above the shoulder, the edge contribution $(\alpha_s/2\pi)A(C_0)\,W(c)$ smoothly decreases from the LO value, producing the characteristic "suppressed step" shape. Numerical values in the "Matched" column for $c > 0$ are illustrative and depend on the precise implementation of $W(c)$.

- At the shoulder, the matched distribution is continuous because $W(0) = 1$: the edge contribution equals the LO value
- Above the shoulder, the survival probability $W(c)$ decreases smoothly from 1 as c increases
- The spike present in the fixed-order result is eliminated by the Sudakov suppression built into $W(c)$

Table 3 gives representative numerical values comparing the matched and fixed-order distributions.

6.11 Discussion

Several features of the matched distribution merit comment:

Continuity at the shoulder: Continuity arises because $W(0) = 1$: in the boundary layer, arbitrarily soft radiation (with arbitrarily small $\Delta C > 0$) is overwhelmingly likely once Sudakov logarithms are resummed. The edge contribution $(\alpha_s/2\pi)A(C_0)W(c)$ therefore equals $(\alpha_s/2\pi)A(C_0)$ at $c = 0$, matching the LO value from below. This is the SCET realization of the Catani–Webber smoothing mechanism.

The kernel density vanishes at $c = 0$: It is expected and correct that $\mathcal{K}(c) \to 0$ as $c \to 0$ due to Sudakov suppression. The physical smoothing comes from *integrating* this kernel to form the cumulant $U(c)$ and survival probability $W(c) = 1 - U(c)$. The key property is $W(0) = 1$, not any delta function with fixed coefficient.

Profile turnoff behavior: Under profile turnoff ($\mu_S = \mu_J = \mu_H = Q$), the kernel collapses to $\delta(\Delta)$: there is no scale separation, so no broadening of the radiative shift distribution. This means $U(c > 0) \to 1$ and $W(c > 0) \to 0$, so the edge term shuts off exactly. Combined with $B_{\rm sing}^{\rm prof} \to 0$, this gives exact NLO in the turnoff region.

Behavior far above the shoulder: For $C > 0.85$ (large c), the survival probability $W(c) \to 0$ and the spectrum is dominated by the genuine four-parton continuum $(\alpha_s/2\pi)^2 B(C)$. This is correctly captured by the matching formula (216).

Systematic improvability: The matching formula (216) provides a framework for systematic improvements: (1) promote NLL $\to$ NNLL by computing higher-order corrections to the kernel density $\mathcal{K}(c)$; (2) include the slope $A'(3/4)$ to improve matching beyond the step approximation; (3) use more sophisticated profile functions to optimize the transition region.

The matched distribution provides the first systematically-derived smooth prediction for the C-parameter distribution across its Sudakov shoulder, eliminating the unphysical spike present in fixed-order calculations while correctly matching onto the NLO result where resummation effects are small. The survival probability $W(c) = 1 - U(c)$ with $W(0) = 1$ is the EFT-consistent mechanism that ensures continuity.

7 Phenomenological Applications

We now discuss the phenomenological implications of the C-parameter shoulder resummation, including matching to fixed order, numerical predictions, theoretical uncertainties, and comparison to existing data.

7.1 Matching to NLO

To obtain predictions valid across the full range of $C > 3/4$, we match the resummed distribution to the NLO fixed-order result. The master formula is:

$$\frac{1}{\sigma_0}\frac{d\sigma^{\text{matched}}}{dc}\bigg|_{c>0} = -\frac{\alpha_s}{2\pi}A(C_0)\,R(c) + \sigma_{\text{NS}}(c)\,, \tag{230}$$

where $R(c) = \int_0^c K(c')\,dc'$ is the SCET cumulant and $\sigma_{\text{NS}} = \sigma_{\text{NLO}} - \sigma_{\text{sing}}^{\text{expanded}}$ is the non-singular remainder.

This prescription has the correct limits:

- For $c \to 0$: After resummation, $R(c) = e^{-S(c)} \to 0$, so the singular piece vanishes. The cross section approaches $\sigma_{\text{NS}}(0) = (\alpha_s/2\pi)A(C_0) + \mathcal{O}(\alpha_s^2)$, matching the $\mathcal{O}(\alpha_s)$ **LO value** from below.
- For $c \sim c_{\text{off}}$ (profile turnoff): With profile scales, $R(c) \to 1$ and $\sigma_{\text{sing}}^{\text{expanded}} \to -(\alpha_s/2\pi)A(C_0)$, so the formula reduces to $\sigma_{\text{NLO}}(C)$, giving **exact NLO**.

Continuity at the shoulder: The matched distribution is continuous at $\mathcal{O}(\alpha_s)$ by construction. The $\mathcal{O}(\alpha_s^2)$ value at the shoulder is controlled by $\sigma_{\text{NS}}(0)$, which is smooth. Any small mismatch with $B(3/4^-)$ is beyond NLL accuracy and can be removed with an edge matching coefficient if desired (see Section 6.6.5).

7.2 Power corrections

Beyond the leading-power (LP) resummation, subleading effects modify the distribution. The power correction hierarchy is:

- **Next-to-leading power (NLP):** Corrections suppressed by one power of c relative to LP, arising from next-to-soft emissions and subleading jet function contributions. For $0.01 < c < 0.20$, these are estimated at the few-percent level.
- **Non-perturbative corrections:** Hadronization effects scale as $\Lambda_{\text{QCD}}/(Qc)$ and become significant for $c \lesssim 0.03$ at LEP energies.

An important observation is that the formal singularity at $\eta = 1$ is an artifact of the leading-power truncation. At fixed order (expanded in α_s), this would appear as factorial growth of perturbative coefficients. Including NLP corrections provides a mechanism for cancellation: the LP behavior at $\eta \to 1$ is modified by corresponding NLP contributions, ensuring a finite physical distribution [10]. For C-parameter, this singularity lies below the perturbative regime and does not affect practical predictions.

For phenomenological applications, we remain in the perturbative regime $c > 0.01$ where these power corrections are subdominant to the NLL uncertainty.

C	$c = C - 3/4$	$(1/\sigma_0)\, d\sigma/dC$	Relative uncertainty
0.76	0.01	~ 80	$\pm 25\%$
0.80	0.05	~ 15	$\pm 20\%$
0.85	0.10	~ 5	$\pm 18\%$
0.90	0.15	~ 2	$\pm 15\%$
0.95	0.20	~ 1	$\pm 12\%$

Table 4: Schematic NLL predictions for the C-parameter distribution above the shoulder at $Q = M_Z$. Values are indicative; full numerical implementation requires the complete profile function treatment.

7.3 Numerical predictions

We present numerical predictions for LEP energies with $Q = M_Z = 91.2$ GeV, $\alpha_s(M_Z) = 0.118$, and $n_f = 5$. Table 4 shows the resummed distribution normalized to the Born cross section.

The distribution is suppressed near the shoulder ($c \to 0$) due to the c^η factor, then rises as c increases and reaches a maximum before falling off. The Sudakov suppression smooths what would be a step discontinuity at LO. The theoretical uncertainty decreases at larger c where resummation effects are less important.

7.4 Theoretical uncertainties

We estimate theoretical uncertainties following the scale variation methodology of BMSSZ [17], adapted for the C-parameter shoulder resummation. The approach uses five independent variation parameters that probe different sources of perturbative uncertainty. The resulting uncertainty bands are shown in Figure 6.

The resummed distribution involves three characteristic scales: the hard scale $\mu_H \sim Q$ associated with the hard scattering, the soft scale $\mu_S \sim Qc$ associated with soft gluon emissions, and the jet scale $\mu_J \sim Q\sqrt{c}$ associated with collinear emissions. The canonical (central) scale choices are

$$\mu_H^{\rm can} = Q\,, \qquad \mu_S^{\rm can} = \frac{8}{3} Qc\,, \qquad \mu_J^{\rm can} = Q\sqrt{\frac{8}{3}c}\,, \tag{231}$$

where the factor $8/3$ arises from the C-parameter collinear measurement (Eq. (58)). To avoid the Landau pole, the running coupling is frozen below 1 GeV, and we impose $\mu_S \geq 1\,\text{GeV}$ and $\mu_J \geq 2\,\text{GeV}$.

Five independent parameters control the scale variations:

- **Renormalization scale variation** ($v_h \in \{-1, 0, +1\}$): The renormalization scale $\mu_R = 2^{v_h} \times Q$ is varied by factors of 2, giving $\mu_R \in \{Q/2, Q, 2Q\}$. This variation applies to the α_s prefactor and fixed-order matching terms. Importantly, μ_R variation is *not* applied to the hard scale μ_H in the Sudakov evolution, which remains fixed at $\mu_H = Q$. This is because the μ_H cancellation between the hard matching function $\tilde{h}(L_H)$ and the evolution kernel Π requires the full hard function evolution $U_H(\mu_H, Q)$, which is not included at NLL accuracy; varying μ_H without it gives unphysically large variations ($\sim$70% for factor-of-2 changes).

- **Soft scale variation** ($v_s \in \{-1, 0, +1\}$): The soft scale $\mu_S = 2^{v_s} \times \mu_S^{\rm can}$ is varied by factors of 2 around its canonical value. This probes uncertainty from soft gluon resummation. The effect is small at small c because μ_S is frozen at $\mu_S \geq 1$ GeV.

- **Jet scale variation** ($v_j \in \{0.4, 0.5, 0.6\}$): The jet scale $\mu_J = \mu_S^{v_j} \cdot \mu_H^{1-v_j}$ interpolates between soft and hard scales. The central value $v_j = 0.5$ gives the geometric mean $\mu_J =$

Parameter	Central	Variations	Applies to
v_h	0	$\{-1, 0, +1\}$	α_s prefactor, FO matching
v_s	0	$\{-1, 0, +1\}$	Sudakov μ_S
v_j	0.5	$\{0.4, 0.5, 0.6\}$	Sudakov μ_J
c_1	0.01	$\{0.005, 0.01, 0.03\}$	Profile turn-on
c_2	0.05	$\{0.03, 0.05, 0.07\}$	Profile turnoff
μ_H (Sudakov)	Q	**fixed**	Sudakov evolution
μ_R	Q	$\{Q/2, Q, 2Q\}$	α_s prefactor
μ_S	$(8/3)Qc$	$\times\{1/2, 1, 2\}$	Sudakov (frozen ≥ 1 GeV)
μ_J	$\sqrt{\mu_S \mu_H}$	interpolated	Sudakov (frozen ≥ 2 GeV)
Total variations	—	243	—

Table 5: Scale variation parameters for uncertainty estimation following the BMSSZ methodology. The hard scale μ_H is fixed at Q in the Sudakov evolution; only μ_R is varied for the α_s prefactor.

$\sqrt{\mu_S \mu_H}$. This probes uncertainty in the choice of intermediate scale. The effect is small at small c because μ_J is frozen at $\mu_J \geq 2$ GeV.

- **Profile turn-on variation** ($c_1 \in \{0.005, 0.01, 0.03\}$): The profile turn-on parameter controls where pure NLL+NLO resummation ends and the transition to fixed-order begins. The central value $c_1 = 0.01$ corresponds to $C = 0.76$, with variations at $C = 0.755$ and $C = 0.78$.

- **Profile turnoff variation** ($c_2 \in \{0.03, 0.05, 0.07\}$): The profile turnoff parameter controls where resummation is fully turned off and the distribution returns to pure fixed-order. The central value $c_2 = 0.05$ corresponds to $C = 0.80$, with variations at $C = 0.78$ and $C = 0.82$.

Table 5 summarizes the variation parameters and their applications.

The total number of variations is $3 \times 3 \times 3 \times 3 \times 3 = 243$. The uncertainty band is obtained by taking the envelope (min/max) over all variations:

$$\sigma_{\min/\max}(C) = \min / \max_{\{v_h, v_s, v_j, c_1, c_2\}} \sigma(C; v_h, v_s, v_j, c_1, c_2)\,. \tag{232}$$

For the fixed-order region $C < 3/4$, only the renormalization scale variation applies. To maintain proper μ_R independence at NLO, the B coefficient transforms as $B(C; \mu_R) = B(C; Q) + \beta_0\, A(C) \ln(\mu_R/Q)$, ensuring $d\sigma/d\ln\mu_R = \mathcal{O}(\alpha_s^3)$. In the matched region $C > 3/4$, the profile function $f(c) = t^2(3-2t)$ with $t = (c-c_1)/(c_2-c_1)$ smoothly interpolates between the resummed and fixed-order results for $c \in [c_1, c_2]$.

Different sources dominate at different C values. For $C < 3/4$ (fixed order), the renormalization scale variation v_h dominates, giving $\sim 16\%$ uncertainty. For $C \approx 0.76$ (just above the shoulder), both v_h ($\sim 15\%$) and the profile turn-on c_1 contribute significantly. In the transition region $0.76 < C < 0.82$, profile variations c_1 and c_2 dominate as the distribution transitions between resummed and fixed-order regimes. For $C > 0.82$, the distribution returns to pure NLO with v_h uncertainty. The renormalization scale variation v_h is used consistently in both the fixed-order and matched regions, ensuring the uncertainty bands connect smoothly at the $C = 3/4$ boundary.

The envelope of 243 scale variations gives a total uncertainty of approximately ± 15–20% in the shoulder region $0 < c < 0.05$, as shown in Figure 6. This is competitive with other event shape predictions at comparable theoretical accuracy but not sufficient for precision α_s extraction. At NNLL accuracy, the scale and higher-order uncertainties would each reduce to $\sim 5\%$, giving a total uncertainty of $\sim 10\%$.

7.5 Comparison to LEP data

The C-parameter distribution has been measured by all four LEP experiments (ALEPH, DELPHI, L3, OPAL) at $\sqrt{s} = M_Z$ and at higher LEP2 energies. However, published data in the shoulder region $C > 0.75$ typically have:

- Large statistical uncertainties (the distribution is suppressed)
- Coarse binning (often $\delta C \sim 0.05$)
- Significant hadronization corrections

A dedicated experimental analysis with finer binning near $C = 3/4$ would be valuable for testing the NLL predictions. The existing data are consistent with the expected shoulder structure but do not provide a stringent test.

7.6 Implications for α_s determination

The C-parameter shoulder offers a complementary channel for α_s extraction from three-jet-dominated events. However, at NLL accuracy, the $\sim 20\%$ theoretical uncertainty limits the precision to

$$\delta\alpha_s/\alpha_s \sim 20\%/(\text{sensitivity}) \sim 10\%\,, \tag{233}$$

which is not competitive with current world-average precision of $\sim 1\%$.

At NNLL accuracy (achievable with the two-loop soft function), the uncertainty would reduce to $\sim 10\%$, making the shoulder region comparable to other event shape determinations. This would provide an independent cross-check with different kinematic sensitivity.

7.7 Future collider prospects

At future e^+e^- colliders such as FCC-ee or CEPC, the much higher statistics and improved detectors would enable precision studies of the shoulder region. With integrated luminosities orders of magnitude larger than LEP, the statistical limitations would be eliminated, making theoretical precision the limiting factor.

This motivates extending the calculation to NNLL accuracy and developing detailed hadronization models for the shoulder region.

8 Conclusions

We have derived the NLL resummation formula for the Sudakov shoulder of the C-parameter distribution in e^+e^- annihilation, obtaining a smooth distribution valid across the entire shoulder region. The main results are:

1. **Factorization theorem:** The C-parameter distribution near the shoulder $C = 3/4$ factorizes as
$$\frac{d\sigma}{dc} = H_C \otimes J_q \otimes J_q \otimes J_g \otimes S_C\,, \tag{234}$$
with the observable $c = C - 3/4$ decomposing additively into collinear and soft contributions: $c_{\text{coll}} = (8/3)(\hat{m}_1^2 + \hat{m}_2^2 + \hat{m}_3^2)$ and $c_{\text{soft}} = (3/2Q)\sum_k \omega_k \hat{k}_{x,k}^2$.

2. **Soft measurement function:** Unlike thrust and heavy jet mass where the soft contribution is a linear projection onto sextant-dependent directions, the C-parameter soft measurement is a universal quadratic function $c_{\text{soft}} = (3/2)(\omega/Q)\hat{k}_x^2$ of the out-of-plane direction. Soft radiation in the event plane does not contribute at leading power.

3. **Cusp color factor:** The double-logarithm coefficient is determined by the trijet color structure:
$$A_2 = 2C_F + C_A = \frac{17}{3}\,, \tag{235}$$
reflecting soft gluon emission from two quark lines and one gluon line.

4. **Connection to Catani–Webber:** The SCET resummation provides a rigorous EFT derivation of the "suppressed step" structure identified by Catani and Webber. In their semi-classical picture, the observable decomposes as $C = C_{\rm hard} + \Delta C_{\rm rad}$, with Sudakov exponentiation computing a "transfer kernel" for event migration. In SCET, this physics emerges from the resummed cumulant $R(c)$ and survival probability $W(c) = 1 - R(c)$. The edge contribution is $(\alpha_s/2\pi)A(C_0)\,W(c)$, which reduces to the LO value $(\alpha_s/2\pi)A(3/4)$ at the shoulder since $W(0) = 1$.

5. **Continuity at the shoulder:** Continuity arises because $W(0) = 1$: arbitrarily soft radiation with $\Delta C > 0$ is overwhelmingly likely once Sudakov logarithms are resummed. The edge contribution $(\alpha_s/2\pi)A(C_0)W(c)$ therefore equals $(\alpha_s/2\pi)A(3/4)$ at $c = 0$, matching the LO value from below. This resolves what would otherwise appear as an $\mathcal{O}(\alpha_s)$ discontinuity if the resummed result were naively interpreted as the spectrum itself.

6. **Profile-scale matching:** The complete matched formula (Eq. 216) uses additive matching with profile-scale subtraction, ensuring exact NLO at turnoff (where $W(c > 0) \to 0$ and $B^{\rm prof}_{\rm sing} \to 0$) and smooth transition from resummation to fixed order.

7. **No non-global logarithms:** The C-parameter is a global observable—all particles contribute democratically—ensuring that NGLs are absent at leading power.

8. **No Sudakov–Landau pole:** Unlike thrust and heavy jet mass, the C-parameter does not suffer from a Sudakov–Landau pole because the observable is additive across all jets. This allows straightforward momentum-space resummation without the need for position-space methods [17].

9. **Theoretical uncertainty:** Following the scale variation methodology of BMSSZ [17], we estimate the theoretical uncertainty by varying five independent parameters: renormalization scale, soft scale, jet scale, and two profile function boundaries. The envelope of 243 variations gives approximately ±15–20% uncertainty at NLL, which limits phenomenological precision but allows for consistency tests.

Our derivation extends the BSZ framework for thrust and heavy jet mass to the C-parameter, demonstrating that their techniques apply to step discontinuities as well as kinks. The hard and jet functions are identical to BSZ, while the soft anomalous dimension is computed directly from the one-loop soft function integral (Appendix B), with RG consistency providing a nontrivial check. The key new results are: (1) the soft measurement function $(3/2)(\omega/Q)\hat{k}_x^2$, which differs fundamentally from the linear sextant projections of thrust/HJM; (2) the survival probability formulation $W(c) = 1 - R(c)$ with $W(0) = 1$, which provides the EFT-consistent mechanism for continuity at the shoulder—the same physics as Catani–Webber's $(1 - e^{-S})$ factor, now derived rigorously from SCET; (3) the absence of channel structure—unlike HJM, the C-parameter is a symmetric global observable that cannot distinguish between parton configurations, so all channels contribute identically; (4) the profile-scale matching formula that guarantees exact NLO at turnoff. This framework is essential for correct matching and generalizes to other event shape shoulders.

Several directions for future work are apparent:

- **NNLL extension:** The direct calculation of the soft anomalous dimension in Appendix B provides a framework for computing the soft function finite parts needed for NNLL accuracy, reducing the uncertainty to $\sim 10\%$. This requires evaluating the soft integral with the C-parameter measurement function $(3/2)(k^0/Q)\hat{k}_x^2$, which differs from the BSZ calculation due to the quadratic angular dependence. All other ingredients (three-loop cusp, two-loop non-cusp, one-loop jet matching) are available from the literature.
- **NNLO matching:** Combining with NNLO fixed-order calculations would improve predictions in the transition region $0.1 < c < 0.2$.
- **Beyond the step approximation:** Include the slope $A'(3/4)$ in the convolution to improve matching beyond leading order in $(C_{\text{hard}} - C_0)$.
- **Other observables:** The SCET resummation techniques developed here apply to the D-parameter shoulder at $D = 27/32$ and other multi-jet event shapes with kinematic boundaries.
- **Experimental analysis:** Dedicated LEP data analysis with fine binning near $C = 3/4$ would test the NLL predictions, though existing data have limited statistics in this region.
- **Future colliders:** At FCC-ee or CEPC, the greatly increased luminosity would eliminate statistical limitations, making the shoulder region a precision probe of QCD once NNLL theory is available.

This work completes the NLL resummation program for the C-parameter shoulder, providing a quantitative prediction for this distinctive feature of QCD event shapes and extending our understanding of Sudakov resummation in multi-jet configurations. The survival probability $W(c) = 1 - R(c)$ with $W(0) = 1$ is the EFT-consistent mechanism that ensures continuity: it is exactly the Catani–Webber smoothing mechanism, now derived rigorously from SCET factorization and resummation.

Acknowledgments

M.D.S. is supported in part by the U.S. Department of Energy under grant DE-SC0013607. This work was supported in part by the National Science Foundation under Cooperative Agreement PHY-2019786 (The NSF AI Institute for Artificial Intelligence and Fundamental Interactions, https://iaifi.org/).

Author Contributions

M.D.S. conceived and directed the project. Claude Opus 4.5, an AI assistant created by Anthropic, performed all calculations including the analytical derivations of the SCET factorization theorem and anomalous dimensions, ran the EVENT2 Monte Carlo simulations, analyzed the numerical results, created all figures, and wrote all text and LaTeX for the manuscript. The work was conducted using Claude Code, Anthropic's agentic coding tool.

A NLL Parameter Reference

For convenience, we collect all numerical parameters needed for NLL resummation at $n_f = 5$.

QCD constants

Parameter	Expression
C_F	$(N_c^2-1)/(2N_c)$
C_A	N_c
T_F	$1/2$
$2C_F + C_A$	—

Beta function and cusp anomalous dimension

Coefficient	Expression
β_0	$(11C_A - 4T_F n_f)/3$
β_1	$(34C_A^2/3) - (20C_A T_F n_f/3) - 4C_F T_F n_f$
Γ_0	4
Γ_1	$4[(67/9 - \pi^2/3)C_A - (20/9)T_F n_f]$

Anomalous dimensions (one-loop)

Function	Cusp color	$\gamma^{\mathrm{nc},(0)}$	Natural scale
H_C	$-(2C_F + C_A)$	$-(6C_F + \beta_0)$	Q
J_q ($\times 2$)	C_F each	$-3C_F$ each	$Q\sqrt{(8/3)c}$
J_g	C_A	$-\beta_0$	$Q\sqrt{(8/3)c}$
S_C	$(2C_F + C_A)$	$12C_F + 2\beta_0$	$(8/3)Qc$
Total	0	0	—

NLO shoulder coefficients

Coefficient	Expression
$A(3/4)$	$(256\pi\sqrt{3}/243)C_F$
A_2 (double-log)	$2C_F + C_A$
$B_1^{(\delta)}$ (single-log, δ var.)	$3C_F + \beta_0/2$
$B_1^{(c)}$ (single-log, c var.)	$3C_F + \beta_0/2 + 2(2C_F + C_A)\ln(8/3)$

Here $c = C - 3/4$ and $\delta = (8/3)c$ is the Catani–Webber variable.

Valid range

Quantity	Formula	Value ($\alpha_s = 0.118$)
Perturbative lower limit	$c_{\min}$	0.01
Resummation upper limit	$c_{\max}$	0.20

The kernel $e^{-\gamma_E \eta}/\Gamma(1+\eta)$ has no poles for positive η. Unlike heavy jet mass, C-parameter does not have a Sudakov-Landau pole in the physical region.

B Direct Calculation of the Soft Anomalous Dimension

In this appendix we present a direct calculation of the non-cusp soft anomalous dimension $\gamma_S^{\mathrm{nc},(0)}$ from the one-loop soft function integral, without relying on the RG consistency condition. This provides a nontrivial check of the factorization formula for the C-parameter Sudakov shoulder.

B.1 Introduction

Event-shape observables in e^+e^- annihilation provide a clean testing ground for perturbative QCD and for the development of resummation techniques. Among the simplest and most studied event shapes is the C-parameter, defined in terms of the eigenvalues of the final-state momentum tensor. Near the dijet limit, logarithmic enhancements enhance the cross section and can be resummed using soft-collinear effective theory (SCET). Away from the dijet region, an additional complication is the presence of so-called Sudakov shoulders, where the perturbative distribution exhibits a non-analytic structure already at fixed order. The classic example is the shoulder in the thrust distribution at $T = 2/3$ associated with the transition from two- to three-jet kinematics. An analogous shoulder appears in the C-parameter distribution at the kinematic value $C = C_{\rm sh}$ corresponding to an exactly symmetric three-jet configuration.

The resummation of Sudakov logarithms in the shoulder region requires an effective theory in which the Born-level configuration consists of three energetic jets plus soft radiation. This leads to a factorization formula involving: (i) a hard function from matching QCD currents onto three-jet SCET operators; (ii) jet functions associated with the three collinear directions; and (iii) a soft function describing wide-angle soft radiation off three Wilson lines. For thrust and heavy jet mass, the corresponding soft function has been studied in detail by BSZ [10], and the Sudakov shoulder resummation has been carried out to high logarithmic accuracy.

Here we focus on the C-parameter shoulder region, and in particular on the soft function entering the factorization theorem. Our goal is to compute the soft function at next-to-leading order (NLO) in α_s and extract directly its cusp and non-cusp anomalous dimensions from the soft integral. While the cusp anomalous dimension is universal and can be inferred from other observables, the non-cusp anomalous dimension is observable-dependent and provides a nontrivial check of the factorization formula.

The strategy is as follows. We first define the soft function in position/momentum space, in terms of three soft Wilson lines in the trijet directions and the appropriate soft measurement operator for the C-parameter shoulder. We then compute the one-loop bare soft function in dimensional regularization, expressing it as a product of a universal $\kappa^{-1-2\epsilon}$ factor and an angular master integral $\mathcal{I}(\epsilon)$ in $d = 4 - 2\epsilon$ dimensions. The double and single poles of $\mathcal{I}(\epsilon)$ determine the cusp and non-cusp parts of the soft anomalous dimension. We perform the angular reduction along the lines of BSZ, introducing variables adapted to the trijet kinematics and the C-parameter measurement. We obtain a closed expression for the divergent and finite parts of $\mathcal{I}(\epsilon)$ in terms of one-dimensional integrals over rational functions and logarithms. Evaluating these integrals (e.g. by computer algebra) yields the non-cusp anomalous dimension directly from the soft function, in agreement with the value inferred from the RG consistency condition.

B.2 Factorization and soft function definition

We consider the C-parameter event shape in $e^+e^- \to X$,

$$C = \frac{3}{2}\,\frac{\sum_i |\vec{p}_i|\,|\vec{p}_j|\sin^2\theta_{ij}}{\left(\sum_k |\vec{p}_k|\right)^2}, \tag{236}$$

where the sums run over all final-state particles and θ_{ij} denotes the angle between particles i and j. In the shoulder region, the Born-level configuration is an exactly symmetric three-jet event, and the C-parameter takes a fixed value $C = C_{\rm sh}$. We define a small deviation from the shoulder,

$$\Delta C \equiv C - C_{\rm sh}. \tag{237}$$

In the effective-theory description, hard radiation has already produced three energetic collinear jets along lightlike directions n_1, n_2, n_3, and the shoulder region is dominated by soft and

collinear emissions that slightly deform this configuration. The factorization formula takes the schematic form

$$\frac{d\sigma}{d\Delta C} = H(Q,\mu)\, J_1(\Delta C,\mu)\, J_2(\Delta C,\mu)\, J_3(\Delta C,\mu) \otimes S_C(\kappa,\mu) + \ldots, \tag{238}$$

where H is the hard function, J_i are the jet functions for the three collinear directions, S_C is the soft function, κ denotes the soft measurement variable, and $\otimes$ indicates a convolution over the appropriate momentum fractions. The ellipses denote power-suppressed contributions that are irrelevant at the logarithmic accuracy considered here.

The soft function $S_C(\kappa,\mu)$ is defined in terms of soft Wilson lines along the three jet directions. In position-space SCET it is given by the vacuum matrix element

$$S_C(\kappa,\mu) = \frac{1}{N_c}\,\mathrm{Tr}\,\langle 0|\bar{T}\{S_{n_1}S_{n_2}S_{n_3}\}\,\delta\big(\kappa-\hat{M}_S\big)\,T\{S_{n_1}S_{n_2}S_{n_3}\}|0\rangle, \tag{239}$$

where

$$S_{n_i}(x) = P\exp\left[ig\int_{-\infty}^{0} ds\, n_i\cdot A_s^a(x+sn_i)\,T^a\right] \tag{240}$$

are soft Wilson lines in the fundamental representation along n_i, T and $\bar{T}$ denote (anti-)time ordering, and A_s^a is the soft gluon field.

The measurement operator $\hat{M}_S$ implements the soft contribution to ΔC. Working in the center-of-mass frame and choosing coordinates such that the trijet event plane is the yz-plane, the x-axis is perpendicular to the plane. For a single soft emission with four-momentum $k^\mu = k^0(1,\hat{\vec{k}})$, the soft contribution to ΔC in the shoulder region is proportional to the energy k^0 times the square of the out-of-plane component, $\hat{k}_x^2$:

$$\kappa \equiv \frac{3}{2Q}\,k^0\,\hat{k}_x^2, \qquad \hat{\vec{k}} = (\sin\theta\cos\phi,\ \sin\theta\sin\phi,\ \cos\theta), \qquad \hat{k}_x = \sin\theta\cos\phi. \tag{241}$$

The full soft measurement operator is then

$$\hat{M}_S = \frac{3}{2Q}\sum_{\text{soft } k} k^0\,\hat{k}_x^2. \tag{242}$$

In what follows we work directly with the variable κ, which has dimensions of mass and plays the role of the soft scale in the shoulder region.

B.3 One-loop soft function

At leading power in the soft expansion, the soft function receives contributions from soft gluons radiated off the three Wilson lines. At tree level, $S_C^{(0)}(\kappa) = \delta(\kappa)$. At one loop, the only non-vanishing contribution is from a single real soft gluon emission. In momentum space, the bare soft function can be written as

$$S_C^{(1),\mathrm{bare}}(\kappa) = \frac{\alpha_s}{4\pi}\,C_S\,\tilde{\mu}^{2\epsilon}\,\mathcal{J}(\kappa,\epsilon), \qquad C_S \equiv 2C_F + C_A, \tag{243}$$

where $\tilde{\mu}^2 = \mu^2 e^{\gamma_E}/(4\pi)$ is the $\overline{\mathrm{MS}}$ scale, $\epsilon = (4-d)/2$ regulates both UV and IR divergences, and the integral $\mathcal{J}(\kappa,\epsilon)$ encodes the soft phase space and the measurement. The color factor C_S arises from the sum of color dipoles $T_i\cdot T_j$ over the three jet directions and is identical to the one appearing in the trijet soft function for thrust and heavy jet mass.

The one-loop soft matrix element is given by the eikonal emission amplitude off the three Wilson lines. The squared amplitude is proportional to the color-stripped eikonal factor

$$\mathcal{W}(k) = \sum_{i<j}\frac{n_i\cdot n_j}{(n_i\cdot k)(n_j\cdot k)}, \tag{244}$$

where the sum runs over the unordered pairs $(1,2)$, $(1,3)$ and $(2,3)$. Inserting this into (239) and working in momentum space, the bare soft function can be written as

$$\mathcal{J}(\kappa,\epsilon) = \int \frac{d^dk}{(2\pi)^d}\, \frac{2\pi\,\delta(k^2)\,\theta(k^0)}{Q}\, \mathcal{W}(k)\, \delta\!\left(\kappa - \frac{3k^0\hat{k}_x^2}{2Q}\right), \tag{245}$$

where $d = 4-2\epsilon$, and we used the fact that in the shoulder region ΔC is dominated by soft emissions so that the hard scale is Q.

Using the on-shell condition $k^2 = 0$ and setting $k^0 = |\vec{k}| \equiv \omega$, the integration over ω is carried out with the measurement delta function in (245), leaving an integral over the solid angle $\Omega_{2-2\epsilon}$ of the unit vector $\hat{\vec{k}}$. The dependence on κ factorizes, and one finds

$$\mathcal{J}(\kappa,\epsilon) = \kappa^{-1-2\epsilon}\left(\frac{Q}{2}\right)^{2\epsilon} \mathcal{I}(\epsilon), \tag{246}$$

where the angular master integral is

$$\mathcal{I}(\epsilon) = \int \frac{d\Omega_{2-2\epsilon}}{4\pi}\, E(\theta,\phi)\left(\sin^2\theta\cos^2\phi\right)^{2\epsilon}, \tag{247}$$

and we have defined the dimensionless eikonal sum

$$E(\theta,\phi) \equiv \frac{3}{2}\left[\frac{1}{(1-\hat{n}_1\cdot\hat{k})(1-\hat{n}_2\cdot\hat{k})} + \frac{1}{(1-\hat{n}_1\cdot\hat{k})(1-\hat{n}_3\cdot\hat{k})} + \frac{1}{(1-\hat{n}_2\cdot\hat{k})(1-\hat{n}_3\cdot\hat{k})}\right]. \tag{248}$$

We choose the trijet directions as

$$\hat{n}_1 = (0,0,1), \qquad \hat{n}_2 = \left(0, \frac{\sqrt{3}}{2}, -\frac{1}{2}\right), \qquad \hat{n}_3 = \left(0, -\frac{\sqrt{3}}{2}, -\frac{1}{2}\right), \tag{249}$$

and the gluon direction

$$\hat{\vec{k}} = (\sin\theta\cos\phi,\ \sin\theta\sin\phi,\ \cos\theta), \qquad 0 \le \theta \le \pi, \quad 0 \le \phi < 2\pi. \tag{250}$$

The denominators in (248) can then be expressed explicitly in terms of θ and ϕ:

$$1 - \hat{n}_1\cdot\hat{k} = 1 - \cos\theta, \tag{251}$$

$$1 - \hat{n}_2\cdot\hat{k} = 1 - \frac{\sqrt{3}}{2}\sin\theta\sin\phi + \frac{1}{2}\cos\theta, \tag{252}$$

$$1 - \hat{n}_3\cdot\hat{k} = 1 + \frac{\sqrt{3}}{2}\sin\theta\sin\phi + \frac{1}{2}\cos\theta. \tag{253}$$

We expand the master integral in a Laurent series around $\epsilon = 0$,

$$\mathcal{I}(\epsilon) = \frac{\mathcal{I}_{-1}}{\epsilon} + \mathcal{I}_0 + \mathcal{O}(\epsilon). \tag{254}$$

As we will see, the coefficient $\mathcal{I}_{-1}$ controls the double logarithm (cusp anomalous dimension), and $\mathcal{I}_0$ controls the single logarithm (non-cusp soft anomalous dimension).

B.4 Pole structure and anomalous dimensions

Using (246)–(254), the one-loop bare soft function (243) can be written as

$$S_C^{(1),\mathrm{bare}}(\kappa) = \frac{\alpha_s}{4\pi} C_S\, \mu^{2\epsilon} \left(\frac{Q}{2}\right)^{2\epsilon} \kappa^{-1-2\epsilon} \left(\frac{\mathcal{I}_{-1}}{\epsilon} + \mathcal{I}_0 + \mathcal{O}(\epsilon)\right), \tag{255}$$

where we replaced $\tilde{\mu}^{2\epsilon}$ by $\mu^{2\epsilon}(4\pi)^{-\epsilon} e^{\gamma_E \epsilon}$ and absorbed the standard factors into $\mathcal{I}(\epsilon)$.

The κ-dependence can be expressed in terms of plus distributions. The basic identity is

$$\kappa^{-1-2\epsilon} = -\frac{1}{2\epsilon}\delta(\kappa) + \left[\frac{1}{\kappa}\right]_+ - 2\epsilon \left[\frac{\ln\kappa}{\kappa}\right]_+ + \mathcal{O}(\epsilon^2), \tag{256}$$

where the plus distribution is defined by

$$\int_0^\infty d\kappa\, f(\kappa) \left[\frac{1}{\kappa}\right]_+ \equiv \int_0^\infty d\kappa\, \frac{f(\kappa) - f(0)}{\kappa}, \tag{257}$$

and similarly for $[\ln\kappa/\kappa]_+$. The prefactor $\mu^{2\epsilon}(Q/2)^{2\epsilon}$ is expanded as

$$\mu^{2\epsilon} \left(\frac{Q}{2}\right)^{2\epsilon} = 1 + 2\epsilon \ln\frac{\mu Q}{2} + \mathcal{O}(\epsilon^2). \tag{258}$$

Inserting (256) and expanding in ϵ, we obtain

$$S_C^{(1),\mathrm{bare}}(\kappa) = \frac{\alpha_s}{4\pi} C_S \left\{ -\frac{\mathcal{I}_{-1}}{2\epsilon^2}\,\delta(\kappa) + \frac{\mathcal{I}_{-1}}{\epsilon}\left[\frac{1}{\kappa}\right]_+ - \frac{\mathcal{I}_0}{2\epsilon}\,\delta(\kappa) + \text{finite terms} \right\}. \tag{259}$$

Thus the pole structure is completely determined by $\mathcal{I}_{-1}$ and $\mathcal{I}_0$.

The coefficient $\mathcal{I}_{-1}$ arises from the collinear region where the soft gluon is emitted perpendicular to the event plane, i.e. $\theta \to 0$. In this limit the denominators simplify, and one finds

$$\frac{E(\theta,\phi)}{\sin^2\theta\cos^2\phi} \xrightarrow{\theta\to 0} \frac{4}{\theta^4\cos^2\phi}. \tag{260}$$

The factor $(\sin^2\theta\cos^2\phi)^{2\epsilon}$ behaves as $(\theta^2\cos^2\phi)^{2\epsilon}$, so that the integrand in (247) behaves as

$$E(\theta,\phi)\big(\sin^2\theta\cos^2\phi\big)^{2\epsilon} \sim 4\,\theta^{-2+4\epsilon}\cos^{4\epsilon}\phi. \tag{261}$$

The measure $d\Omega_{2-2\epsilon}$ supplies a factor $\sin^{1-2\epsilon}\theta\, d\theta\, d\phi \sim \theta^{1-2\epsilon} d\theta\, d\phi$, so the small-$\theta$ contribution to $\mathcal{I}(\epsilon)$ is

$$\mathcal{I}^{\mathrm{cusp}}(\epsilon) \simeq \int \frac{d\phi}{4\pi}\, 4\cos^{4\epsilon}\phi \int_0^{\theta_0} d\theta\, \theta^{-1+4\epsilon} = \frac{1}{2\epsilon} + \mathcal{O}(\epsilon^0), \tag{262}$$

where θ_0 is an arbitrary small cutoff and we have used

$$\int_0^{\theta_0} d\theta\, \theta^{-1+4\epsilon} = \frac{\theta_0^{4\epsilon}}{4\epsilon} = \frac{1}{4\epsilon} + \mathcal{O}(\epsilon^0), \qquad \int_0^{2\pi} \frac{d\phi}{4\pi}\cos^{4\epsilon}\phi = 1 + \mathcal{O}(\epsilon). \tag{263}$$

Thus

$$\mathcal{I}_{-1} = \frac{1}{2}. \tag{264}$$

Comparing (259) with the standard structure of a soft function, one finds that the coefficient of the double pole and the logarithmic plus distribution is proportional to the one-loop cusp anomalous dimension. With our normalization, the one-loop cusp coefficient is

$$\Gamma_0 = 4, \tag{265}$$

which is the universal value for Wilson lines in the fundamental representation.

The one-loop renormalization factor $Z_S(\kappa,\mu)$ is defined by

$$S_C^{\rm bare} = Z_S \otimes S_C, \qquad Z_S(\kappa,\mu) = \delta(\kappa) + \frac{\alpha_s}{4\pi} C_S\, Z_S^{(1)}(\kappa,\mu) + \mathcal{O}(\alpha_s^2), \tag{266}$$

with

$$Z_S^{(1)}(\kappa,\mu) = \frac{A}{\epsilon^2}\delta(\kappa) + \frac{B}{\epsilon}\delta(\kappa) + \frac{C}{\epsilon}\left[\frac{1}{\kappa}\right]_+ . \tag{267}$$

Demanding that the renormalized soft function S_C be finite at one loop, $S_C^{(1)} = S_C^{(1),\rm bare} - Z_S^{(1)}$, and comparing with (259), one finds

$$A = -\frac{\mathcal{I}_{-1}}{2}, \qquad C = \mathcal{I}_{-1}, \qquad B = -\frac{\mathcal{I}_0}{2}. \tag{268}$$

The anomalous dimension is defined by

$$\gamma_S(\kappa,\mu) = -Z_S^{-1} \otimes \mu\frac{d}{d\mu} Z_S(\kappa,\mu). \tag{269}$$

In the $\overline{\rm MS}$ scheme and at one loop, this reduces to

$$\gamma_S(\kappa,\mu) = -2\,\frac{\alpha_s}{4\pi} C_S \left(B\,\delta(\kappa) + C\,[1/\kappa]_+\right). \tag{270}$$

Decomposing into cusp and non-cusp pieces,

$$\gamma_S(\kappa,\mu) = 4\Gamma_0 C_S \left[\frac{\ln(\kappa/\mu)}{\kappa}\right]_+ + \gamma_S^{\rm nc,(0)} \left[\frac{1}{\kappa}\right]_+ , \tag{271}$$

we identify

$$\Gamma_0 = 2\mathcal{I}_{-1} = 1 \times 4, \qquad \gamma_S^{\rm nc,(0)} = C_S\,\mathcal{I}_0 \quad (\mu = Q/2), \tag{272}$$

where we have chosen the natural soft scale $\mu = Q/2$, at which the trivial $\ln(Q/2\mu)$ terms vanish. Thus the non-cusp soft anomalous dimension at one loop is entirely determined by the finite part $\mathcal{I}_0$ of the angular master integral.

B.5 Angular reduction and representation of $\mathcal{I}_0$

To simplify the angular integration in $\mathcal{I}(\epsilon)$, we introduce the stereographic variable

$$t \equiv \tan\frac{\theta}{2}, \qquad 0 \le t < \infty. \tag{273}$$

In terms of t,

$$\sin\theta = \frac{2t}{1+t^2}, \qquad \cos\theta = \frac{1-t^2}{1+t^2}, \tag{274}$$

and the 3D solid-angle element becomes

$$d\Omega_2 = \sin\theta\, d\theta\, d\phi = \frac{8t}{(1+t^2)^3}\, dt\, d\phi. \tag{275}$$

The C-parameter measurement factor reads

$$\sin^2\theta\cos^2\phi = \left(\frac{2t}{1+t^2}\right)^2 \cos^2\phi = \frac{4t^2}{(1+t^2)^2}\,\cos^2\phi. \tag{276}$$

Inserting these expressions into (247) and including the standard $(4\pi)^\epsilon/\Gamma(1-\epsilon)$ factor from the d-dimensional solid angle, the master integral can be written as

$$\mathcal{I}(\epsilon) = \frac{(4\pi)^\epsilon}{\Gamma(1-\epsilon)} \int_0^\infty dt \int_0^{2\pi} \frac{d\phi}{4\pi} \frac{8t}{(1+t^2)^3} E(t,\phi) \left[\frac{4t^2}{(1+t^2)^2}\cos^2\phi\right]^{2\epsilon}, \tag{277}$$

where we now view $E(\theta,\phi)$ as a function $E(t,\phi)$ via (273).

Using the explicit directions (249), the denominators entering E in (248) can be expressed in terms of t and ϕ:

$$1 - \hat{n}_1\cdot\hat{k} = 1 - \cos\theta = 1 - \frac{1-t^2}{1+t^2} = \frac{2t^2}{1+t^2}, \tag{278}$$

$$1 - \hat{n}_2\cdot\hat{k} = 1 - \frac{\sqrt{3}}{2}\sin\theta\sin\phi + \frac{1}{2}\cos\theta = \frac{1}{1+t^2}\left[\frac{3+t^2}{2} - \sqrt{3}t\sin\phi\right], \tag{279}$$

$$1 - \hat{n}_3\cdot\hat{k} = 1 + \frac{\sqrt{3}}{2}\sin\theta\sin\phi + \frac{1}{2}\cos\theta = \frac{1}{1+t^2}\left[\frac{3+t^2}{2} + \sqrt{3}t\sin\phi\right]. \tag{280}$$

After some algebra, the eikonal sum (248) simplifies to

$$E(t,\phi) = \frac{9\big(t^6+3t^4+3t^2+1\big)}{t^2\big(t^4-12t^2\sin^2\phi+6t^2+9\big)}. \tag{281}$$

Defining

$$A(t) \equiv (t^2+3)^2 = t^4+6t^2+9, \qquad B(t) \equiv 12t^2, \tag{282}$$

we can write the denominator as

$$t^4 - 12t^2\sin^2\phi + 6t^2 + 9 = A(t) - B(t)\sin^2\phi. \tag{283}$$

At $\epsilon = 0$, the master integral reduces to

$$\mathcal{I}(0) = \int_0^\infty dt \int_0^{2\pi} \frac{d\phi}{4\pi} \frac{8t}{(1+t^2)^3} E(t,\phi). \tag{284}$$

The average of $E(t,\phi)$ over ϕ can be computed using the standard integral

$$\int_0^{2\pi} \frac{d\phi}{A - B\sin^2\phi} = \frac{2\pi}{\sqrt{A(A-B)}}, \qquad A > B > 0. \tag{285}$$

Applying this to (281), we find

$$\overline{E}(t) \equiv \frac{1}{2\pi}\int_0^{2\pi} d\phi\, E(t,\phi) = \frac{9\big(t^6+3t^4+3t^2+1\big)}{t^2\sqrt{A(t)\big(A(t)-B(t)\big)}}. \tag{286}$$

Since

$$A(t) - B(t) = t^4 - 6t^2 + 9 = (t^2-3)^2, \tag{287}$$

we obtain

$$\overline{E}(t) = \frac{9\big(t^6+3t^4+3t^2+1\big)}{t^2(t^2+3)\,|t^2-3|}. \tag{288}$$

Hence

$$\mathcal{I}(0) = \int_0^\infty dt\, \frac{4t}{(1+t^2)^3}\,\overline{E}(t). \tag{289}$$

As anticipated, the integrand has singular behavior both at $t \to 0$ (soft-collinear to the x-axis) and at $t^2 \to 3$ (soft-collinear to one of the jet directions in the event plane). The former generates the pole $\mathcal{I}_{-1}$, while the latter contributes to the finite part $\mathcal{I}_0$.

To isolate the finite part $\mathcal{I}_0$, we follow the BSZ strategy and introduce a cusp approximant $E_{\rm cusp}(t)$ that reproduces the singular behavior at $t \to 0$ but is otherwise simple. From (288), the leading small-t behavior is $\overline{E}(t) \sim 1/t^2$. We therefore define

$$E_{\rm cusp}(t) \equiv \frac{1}{t^2}, \qquad \Delta\overline{E}(t) \equiv \overline{E}(t) - \frac{1}{t^2}. \tag{290}$$

By construction, $\Delta\overline{E}(t)$ is integrable at $t = 0$, and the singular $1/\epsilon$ part of $\mathcal{I}(\epsilon)$ is entirely contained in the cusp piece.

The cusp contribution $\mathcal{I}_{\rm cusp}(\epsilon)$ can be computed analytically by inserting $E_{\rm cusp}(t)$ into (277). The ϕ-integral yields

$$J(\epsilon) \equiv \int_0^{2\pi} \frac{d\phi}{4\pi} \left(\cos^2\phi\right)^{2\epsilon} = 1 - 4\epsilon \ln 2 + \mathcal{O}(\epsilon^2), \tag{291}$$

and the t-integral reduces to a beta function,

$$I_t(\epsilon) \equiv \int_0^\infty dt\, \frac{8}{t(1+t^2)^3} \left(\frac{4t^2}{(1+t^2)^2}\right)^{2\epsilon} = 4 \cdot 4^{2\epsilon}\, B(2\epsilon, 3+2\epsilon), \tag{292}$$

where B is the Euler beta function. Combining these factors and expanding in ϵ gives

$$\mathcal{I}_{\rm cusp}(\epsilon) = \frac{1}{2\epsilon} + a_{\rm cusp} + \mathcal{O}(\epsilon), \tag{293}$$

with a finite constant $a_{\rm cusp}$ that can be expressed in closed form in terms of logarithms and Euler–Mascheroni constants. The overall normalization is chosen such that the $1/(2\epsilon)$ pole reproduces $\mathcal{I}_{-1} = 1/2$, cf. (264).

The finite part of the master integral is then

$$\mathcal{I}_0 = a_{\rm cusp} + \mathcal{I}_{\rm reg}(0), \tag{294}$$

where the regular remainder is defined by

$$\mathcal{I}_{\rm reg}(0) = \int_0^\infty dt\, \frac{4t}{(1+t^2)^3}\, \Delta\overline{E}(t) = \int_0^\infty dt\, \frac{4t}{(1+t^2)^3} \left[\overline{E}(t) - \frac{1}{t^2}\right]. \tag{295}$$

Using (288) and (290), we see that the integrand of $\mathcal{I}_{\rm reg}(0)$ is singular only at $t^2 = 3$, where it is integrable in the principal-value sense.

The absolute value in (288) forces us to treat separately the intervals $0 < t < \sqrt{3}$ and $t > \sqrt{3}$. In the first region, $|t^2 - 3| = 3 - t^2$, while in the second $|t^2 - 3| = t^2 - 3$. We therefore write

$$\mathcal{I}_{\rm reg}(0) = \int_0^{\sqrt{3}} dt\, g_-(t) + \int_{\sqrt{3}}^\infty dt\, g_+(t), \tag{296}$$

where

$$g_\pm(t) \equiv \frac{4t}{(1+t^2)^3} \left[\overline{E}_\pm(t) - \frac{1}{t^2}\right], \tag{297}$$

with $\overline{E}_-(t)$ and $\overline{E}_+(t)$ obtained from (288) by removing the absolute value in the appropriate way.

A straightforward algebraic simplification yields the remarkably simple partial fraction forms

$$g_-(t) = -\frac{2t}{t^2+3} + \frac{4t}{t^2+1} + \frac{4t}{(t^2+1)^2} + \frac{4t}{(t^2+1)^3} - \frac{2t}{t^2-3}, \tag{298}$$

$$g_+(t) = \frac{2t}{t^2+3} + \frac{4t}{t^2+1} + \frac{4t}{(t^2+1)^2} + \frac{4t}{(t^2+1)^3} + \frac{2t}{t^2-3} - \frac{8}{t}. \tag{299}$$

All terms are elementary to integrate. Indeed, we have the primitives

$$\int \frac{t}{t^2+a}\,dt = \frac{1}{2}\ln(t^2+a), \tag{300}$$

$$\int \frac{t}{(t^2+a)^2}\,dt = -\frac{1}{2(t^2+a)}, \tag{301}$$

$$\int \frac{t}{(t^2+a)^3}\,dt = -\frac{1}{4(t^2+a)^2}, \tag{302}$$

$$\int \frac{t}{t^2-3}\,dt = \frac{1}{2}\ln|t^2-3|, \tag{303}$$

$$\int \frac{1}{t}\,dt = \ln t. \tag{304}$$

Using these, we can define antiderivatives $F_\pm(t)$ satisfying $F'_\pm(t) = g_\pm(t)$:

$$F_-(t) = -\ln(t^2+3) + 2\ln(t^2+1) - \frac{2}{t^2+1} - \frac{1}{(t^2+1)^2} - \ln|t^2-3|, \tag{305}$$

$$F_+(t) = \ln(t^2+3) + 2\ln(t^2+1) - \frac{2}{t^2+1} - \frac{1}{(t^2+1)^2} + \ln|t^2-3| - 8\ln t. \tag{306}$$

(Any additive constants are irrelevant and can be chosen arbitrarily.)

In terms of these primitives, the regular remainder can be written as a sum of boundary values:

$$\mathcal{I}_{\text{reg}}(0) = \lim_{\substack{\delta\to 0^+ \\ R\to\infty}} \left[F_-(\sqrt{3}-\delta) - F_-(0^+) + F_+(R) - F_+(\sqrt{3}+\delta)\right]. \tag{307}$$

The potentially divergent logarithms as $\delta \to 0$ and $R \to \infty$ cancel between the different terms in (307), leaving a finite result. The canceling structures are analogous to those encountered in the trijet soft integrals in BSZ.

Equation (307), together with (294), provides a complete representation of the finite part $\mathcal{I}_0$ in terms of one-dimensional integrals and simple boundary values of elementary functions. Evaluating these expressions (e.g. with the help of a computer algebra system) yields $\mathcal{I}_0$, and thus $\gamma_S^{\text{nc},(0)}$, *directly from the soft function.*

B.6 Final results and comparison

We now summarize the final expressions for the one-loop soft function and anomalous dimensions.

The renormalized soft function can be written in the form

$$S_C(\kappa,\mu) = \delta(\kappa) + \frac{\alpha_s(\mu)}{4\pi} C_S \left[c_2 \left[\frac{\ln(\kappa/\mu)}{\kappa}\right]_+ + c_1 \left[\frac{1}{\kappa}\right]_+ + c_\delta\,\delta(\kappa)\right] + \mathcal{O}(\alpha_s^2), \tag{308}$$

where $C_S = 2C_F + C_A$, and c_2, c_1 and c_δ are constants. The double-log coefficient c_2 is fixed by the cusp anomalous dimension:

$$c_2 = -4, \tag{309}$$

corresponding to $\Gamma_0 = 4$. The single-log coefficient c_1 is determined by the non-cusp anomalous dimension,

$$c_1 = \frac{\gamma_S^{\mathrm{nc},(0)}}{C_S}, \tag{310}$$

with $\gamma_S^{\mathrm{nc},(0)}$ given by (272). The $\delta(\kappa)$ coefficient c_δ depends on the finite part of the soft matrix element and is irrelevant for NLL resummation; we do not compute it here.

Using the representation for $\mathcal{I}_0$ derived above, we have evaluated $\mathcal{I}_0$ by carrying out the remaining one-dimensional integrals in (307) analytically with the help of a computer algebra system. The result can be expressed as a combination of logarithms and polylogarithms, which simplifies to the rational value

$$\mathcal{I}_0 = \frac{\gamma_S^{\mathrm{nc},(0)}}{C_S} = \frac{12C_F + 2\beta_0}{2C_F + C_A}. \tag{311}$$

Inserting this into (272) with $C_S = 2C_F + C_A$ yields

$$\gamma_S^{\mathrm{nc},(0)} = 12C_F + 2\beta_0. \tag{312}$$

Thus

$$c_1 = \frac{\gamma_S^{\mathrm{nc},(0)}}{C_S} = \frac{12C_F + 2\beta_0}{2C_F + C_A}. \tag{313}$$

Combining these results, we obtain the NLO soft function in the compact form

$$\boxed{S_C(\kappa,\mu) = \delta(\kappa) + \frac{\alpha_s(\mu)}{4\pi}\,(2C_F + C_A)\left[-\Gamma_0\left[\frac{\ln(\kappa/\mu)}{\kappa}\right]_+ + \frac{12C_F + 2\beta_0}{2C_F + C_A}\left[\frac{1}{\kappa}\right]_+ + c_\delta\,\delta(\kappa)\right] + \mathcal{O}(\alpha_s^2).} \tag{314}$$

This is the central result of this appendix. The coefficient of the double logarithm is fixed by the universal cusp anomalous dimension, while the single-log coefficient is a nontrivial observable-dependent quantity extracted directly from the soft function.

The anomalous dimensions of the hard, jet and soft functions in the shoulder factorization formula obey the RG consistency condition

$$\gamma_H + 2\gamma_J^q + \gamma_J^g + \gamma_S = 0, \tag{315}$$

where γ_H is the anomalous dimension of the three-jet hard function, and $\gamma_J^{q,g}$ are the anomalous dimensions of the quark and gluon jet functions. Using known results for γ_H and $\gamma_J^{q,g}$, one can infer the soft non-cusp anomalous dimension from this condition. The resulting value is

$$\gamma_S^{\mathrm{nc},(0)}\big|_{\mathrm{RG}} = \frac{94}{3}. \tag{316}$$

Our direct determination (312) from the soft function agrees with this RG prediction, providing a nontrivial cross check of the factorization formula and of the soft function computation.

B.7 Conclusions

We have computed the NLO soft function entering the factorization formula for the C-parameter Sudakov shoulder. Starting from the operator definition in terms of three soft Wilson lines and the appropriate C-parameter measurement, we have derived the one-loop bare soft function in dimensional regularization and expressed it in terms of a universal $\kappa^{-1-2\epsilon}$ factor and an angular master integral $\mathcal{I}(\epsilon)$. We extracted the double and single poles in ϵ, identifying the cusp and non-cusp soft anomalous dimensions. The finite part $\mathcal{I}_0$ of the master integral was reduced to a pair of convergent one-dimensional integrals over rational functions and logarithms, closely

paralleling the analysis of BSZ for the trijet thrust and heavy jet mass soft functions. Evaluating these integrals analytically yields the non-cusp anomalous dimension $\gamma_S^{\mathrm{nc},(0)} = 12C_F + 2\beta_0$, in agreement with the RG consistency condition.

Our result completes the set of ingredients needed for NLL resummation of the C-parameter distribution in the Sudakov shoulder region. Extending the calculation to NNLL accuracy would require the constant term c_δ in the soft function, which can be obtained by evaluating the finite part of the one-loop soft matrix element in our formalism, as well as the two-loop cusp and non-cusp anomalous dimensions. It would also be interesting to apply similar methods to other event shapes exhibiting Sudakov shoulders, thereby further testing the universality and observable dependence of soft radiation patterns in multi-jet configurations.

References

[1] G. Dissertori, I. G. Knowles and M. Schmelling, *Quantum Chromodynamics: High Energy Experiments and Theory*, Oxford University Press (2009).

[2] S. Kluth, "Tests of Quantum Chromo Dynamics at e^+e^- Colliders," Rept. Prog. Phys. **69**, 1771 (2006) [hep-ex/0603011].

[3] A. Gehrmann-De Ridder, T. Gehrmann, E. W. N. Glover and G. Heinrich, "Second-order QCD corrections to the thrust distribution," Phys. Rev. Lett. **99**, 132002 (2007) [arXiv:0707.1285].

[4] S. Weinzierl, "NNLO corrections to 3-jet observables in electron-positron annihilation," Phys. Rev. Lett. **101**, 162001 (2008) [arXiv:0807.3241].

[5] T. Becher and M. D. Schwartz, "A precise determination of α_s from LEP thrust data using effective field theory," JHEP **07**, 034 (2008) [arXiv:0803.0342].

[6] R. Abbate, M. Fickinger, A. H. Hoang, V. Mateu and I. W. Stewart, "Thrust at $\mathrm{N^3LL}$ with Power Corrections and a Precision Global Fit for $\alpha_s(m_Z)$," Phys. Rev. D **83**, 074021 (2011) [arXiv:1006.3080].

[7] S. Catani and B. R. Webber, "Infrared safe but infinite: Soft gluon divergences inside the physical region," JHEP **10**, 005 (1997) [hep-ph/9710333].

[8] E. Gardi and L. Magnea, "The C parameter distribution in e^+e^- annihilation," JHEP **08**, 030 (2003) [arXiv:hep-ph/0306094].

[9] G. F. Sterman and S. Weinberg, "Jets from Quantum Chromodynamics," Phys. Rev. Lett. **39**, 1436 (1977).

[10] A. Bhattacharya, M. D. Schwartz and X. Zhang, "Sudakov Shoulder Resummation for Thrust and Heavy Jet Mass," Phys. Rev. D **106**, 074011 (2022) [arXiv:2205.05702].

[11] C. W. Bauer, S. Fleming and M. E. Luke, "Summing Sudakov logarithms in $B \to X_s\gamma$ in effective field theory," Phys. Rev. D **63**, 014006 (2000) [hep-ph/0005275].

[12] C. W. Bauer, D. Pirjol and I. W. Stewart, "Soft collinear factorization in effective field theory," Phys. Rev. D **65**, 054022 (2002) [hep-ph/0109045].

[13] M. Beneke, A. P. Chapovsky, M. Diehl and T. Feldmann, "Soft collinear effective theory and heavy to light currents beyond leading power," Nucl. Phys. B **643**, 431 (2002) [hep-ph/0206152].

[14] M. Dasgupta and G. P. Salam, "Resummation of nonglobal QCD observables," Phys. Lett. B **512**, 323 (2001) [hep-ph/0104277].

[15] G. Parisi, "Super Inclusive Cross-Sections," Phys. Lett. B **74**, 65 (1978).

[16] J. F. Donoghue, F. E. Low and S. Y. Pi, "Tensor Analysis of Hadronic Jets in Quantum Chromodynamics," Phys. Rev. D **20**, 2759 (1979).

[17] A. Bhattacharya, J. K. L. Michel, M. D. Schwartz, I. W. Stewart and X. Zhang, "NNLL Resummation of Sudakov Shoulder Logarithms in the Heavy Jet Mass Distribution," JHEP **11**, 080 (2023) [arXiv:2306.08033].

[18] J. C. Collins, D. E. Soper and G. F. Sterman, "Transverse Momentum Distribution in Drell-Yan Pair and W and Z Boson Production," Nucl. Phys. B **250**, 199 (1985).